SPORT INJURY BIOMECHANICS AND STRESS CHANGES IN ADJACENT INTERVERTEBRAL DISCS AFTER PARTIAL DISCECTOMIES AND FUSION OF THE CERVICAL SPINE

BY

ABRAHAM TCHAKO

A dissertation submitted to the Graduate Faculty in Engineering in partial fulfillment of the requirements for the degree of Doctor of Philosophy, The City University of New York

2004

UMI Number: 3187798

ProQuest Information and Learning Company
300 North Zeeb Road
P.O. Box 1346
Ann Arbor, MI 48106-1346

This manuscript has been read and accepted for the Graduate Faculty in Engineering in satisfaction of the dissertation requirement for the degree of Doctor of Philosophy.

Date

Professor Ali M. Sadegh, Ph.D., Dept. of ME, CCNY
Chair of Examining Committee

Date

Professor Mumtaz K. Kassir, Ph.D., Executive Officer

Stephen C. Cowin, Ph.D., CUNY Distinguished Professor of Mechanical and Biomedical Engineering, CCNY.

Susannah P. Fritton, Ph.D., Professor of Biomedical Engineering, CCNY.

Peter A. Torzilli, Ph.D., Senior Scientist and Director, Laboratory for Soft Tissue Research, HSS, NY.

Supervisory Committee

THE CITY UNIVERSITY OF NEW YORK

ABSTRACT

SPORT INJURY BIOMECHANICS AND STRESS CHANGES IN ADJACENT INTERVERTEBRAL DISCS AFTER PARTIAL DISCECTOMIES AND FUSION OF THE CERVICAL SPINE

By

ABRAHAM TCHAKO

Adviser: Professor Ali M. Sadegh

Cervical spine injuries and degeneration of cervical spinal components as well as surgical intervention such as discectomy and fusion are among the major concerns that spinal surgeons have to deal with on a continuous basis. Physico-geometrical and medical considerations taken into account during the surgery will affect the long-term (biomechanical and medical) outcomes of the surgical procedure.

To simulate sport injury mechanisms and the long-term biomechanical effect of the cervical discectomy surgery, two complete 3D Finite Element models (FEM) of the human c-spine (C1-T1) were created.

The first model was a geometrically simplified model that was used to study the vertebrae and disc stresses under high G-z and G-y accelerations while considering the dynamic nature of the forces and visco-elastic properties of the disc and ligaments. The primary results using this model revealed that the stresses in the vertebral bodies, for 10 to 12 G-z accelerations, were under the injury threshold level.

The second complete model was an improved and geometrically detailed non-linear 3D FE model of the human c-spine (C1-T1). The modeling took into consideration

the inhomogeneity and the non-linearity of the hard and soft tissues of the cervical spine. The major components of the c-spine were individually materialized in the second model. The model was validated against existing in-vivo experimental studies. This model was first utilized to investigate sport and accident injuries. The results showed that minimal shear forces and eccentric compression forces could generate enough flexion moment to put the c-spine at the onset of discs injuries and/or clinically instability.

The second model was further utilized to investigate the change in stresses in adjacent discs after partial discectomies and fusion. Discectomy and fusion is a surgical procedure commonly used to correct and/or stabilize an injured or degenerated cervical spine. After fusion, the stresses in adjacent intervertebral discs change and could lead to another surgery. It was determined that the percentage of the contact area between the bone graft and the vertebral body is directly related to the changes in stresses in adjacent discs and to the extent of the bone graft subsidence into the vertebral body.

ACKNOWLEDGMENTS

I express my profound gratitude to the Committee Chairman and my mentor, Professor Ali M. Sadegh, for his invaluable guidance, tireless support and motivation throughout this project. My appreciation and special thanks to Professor Susannah P. Fritton, Ph.D., Distinguished Professor Stephen C. Cowin, Ph.D. and Senior Researcher Peter A. Torzilli, Ph.D. for their individual help and their participation in the examining Committee.

I wish to thank the current and former Chairman, Professor Feridun Delale and Professor Yannis Andreopoulos, of the Department of Mechanical Engineering at CCNY, and their staff for the continuous logistical and financial support. I also thank the Department of Biomedical Engineering for its support.

I will forever be indebted to Professor Alfred S. Posamentier, Ph.D., Dean of the School of Education at CCNY, and his former Assistant, Ms. Jill Cotter for the opportunity and assistance they gave, and which allowed me to undertake this research project. I am really grateful.

Great appreciation goes to all my friends who were encouraging. I am very grateful to my family members for their relentless support. Finally, my deepest indebtedness to my wife and children, they were instrumental in my pursuit of this research work. Their smiles, motivational teases and encouragements during difficult times motivated me to complete this project.

This research was supported by grant from the U.S. Air Force. The PSC-CUNY, the Research Foundation and the Graduate Center of the City University of New York provided further financial supports.

To

My Mother

And

In memories of my Father and my Sister-in-law

TABLE OF CONTENTS

LIST OF TABLES

LIST OF FIGURES

1. INTRODUCTION

The biomechanics of the human cervical spine after traumatic situations and partial discectomy and fusion is the main subject of this research. Problems that are often associated with the cervical spine are injuries and degeneration. Whilst injuries can result from any professional or recreational activities, degeneration is a more complex process that may be due to the aging process, the pathological or biochemical development. Injury as well as degeneration could alter the biomechanics and the normal structure of the spine and lead to severe pain and dysfunction that may require surgery. According to the American Academic of Orthopedic Surgeons (AAAOS), cervical spine surgeries in the U.S. cost hundreds of billions dollars every year, and about 45% of spinal surgeries performed in the U.S in year 2000 were done on the cervical spine column. The study of disc degeneration process itself is beyond the scope of this research and only the biomechanics effects of some of its curative surgery will be studied. In contrast, it is well known that injuries to the human neck result from forces generated in the neck when the head is subjected to traumatic impact or high single and multidirectional accelerations such as in high-velocity contact sports, automobile accidents or fighter pilot ejections.

The primary goal of this research is to use a FE model of the cervical spine to study its responses when it is subjected to high g-accelerations forces, such as those experienced by fighter jet pilots during the ejection process. Advancements in aerospace technology have made the increase in airspeed of aircrafts possible. However, increased airspeed has made the safe ejection of crewmembers from disabled aircrafts difficult. In an emergency situation requiring ejection from cockpit, a fighter pilot's torso is subjected to high acceleration on the order of 15 G's (Guill et al. 1990). The time required for an

ejection is in the order of milliseconds. The high acceleration, which is achieved in an extraordinarily brief period of time, applies an extremely high magnitude of loads to the spinal column, particularly the cervical spine. The high magnitude loads often causes injuries; many of which occur in the lumber and thoracic spine, but frequently in the cervical spine and the neck. (Guill et al. 1990). In an ejection process, the initial orientation of the head and the direction of the acceleration vector both play important roles in the magnitude of the load that is applied to the neck. That is, the head acceleration varies considerably depending on whether the airplane is in roll or spin conditions. Additional instrumentation, such as night vision goggles and helmet-mounted displays, while profiding significant advantages over panel-mounted instruments, have increased the mass of the helmet system, which also increases the risk of a major neck injury in an emergency escape situation. Recent advances in seat design and pilot training have added more restraint to the pilot's lumbar and thoracic regions thereby reducing the risk of lower back injuries. However, lack of restraint in the neck and head regions has made the pilot's cervical spine vulnerable to injuries. This is due to the fact that the pilot's head must have a reasonable freedom of motion in order to ensure an adequate field of view. High magnitude loads are also present during automotive and sport accidents where the unrestraint head and neck of a passenger or a sportsperson are subjected to high acceleration.

There have been several studies on head and neck injury after a sled test in G-x, G-z accelerations, (Miller, 1993 and Perry, 1994). Sadegh, 1995 developed and validated a head and neck model. He employed the experimental data collected from the biodynamic responses of human volunteers during acceleration in the y direction on a

sled at the sled track facility at Armstrong Laboratory at Wright-Patterson Air Force Base (WPAFB) in Dayton, Ohio. He used the Articulate Total Body (ATB) software and determined the loads and torques at the neck/head and neck/torso joints. In all these studies the global rigid body dynamic response of the head and neck due to the accelerations were determined. In addition, the global loads and torques at the head joint, occipital condyle (OC), and the neck joints (C1-T1) were also determined. However, the local internal loads (stresses) on the vertebra, discs and endplates were not quantified. These lapses are the main subject of the preliminary studies of this research. In order to obtain local stresses in the vertebral bodies and intervertebral discs, the dynamic responses of the head and neck, determined by Sadegh (1995), were then used in a more detailed model. This could not be done using the articulated model. Furthermore, experimental studies on injuries have limited application due to the low tolerance limits of human volunteers. Even cadavers and mannequins are only subjected to near-tolerance limits and the attempt to recreate injury is rarely successful. In contrast, computer generated models, such as finite element models, have multiple usage and can be easily modified in term of material properties and boundary conditions during analytical analyses. There is therefore a need in creating finite element models that could be used to resolve the lapses of the articulated model and help close the gap that exists between low G amplitude in human-volunteer tests and the actual high acceleration to which pilots, passengers of automobile and sportpersons are subjected during the ejection process or accidents. A 3-D complete but simplified finite element model (FEM) of the cervical spine was then created to conduct the preliminary studies of this research and encouraging results were obtained regarding the stress in the cervical spinal components

as well as the response of the model to high (20 G-z) acceleration.

The secondary goal of this study was to simulate sport accidents and the effect of correction surgery after injuries or degenerations. Subsequently, an improved accurate and more detail cervical spine model was created. Degeneration in the cervical spine causes clinical conditions, which involve disc herniation or spondylosis. Cervical spondylosis denotes progressive changes in the spine that begin in the cervical intervertebral disc and extend to the surrounding bone and soft tissue (The Cervical Spine, 1998). Spondylosis could become symptomatic in the form of stenosis (narrowing of the spinal canal), myelopapathy (compression of the spinal cord), radiculopathy (pinching and irritation of the nerves) or myeloradiculopathy (compression of the nerves and spinal cord). The general problems associated with disc degeneration are physical narrowing of disc space, loss of normal intervertebral motion, and development of spondylotic osteophytes, neurologic dysfunction and chronic pain. The pain is usually caused by compression of the herniated disc material on the neural elements. Surgical treatment to correct degeneration involves the removal of the damaged disc material and its replacement by a different usually harder material (bone graft / implant). Disc removal is clinically known as discectomy, which is a surgical procedure that can be performed from the anterior or posterior side of the neck. This surgical alteration directly affects the biomechanics of the involved spinal components in particular and that of the cervical spine in general. Clinical studies revealed that up to 25 % of the patients that undergo surgical discectomy and fusion would have another operation at a different disc level within the decade following the first surgery. This long-term complication is clinically known as the adjacent level syndrome. The causes of the adjacent level

syndrome are many, and changes in motion and stress redistribution in the spine after discectomy and fusion are thought to be some of the factors that contribute to the long-term complication. Surgical procedures, used to correct injuries and degeneration, are in some cases similar. In addition, any surgical attempt to restore the spinal integrity after injury or degeneration is a mechanical alteration that would affect in many ways the function and movement of unaltered components in particular and of the cervical spine as a whole. Clinical studies on treatment of spine degeneration show good to excellent outcome of the surgery but the resulting changes in biomechanics and their long-term consequences on the rest of the structure are generally unevaluated. There is also, therefore, a gap between clinical outcome of the spinal surgery and long-term complications due to the modified biomechanics. Computer models again are appropriate means for closing this gap. They are reliable tools for analytical prediction of the dynamic and quasi-static responses of the neck and the head, for the simulation of accidents and surgeries. Literature review shows that 3D Finite Element (FE) models of the cervical spine that exist are mostly segmental models and are frequently used to study external responses. It is therefore highly desirable to develop multi-purpose models that can be used to predict the stresses and displacements of the cervical spine components under dynamic and quasi-static loadings. Such models could be altered to simulate surgeries and its effects on the biomechanics of altered spine. Such models can also be useful for predicting neck loads for passengers involved in automotive accidents or for sportsperson involved in sport accidents. It has been claimed that about two-thirds of all traffic fatalities involve injuries to the head and the neck. Other extended applications may include optimum design of fusion cages, car seats restrains or better training

methods.

Therefore, the hypotheses of the current research are:

1) The stresses in the intervertebral disc reach critical values before the onset of the translational and rotational displacements, of adjacent vertebrae, that lead to the clinical instability. That is, disc herniation and/or bulging occur before the clinical instability.
2) Segmental discectomy and fusion induces changes in stresses in neighboring discs of the cervical spine. These changes in stresses are non-linear and are directly related to the percentage of contact area between the bone graft and the vertebral body. There is an optimum percentage of bone graft and partial discectomy for each disc, an average of 20% – 60%, at which the changes in stresses in adjacent discs are less critical.

Objectives: The aims of this research are:

a) Use experimentally obtained data to gain insights into the global responses of the cervical spine when it is subjected to acceleration forces.
b) Create and validate an anatomically accurate and detailed FE model of the complete cervical spine column.
c) Simulate local contact and non-contact sport injuries that could lead to clinical instability and/or intervertebral discs injuries.
d) Simulate segmental partial discectomies and fusions with purpose of obtaining optimum percentage of contact area between the vertebral body and the bone graft.

The three-dimensional finite element models of the complete cervical spine will be used to attain the proposed objectives.

Dissertation outline:

This research consists of two major parts:

1) A background/ review part, presented in chapters 1, 2, 3, and 4.
2) An investigation/analytical part, presented in chapters 5, 6, 7, 8 and 9.

Following the introduction, chapter 1, a detailed anatomy of the cervical spine is presented in chapter 2. The literature review and the mechanism of cervical spine injuries are covered in chapters 3 and 4, respectively. Chapter 5 describes the first model and the preliminary study. This chapter also concludes the background/review part of the research.

The hypotheses of the study are examined in the second part of the dissertation and are covered in chapters 6, 7 and 8. An improved 3-D FE model and its validation are the subjects of the sixth chapter. Chapter seven tests the first hypothesis, which deals with Panjabi and White clinical instability criteria and their probable initiation of the intervertbral disc injury and instability. The second hypothesis, that correlates the change in stresses in adjacent discs, after discectomy and fusion, to the contact area between the bone craft and the vertebral body, is simulated in chapter eight.

For quick reference and convenience, the figures and tables of each chapter are directly shown following the corresponding chapter.

While each chapter has its own conclusions and discussions, a global summary concludes the dissertation in chapter 9.

2. ANATOMY OF THE CERVICAL SPINE

The modeling of the cervical spine is a tedious and complex task that requires a good knowledge of the anatomy of the neck. The modeling must take into consideration the complex geometrical and functional aspects of the spinal components and their interconnection and interaction.

The cervical spine is the superior part of the human spine column, Figure 2.1. It starts just below the head and ends at the top of the torso. It has a backward "C" shape (lordotic curve) in neutral position and is the most mobile region of the spine column. It consists of the first seven vertebrae (osseous components), C1-C7, Figure 2.1, Figure 2.2 and Figure 2.3. The vertebrae are connected by soft tissues such as the intervertebral discs, the facet joints and the ligaments. It carries the head and provides structural protection to the spinal cord and to the arteries that carry blood to the brain. In each area of the spinal cord, there are nerves, which connect to specific parts of the body. The nerve roots run through the bony canal, and at each level of the cervical spine a pair of nerve roots exits from the spine and go to the upper chest and arms. The nerves also carry electrical signals back to the brain. The major stability and the rotational function of the cervical spine are provided by major ligaments and muscles. Damage to the soft and hard tissue can lead to pain, dysfunction or impairment. Abnormal compression on the nerves, nerve roots, or spinal cord can lead to symptoms such as pain, tingling, numbness and weakness. A detailed description of the anatomy of the individual cervical spine components is presented below. It is collected from a variety of studies and publications on the human anatomy (de Jarger et al. 1994, Hukins 1988, Kleinberger et al. 1993, Woodburne 1982, Yoganandan et al. 1987, Malanga et al. 2002).

2.1 Anatomy of the cervical vertebrae

There are two atypical vertebrae in the upper region, Figure 2.3 of the cervical spine: the atlas (C1), see Figure 2.4, and the Axis (C2), see Figure 2.5. Their uniqueness in form and shape has both physiological and biomechanical importance. The atlas has the primary function of supporting the weight of the head. The atlas and the axis are especially critical to the overall mobility of the head and the neck. About one half of the flexion /extension movement is provided by the atlanto-occipital articulation and about one half of the neck rotation takes place between the altas and the axis.

The atlas (C1), see Figure 2.4, is unique among vertebrae in that it does not have a vertebral body. Its vertebral body is absorbed into the formation of the axis during the skeletal development process. Its other particularities are that it does not have a spinous process is ring-like, and consists of an anterior and posterior arch and two lateral masses. On the superior aspect of the lateral masses are the upward and inward facing kidney-shaped articulations that support the occiput. The inferior facets are flatter and face downward and inward to transmit the weight of the skull onto the superior facets of the Axis (C2). The posterior arch of the atlas corresponds to the lamina of the other vertebrae**.** The anterior arch forms about one-fifth of the ring: its anterior surface is convex and presents at its center the anterior tubercle for the attachment of the Longus colli muscles; posteriorly it is concave, and marked by a smooth, oval or circular facet, for articulation with the odontoid process (dens) of the axis. The upper and lower borders, respectively, give attachment to the anterior atlantooccipital membrane and the anterior atlantoaxial ligament. The atlantooccipital membrane connects the atlas with the occipital bone above, and the atlantoaxial ligament with the axis below.

The second vertebra (C2), see Figure 2.5, is named the axis because it forms the pivot upon which the first vertebra (C1), carrying the head, rotates. The most distinctive characteristic of this vertebra is the strong odontoid process (dens), which rises perpendicularly from the upper surface of the body. The body is deeper in front than behind, and prolonged downward anteriorly so as to overlap the upper and fore part of the third vertebra. It presents in front a median longitudinal ridge, separating two lateral depressions for the attachment of the longus colli muscles. Its under surface is concave from the front backward and convexe from side to side. The dens or odontoid process exhibits a slight constriction or neck, where it joins the body. On the anterior surface of the dens is an oval or nearly circular facet for articulation with the facet on the anterior arch of the atlas. On the back of the neck, and frequently extending on to its lateral surfaces, is a shallow groove for the transverse atlantal ligament, which retains the process in position. The odontoid ligament and the alar ligaments connect the process to the occipital bone. The inferior surface of the axis resembles those of the typical vertebrae (C3-C7) in the mid- and lower cervical spine. The laminae of the axis are heavy and strong. Because of its thick transverse processes the axis gives attachment to the longissimus cervicis, splenius cervicis and other major muscles. The superior articular facets are large and slightly convex, and face upward and outward to articulate with the inferior facets of the atlas vertebra.

There are five typical vertebrae of cervical spine (C3-C7) located in the mid- and lower cervical spine regions. The bony anatomy of these regions shows minimal variations in dimensions, except at C7, where there is a transition between the cervical and thoracic spine. Typical vertebra**,** see Figure 2.6**,** comprises a vertebral body, pedicles,

laminae, lateral masses, an arch and several processes for muscular and ligament attachment and articulation. The vertebral body supplies the strength and carries about two thirds of the vertebral load (Kleinberger et al. 1993). It is geometrically and physically concave on its superior surface. It is correspondingly convex on its inferior surface. The pedicles project posterior-laterally from the vertebral bodies and attach to the lateral masses. The laminae project postero-medially from the lateral masses and join in the midline. The pedicles, the lateral masses and the laminae together form the vertebral arch. The vertebral arch encloses the vertebral foramen, which combines with the foramen at adjacent levels to form the spinal canal. The spinous process projects posteriorly from the junction of the lamina. The lateral mass forms at the junction of the lamina and pedicle and gives rise to the superior and inferior articular facets. The superior facet at each level faces upward and posteriorly; the inferior facet faces downward and anteriorly.

2.2 Anatomy of the soft tissues

2.2.1 Intervertebral disc

The intervertebral discs are interposed between the adjacent surfaces of the bodies of adjacent vertebrae from between the second (C2) and the third (C3) vertebrae to the sacrum. They form the major bonds of connection between the vertebrae. They vary in shape, size, and thickness, in different parts of the vertebral column. Their shape and size correspond with the surfaces of the vertebral bodies between which they are placed except in the cervical region where they are slightly smaller from side to side than the corresponding vertebral bodies. Intervertebral disc are thicker in front than behind in the

cervical region, and thus contribute to the anterior convexities of this part of the spinal column. The intervertebral discs constitute about one-third to one-fourth of the length of the spinal column. The cervical and lumbar portions have in proportion to their length a much greater amount of disc material than the thoracic region. The cervical and lumbar therefore parts possess greater bending capacity and larger range of motion. The intervertebral disc has a distinctive structure. It is a fibro-cartilaginous joint that primary creates shock-absorbing pads/cushions between the bodies of adjacent vertebrae. At birth, about eighty percent of the disc is composed of water. With age, the discs dehydrate and become stiffer. A normal disc, see Figure 2.7, is composed of two parts: the outer fibrocartilaginous annulus fibrosos and the gel-like central nucleus pulposus. The fibrous ring of the annulus consists of up to 20 concentrically arranged fiber lamellae and fibrocartilage component. The fibers pass obliquely from the vertebral body above to that below and are arranged in a helicoids manner. They alternate in diagonal direction in successive concentric rings, and are oriented at about 30 degree to the plane of the disc. The alternate arrangement of the fibers makes the annulus and thus the intervertebral disc less resistant in torsion and shear because only haft of the fibers are stretched when the disc is loaded in this mode. The inner one-third of the lamellae of the annulus is attached to the cartilage endplates to form a vessel enclosing the pressurized nucleus. In contrast, the outer two-third of the lamellae is attached to the vertebral bodies. These structural and functional arrangements allow the fibers to be stretched directly when one vertebra moves relative to another during rotating and bending movements. Even minor injury damage to the disc may start a cascade of events that leads to degeneration. To the contrary of many soft-tissue, a damaged disc cannot repair itself because it has very few

nerve endings and no blood supply. Consequently pain created by the damaged disc can last for years.

2.2.2 End-plates

The cartilaginous endplates are the superior and the inferior thin layer surfaces of the intervertebral discs. They are the transitional elements between the intervertebral disc and the vertebral bodies, and they serve as semi-permeable membrane that facilitates the diffusion of solutes from the vertebra to the disc. The endplates are approximately 1 mm thick and are mainly composed of hyaline cartilage, which consist of a gel reinforced by collagen fibrils. In contrast to the articular cartilage, which is also made of hyaline cartilage, and which is firmly attached to the subchondral bone by its collagen fibrils, the end-plates do not have direct collagenous connection to the bone of the underlying vertebral bodies.

2.2.3 Facet Joints

Each vertebra articulates with the one above and below through the zygapophysial (facet) joint. The facets have different orientations at different parts of the spine. In the cervical spine the facets are oriented at about 45 degrees in the horizontal plane, see Figure 2.8. This orientation allows for flexion, extension, and a much larger amount of rotation, and side bending. The facets are surrounded by cartilage (joint capsule) that is innervated and capable of producing pain. The facet surfaces are covered with articular cartilage and the gap between the cartilages is filled with synovial fluid bounded by thin synovial membrane. The joint is enclosed by capsular ligament. The facet joints transmit about 30% of the external load (Kleinberger et al. 1993) and they guide the motion of the

cervical spine by allowing the sliding and rotation actions between the superior and inferior facets, see Figure 2.8.

2.2.4 Ligaments

Ligaments, see Figures 2.9 A and B, provide stability, absorb energy during trauma and act as a joint position transducer during physiological motions. While cervical ligaments along with paracervical muscles prevent motion, between vertebrae, that might injure the spinal cord or nerve roots, (Malanga et al. 2002), ligaments with the intervertebral discs form the primary static stabilizers of the cervical spine**.** A detail description of the major spinal ligaments is given in the subsequent paragraphs.

The anterior longitudinal ligament (ALL) is a broad and strong band of fibers, which extends along the anterior surfaces of the bodies of the vertebrae, from the axis to the sacrum. It progressively becomes wider as it runs through the spinal column. It is thinner and narrower in the cervical in comparison to the lower regions of the spine. Its superior section is attached to the body of the axis (C2) and its inferior section is attached to the upper part of the front of the sacrum (S1-S5). It consists of dense longitudinal fibers, which adhere to the intervertebral discs and to the prominent margins of the vertebrae, but not to the middle parts of the bodies. It is made up of three layers of fibers, which vary in length, but are closely interlaced with each other. The most superficial fibers are the longest and extend between four or five vertebrae. A second, subjacent set extends between two or three vertebrae while a third set, the shortest and deepest, reaches from one vertebra to the next.

The posterior longitudinal ligament (PLL) is situated within the vertebral canal, and extends along the posterior surfaces of the bodies of the vertebrae. Similar to ALL, PLL extends from the body of the axis (C2), with the membrana tectoria, to the sacrum (S1-S5). Like the anterior longitudinal ligament, it is narrow and thin in the cervical. It is attached the same way as the anterior longitudinal ligament to the discs and vertebrae. This ligament is composed of smooth, shining, longitudinal fibers, denser and more compact than those of the anterior ligament, and consists of superficial layers occupying the interval between three or four vertebrae, and deeper layers which extend between adjacent vertebrae. The posterior longitudinal ligament (PLL) is not as strong as the anterior longitudinal ligament (ALL) but it is thick in its central portion, which helps prevent a herniated disk from pressing directly on the cord posteriorly.

The ligamentum flavum (LF) consists mainly of elastic fibers and connects the inferior and superior aspects of adjacent lamina and neural arches. It is a stronger ligament and it helps to restrain hyperflexion. The ligamentum flavum becomes shortened and thicker in hyperextension and elongated and thinner in hyperflexion. During hyperextension, it may protrude into the cervical canal as much as 3.5 mm. Impingement on the spinal cord during extension normally is prevented by the mechanical properties of the ligament; however, hypertrophy of the ligamentum flavum or loss of mechanical properties (e.g., modulus) through degeneration may lead to canal narrowing or cord impingement (Malanga et al. 2002).

The capsular ligaments (CL) surround the articular facets of adjacent vertebrae. They are oriented approximately orthogonal to the articular facets and provide maximal

mechanical efficiency in resisting distraction of the facets but relatively poor resistance to shear. They are short and strong fibrous structures that contribute to posterior stability and allow vertebrae to slide and rotate with respect to each other. They offer maximal mechanical resistance to flexion distraction but relatively poor resistance to rotation distraction.

The interspinous ligaments (ISL) are found between the processes from the ligamentum flavum to the tip of the process. They are not as well developed in the cervical region as in other regions of the spinal column, but nevertheless they allow the application of a significant flexion-resisting force to the spine.

The alar ligament (ARL), the transverse ligament (TRL) and the atlantodens (AD) ligament control the articulation and connection between the head, the atlas and the axis vertebrae, see Figure 2.10.

The alar ligaments (ARL) mainly restrain the rotation of the head. They originate from the posterolateral aspect of the dens of C2 and insert on the medial surfaces of the occipital condyles. Alar ligaments are stretched the most when the head is rotated and flexed together, and they are relaxed during extension.

The transverse ligaments (TRL) hold the odontoid process of C2 against the anterior ring of the atlas, the transverse ligament functions as a restraining band on the dens. Flexion and anterior displacement of the atlas is restrained by its orientation. The anterior aspect of the transverse ligament acts as the pivot about which C1 rotates.The

anterior atlantodens ligament is an unusual ligament that connects the base of the dens to the anterior arch of the atlas.

2.2.5 Muscles

Muscles are the major dynamic stabilizers of the neck. They also protect the vertebrae, carry loads and produce motion. The motion of the head occurs by means of complex interaction between the hard and the soft tissues of the neck. Muscles play a very significant role in this interaction by controlling and adding to the stability of the neck. Neck muscles can be grouped according to their anatomical arrangement, (point of origin, point of insertion, prevertebral, postvertebral, posterior, anterolateral) or in terms of their structural contribution to the movement of the neck. Individually or collectively, muscles act to produce tension, flexion, rotation and lateral bending. The major muscles of the neck are given in Table 2.1 with the type of motion they controlled and their insertion point. An illustrative arrangement and attachment of the muscles is shown in Figure 2.11.

The explicatory Figures and tables related to this are shown next. A broad review of the experimental and analytical studies that are relevant to the current study is presented in the upcoming third chapter.

2.3 List of figures and tables

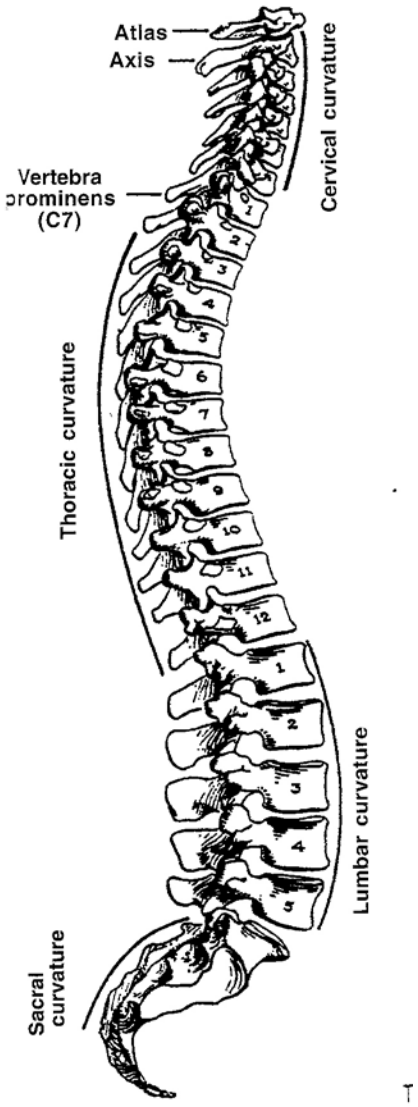

Figure 2.1: The human spinal column, lateral view of sagittal plane

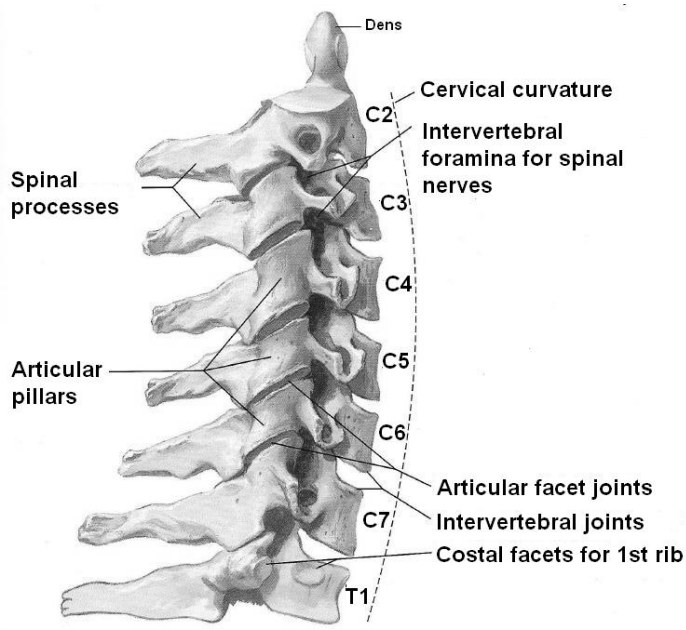

Figure 2.2: Cervical spine (C2-T1), lateral view

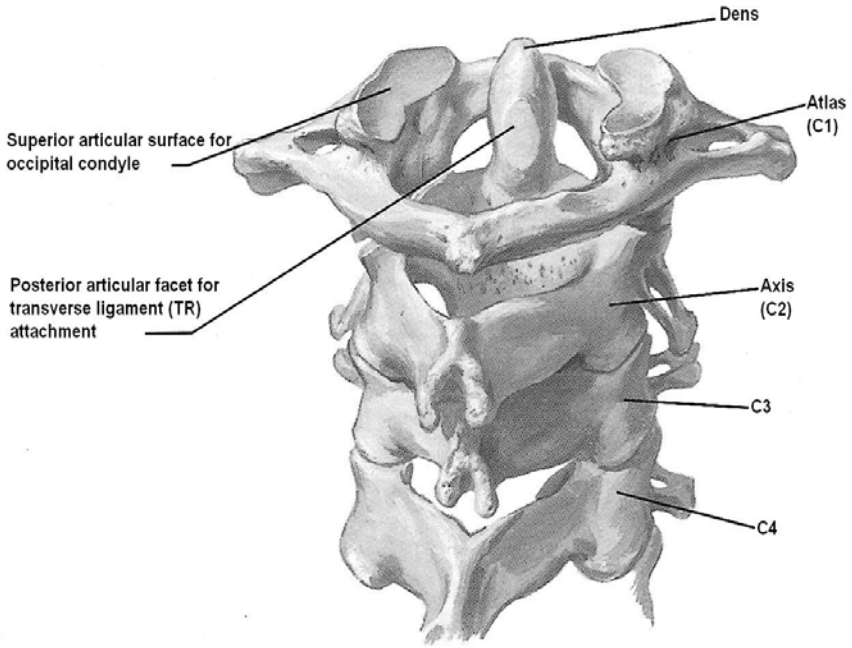

Figure 2.3: Assembly of upper cervical vertebrae (C1-C4), posterior view

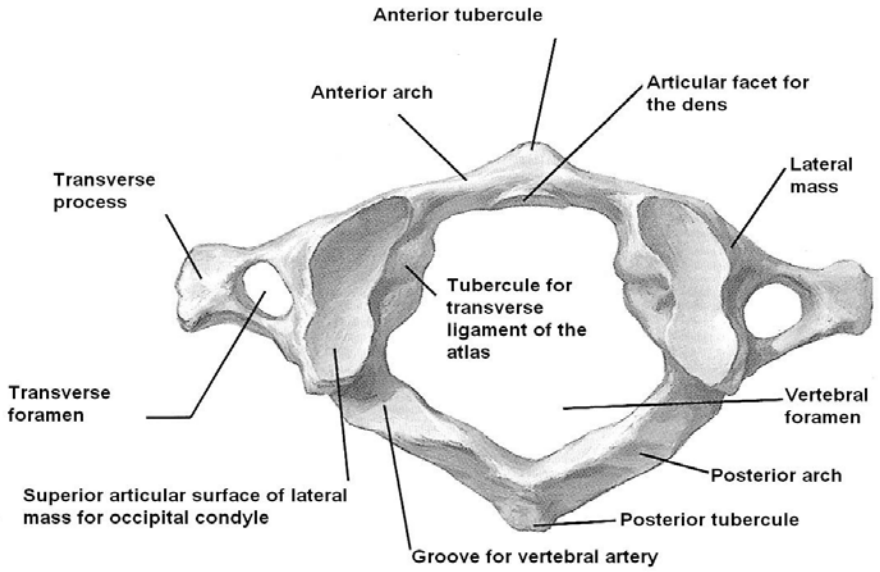

Atlas (C1): Superior view

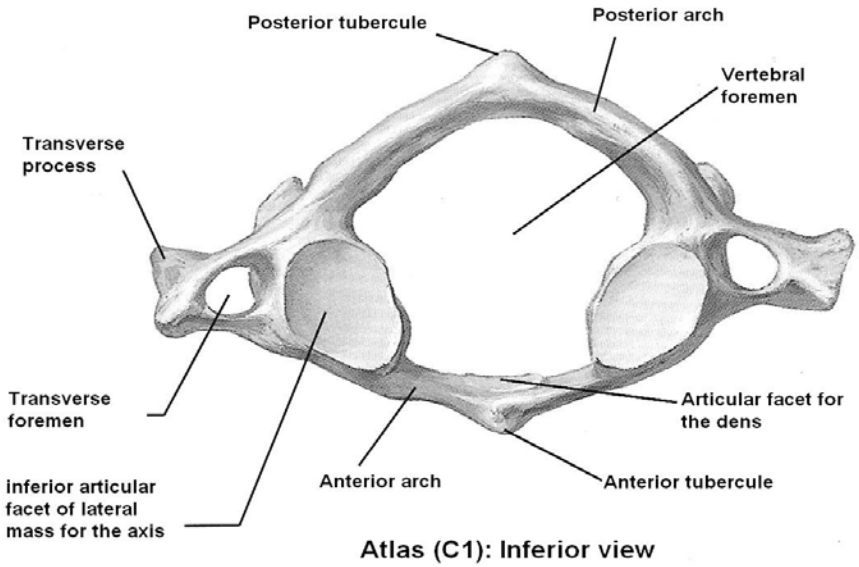

Atlas (C1): Inferior view

Figure 2.4: The atlas vertebra (C1)

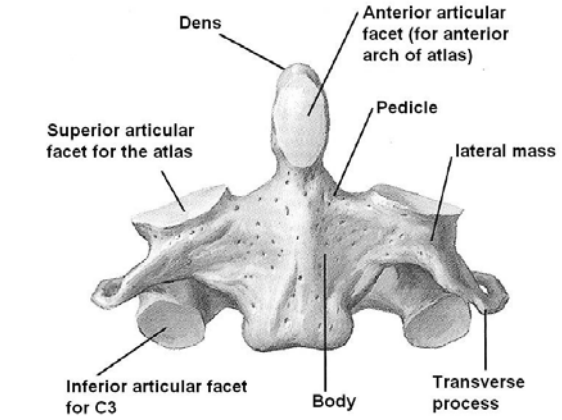

Figure 2.5: The axis vertebra (C2)

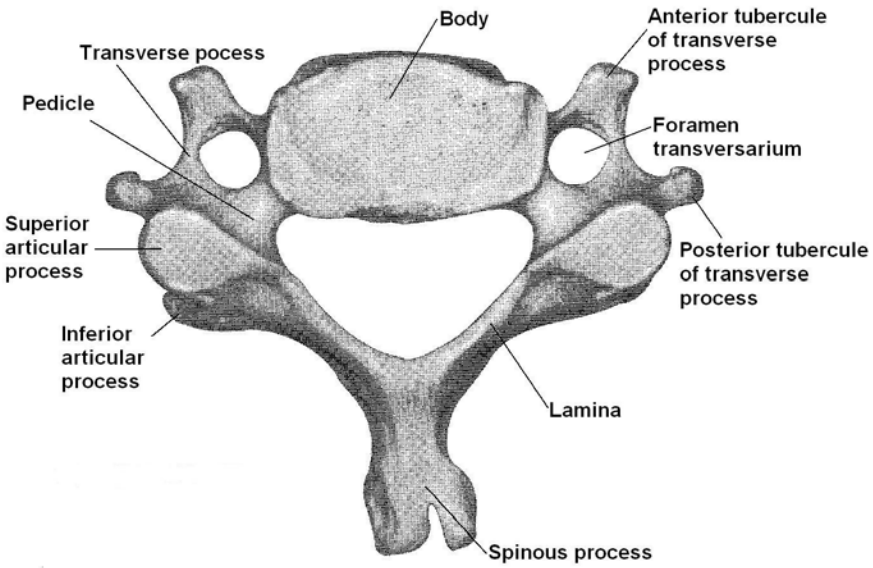

A

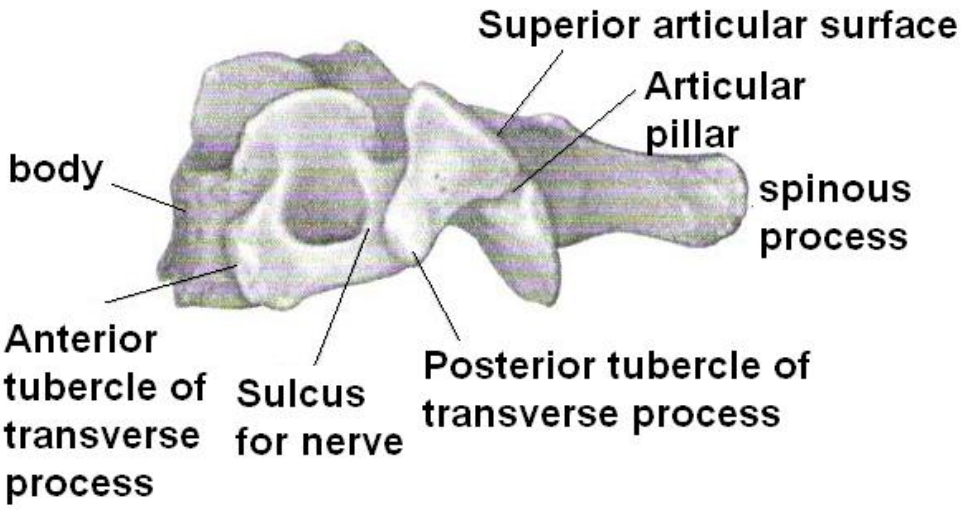

B

Figure 2.6: Typical vertebra; A: top view, B: lateral view.

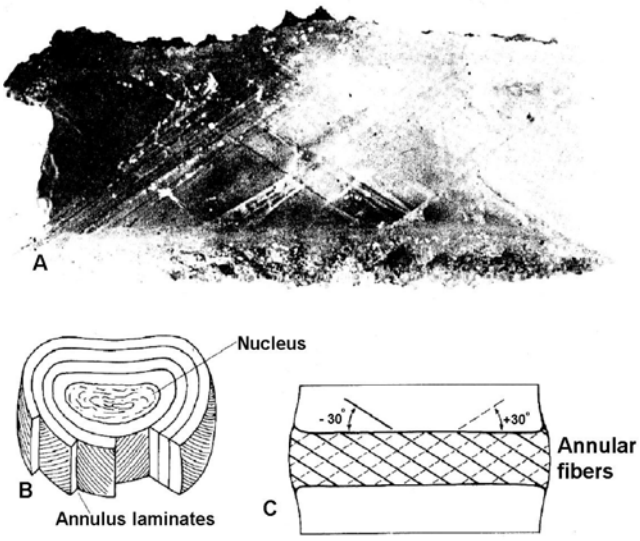

Figure 2.7: Intervertebral disc, (Shirazi et al. 1986)

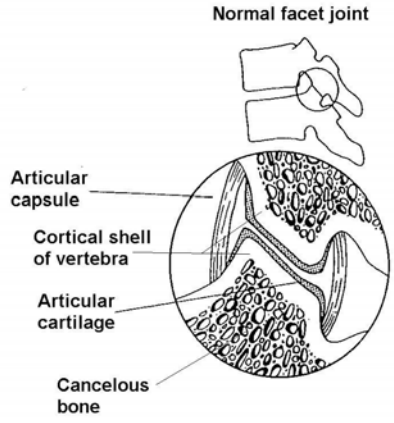

Figure 2.8: Articular facet joint detail, (Kumaresan, 1997)

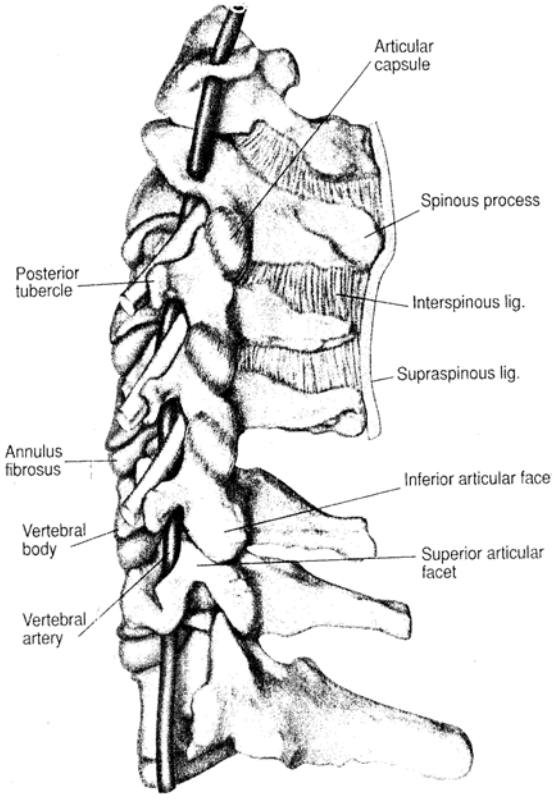

Figure 2.9A: Lateral view of ligaments, (The cervical Spine, 1998)

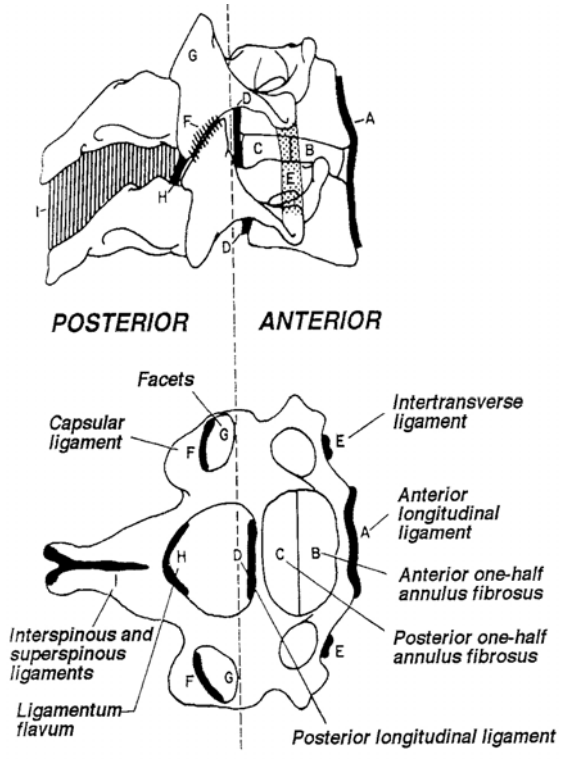

Figure 2.9B: Schematic diagram of the ligaments, (The cervical Spine, 1998)

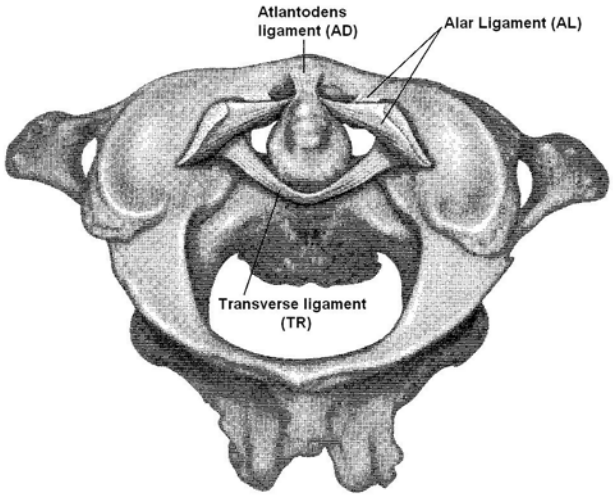

Figure 2.10 : Ligament of C1-C2 assembly

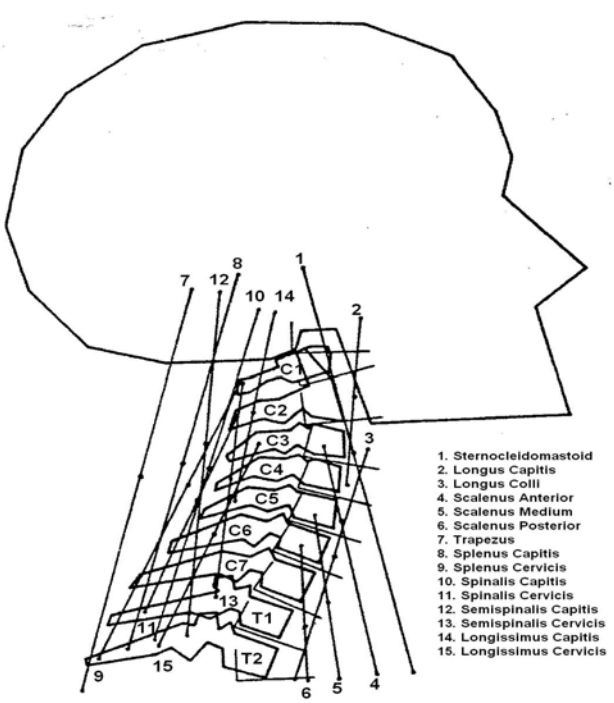

Figure 2.11: Parametric muscles model of Deng and Goldsmith (Deng et al. 1987)

Muscle	Neck motions produced (main)	Insertion points	Ultimate tensile strength
Sternocleidomastoideus	E, F, R, LF	C2 and C7	0.2 – 0.6 MPa (passive) (Katake, 1961) 0.4 – 1.0 MPa (active) (Fick, 1910)
Longus capitis	F,	Co to C3 to C6	
Longus colli	F, R, LF	C1, T3or T4	
Scalenus anterior	R, LF	C3 , upper T	
Scalenus medius	R, LF	C5 , upper T	
Scalenus posterior	R, LF	C6, upper T	
Trapezius	E,	C0, upper T	
Splenus Capitis	E, R, LF	C0, T2	
Splenus cervicis	E, R, LF	C0, T2	
Spinalis Capitis	E	C0, T2	

Table 2.1: Major cervical muscles (*E: extension, F: flexion, R: rotation, LF: lateral flexion).*

3. REVIEW OF LITERATURE

Experimental and analytical studies on the biomechanics of human cervical spine are important and challenging enterprises that can have multiple clinical applications. Numerous analytical and experimental models of the cervical spine have been studied with the purposes of explaining the interaction between the spinal components and the mechanisms of injuries. Experiments on cadaver's necks have been performed on intact spine with or without head and on spinal components such as vertebrae, discs and ligaments. Experimental and clinical studies on the strength and stiffness of the cervical spine column and its individual components are also well documented.

The following literature review is a selection from a large bibliography. They are grouped into two categories: 1) finite element models, and 2) experimental studies, including static and dynamic. A brief summary is given at the end of each category.

3.1 Finite element models:

Several finite element models have been created for the study of the cervical spine. The earliest models were developed to study pilot ejection, head impact and acceleration (Williams and Belytschko, 1983, Deng and Goldsmith , 1987). These models were articulated models that lacked finite element geometry and material details. The first detailed finite element model of the cervical spine did not appear until the beginning of the 90's (Gilbertson et al. 1995). Interest in this area has grown since then, and more models have been created to study the local and global external and the internal responses of the cervical spine.

Dietrich et al. (1991) made the first attempt to duplicate the geometry of the cervical spine. Using the geometry data from a cadaver, the authors were able to create a 3-D finite element model composed of vertebrae C3 through L5. The model included the ribs, muscles and ligaments. The intradiscal pressures and the muscles stresses were reported for the thoracolumbar spine, but no results were given for the cervical spine section.

Saito et al., 1991 created a detailed 2-D model of the cervical spine to investigate the effect of postlaminectomy deformities in young and old patients, (Figure 3.1). The model was made of the base of the skull and the vertebrae C1 trough T2. Four interconnected slice regions in the sagittal plane were considered. The first slice region incorporated the cancellous core of the vertebral body, the endplates, the discs, the laminae, the spinous processes and all the relevant ligaments. The second slice contained the cortical shell of the vertebral body and the articular facets. The third slice contained the transverse process and the intertransverse ligaments, and the fourth slice incorporated the cortex of axis (C2) and the lower part of the cranium. The model was completely constrained at the base of T2 and one point on the cranium was allowed to move in the cranial caudal direction only. The model was then repeatedly loaded with a 150 N to cause gradual deformity. The authors concluded that, depending on the load location, clinically observed postlaminectomy spinal deformity could be reproduced by the finite element model.

Kleinberger (1993) developed a 3-D finite element model of a human cervical spine to study the mechanics of injuries related to automotive crashes. The preliminary model

consists of two identical cervical vertebrae (C5), an intervertebral disc and the major ligaments. The complete cervical spine model was then created by replicating and stacking the preliminary model. The vertebrae were aligned with an appropriate lordosis. The intervertebral discs and the facet joints were then created by filling in the space between adjacent vertebrae body (Figure 3.2). The model was validated using a small strain axial compression test. The total compressive displacement was –1.545 mm, which yielded an axial stiffness of 161.8 N/mm. The author used the model to investigate the large strain response of the neck, by applying a forced axial displacement of 10 mm at C1. The results showed that 7.7 mm of the displacement was carried by the compression of the discs and the bending of the cervical column carried 2.3 mm. It was also noticed that the maximum shear displacement occurred between the C2 and C3 vertebrae. The author also used the model to simulate an 8 G frontal crash sled test and the results revealed that the head rotation lags behind the neck rotation by about 12 degrees.

Bozic et al., 1994 generated a complex and inhomogeneous model of a mid-cervical vertebra (C4) to predict regions of high risk in vertebra during compressive loading (Figure 3.3). The model was automatically generated using quantitative computed tomography (QCT) image of the C4 from a 66-year old male. The material properties of the cortical and cancellous bone were assigned based on the CT scan apparent density. Series of springs of different stiffness located at the superior and the inferior endplates of the vertebral body were used to transmit the loading. The model was subjected to 4 mm axial compression, which generated 3400 N. The authors assumed the shear stress failure criterion. They obtained higher shear stresses (0.5 to 0.8 MPa) in the cancellous core and

concluded that the regions of safety as determined by their model overlapped the fracture lines as frequently discovered clinically in a typical burst fracture. This was model a single vertebra model that lacked ligaments, facets and disk and therefore had very limited extension and applications.

Dauvilliers et al., 1994 developed a complete ligamentous cervical spine and head model to predict neck injury under frontal and lateral loading conditions. The model included vertebral bodies with flat superior and inferior surfaces, identical angle for all the facets and the relevant ligaments (Figure 3.4). The validation of the model compared the computed head displacement and rotation with human volunteer data. No internal response was reported. The model lacked accuracy and some anatomical details of the components, and therefore can only be used for limited applications in basic biomechanics of cervical spine.

Teo et al., 1994 modeled a human axis (C2) to investigate likely sites of failure under prescribed loading. A coordinate measuring machine (CMM) was used to extract the geometry data of the vertebra. The vertebra was assumed symmetrical about the sagittal plane. The CMM was used to digitize in sequence haft of the periphery at each cross-section and at pre-detected points. The stored geometric data were then transferred as input note to the finite element program to generate the solid model. The material properties of the cortical bone were assumed for the solid model. The soft tissues (ligaments and disc) were represented by incorporating spring elements. The analysis was performed by assuming an arbitrary force of 5 KN distributed over a 50 mm^2 area of the anterior surface of the dens. The force was oriented in the anterior posterior direction at

an angle of 45°, 0° and – 45° degree. These angles represented different frontal impact situations. The results of the analysis showed that the stress distribution in the vertebra depended on the direction of the impact force. The authors also observe that the location of the higher stresses agreed with clinically observations of recorded fracture locations. This was a simplified single vertebra model with very limited applications.

Yoganandan et al., 1996 used 1.0 mm CT slices to develop the first most anatomically correct model of the C4, C5 and C6 vertebrae (Figure 3.5) Eight-node brick elements were used to generate the cancellous bone. Two-node cable elements were used for the ligaments and four-node shell elements were used for the cortical bone and the endplates. The model lacked some details at the disc levels. The discs were represented as continuum material and the facets are assumed to be 3-D solids. The validation was done in axial compression and compression flexion using the experimental data from a complete cadaver model of the cervical spine.

Clausen et al., 1996 developed an anatomically accurate and detailed multipurpose finite element model of the C5-C6 motion segment (Figure 3.6). The model included the two vertebrae, a composite disk and all the articulations. The authors used 1.5 mm transverse CT slices of a disease-free cervical spine. The finite element mesh was manually constructed to accurately capture the complex structures of the cervical vertebra. This model was the first model that has been thoroughly validated in all modes of loading. Three validations were conducted. The first and the second validation carried a 76.3 N axial compression load and a moment of 1.6 Nm and 1.8 Nm, to mimic flexion extension,

axial rotation and lateral bending respectively. The third validation predicted the motion of the intact cervical spine motion. This was compared to the experimentally obtained data of 17 cervical spines in response to primary and coupled motions. The model could be used to study fracture mechanics and the effect of various surgical procedures.

Nitsche et al., 1996 created a 3-D finite element model of the neck to study flexion, lateral bending and compression (Figure 3.7). The geometrically simplified model included all the important components of the cervical spine. The disc and the facets were modeled as homogeneous solid elements. The model was validated by comparing the computed condyle displacement with the human volunteer data. The model was completely fixed at the base of C7 for the analysis. Three loading cases were considered: 15 G flexion, 7 G lateral flexion and 5 kg compression. This model lacked accuracy and anatomical details, which limit its application.

Maurel et al., 1997 created a parameterized 3-D finite element model of the mid- and lower-cervical spine to study the effect of the facet joint geometry on its biomechanical response (Figure 3.8). The geometrical data were obtained using a spatial measuring machine. The geometry details were generated to fit regular geometry shapes. The model contained cortical shell, cancellous core, the endplates, composite discs, and the major ligaments. The model was restrained at the base of C7 and four moments of 1.6 Nm simulating lateral bending, flexion extension and axial torsion were applied to C3. The authors computed the principal and the coupled motions for various facet angles and concluded that the orientation of the facets governed both the principal and the couple

motions. No internal results were given. The model included more motion segments and used good material properties for the discs. This is a very good model for clinical and basic biomechanics applications.

Sadegh et al., 1997 created a simplified complete, and an articulation 3-D finite element models of the cervical spine to investigate its internal responses under dynamic load (high G-y acceleration) (Figure 3.9). The solid model of the vertebrae was created using anatomical dimensions (Cervical Research Society). The disc and the vertebrae were assumed isotropic, mono-material. The facet joints, the ligaments and two main muscles were simulated using beam elements. Elastodynamic analysises were performed for different G-y accelerations (8 to 20 G-y). The results indicated that the maximum stress increased sharply as the magnitude of the acceleration increased. The stresses in the 10 to 12 G-y cases were below the threshold of injury. The maximum stresses occurred in C6 and C4 regions. The model lacks some geometrical and anatomical details and has therefore limited clinical and biomechanics applications.

The summary of the FE models reviewed here is given in table 3.1. These models are either single vertebra and motion segments or simplified three-dimensional models. Four of them are complete 3-D finite elements models, (Kleinberger's, Dauvilliers', Nitsche's and Sadegh's). But all the four have oversimplified geometry and/or material properties. The results obtained from single vertebrae and motion segments models do not adequate convert the global, internal as well as external, responses of the complete cervical spine. In the reviewed models, either some soft tissues were missing or the

transfer of physiological boundary conditions and their effects were not simulated. Detailed and anatomical correct 3-D complete models offer better insight and will simulate the physiological situations realistically. There is a clear need for such models, and in light of the first objective of this research, two complete 3-D anatomical correct and detailed cervical spine FE models have been developed and utilized to simulate accidental injuries and partial discectomies and fusion.

INVESTIGATOR	MODEL & ANALYSIS	APPLICATION	LOAD	RESPONSES
Saitoet al. 1991	Occiput to T2, 2-D Linear static	Laminectomy Deformity	150 N, axial load, applied 14 times	Principal stress, Axial response
Kleinberger 1994	C1 to C7, 3-D Linear static & Dynamic	Automotive crashes	10 mm axial compression 8 G frontal impact	Displacement, change in velocity
Bozic et al. 1994	Single vertebra, C4, 3-D Linear static	Predict regions of high stresses, fracture	4 mm axial compression 3400 N resulting force.	Normal and shear stress.
Dauvilliers et al. 1994	Head to C7, 3-D Linear static & dynamic	Predict neck injuries under frontal and lateral loadings.	G-x, G-y and G-z accelerations	Head displacement and rotation.
Teo et al. 1994	Single vertebra, C2, 3-D Linear static	Investigate site of failure under prescribed load.	1000 N over 50 mm^2 at –45, 0 and +45 degrees	Normal stresses
Yoganandan et al. 1996	C4 to C6, 3-D Linear static	Axial compression and flexion bending	10 mm forced displacement	Maximum stress
Clausen et al. 1996	C5-C6, 3-D Non-linear static	Load sharing mechanism	74 N compression 1.8 Nm flexion extension, lat. Bend. and axial torsion.	Internal reaction, force
Nitsche et al. 1996	C1-T1 Linear static and dynamic	Compression flexion, lateral bending	15 G flexion. 7 G lat. Bending 5 Kg compression	Occipital Condyle displacement.
Maurel et al. 1997	C3-C7, 3-D Nonlinear static	Effect of facets orientation	1.6 Nm flexion extension, lateral bending and axial torsion.	Primary and coupled motions
Sadegh et al. 1997	C1-C7, 3-D Linear static, dynamic	Predict neck stress in high g-y acceleration	4 to 10 G-y	Maximum stresses in vertebrae

Table 3.1: Summary of finite element models

3.2 Static and Dynamic Experimental Studies

Investigations on vertebral segments and or complete cervical columns, with and without the presence of ligaments, have been an area of intense research aimed at determining the strengths of the cervical spine components under static and dynamic loads. The experimental studies reported here include the testing of spinal components such as the vertebrae, discs, ligaments or intact spinal columns.

Mckenzie et al., **1971** used a discrete-parameter model of the head-neck-torso to investigate the whiplash problem. They applied a 5 G acceleration at the base of the seat and observed that initial flexion of the head relative to the torso occurred prior to hypertension. The maximum values of loadings in the cervical spine area of the model were in the low cervical region and were reached during the hyperextension motion. Some of the important conclusions in this study were that flexion of the head is the first motion to occur during a rear impact, and low impact accelerations could lead to near critical head acceleration.

Panjabi et al., 1978 created an in vitro laboratory model of the “stretch test”. They induced injury to the soft components of motion segments and analyzed their change in motion as a function of the applied load and the transected spine component. They used four cervical spines for the experiment. Loads were applied in an increment of 5 kg until about 1/3 of the body weight was reached. The results indicated that failure takes place when at least all of the anterior ligaments or all of the posterior ligaments and two other

anterior components have been transected. The changes in the anterior disc space height at the beginning of failure ranged from 1.1 to 7.1 mm for a load of 7.5 N.

Kabo et al.,1983 tested a geometrically equivalent, reproducible and mechanically representative model of human neck system. They studied the disc pressures and the inter-cranial responses to transient sagittal pendulum type plane loading. Peak intradiscal pressures occurred at C5/C6 level and the second maximum at C7/T1. The authors observed that rear impacts to the head generally induced higher amplitude acceleration of shorter duration than frontal impacts of the same initial energy.

Yoganandan et al., 1986 conducted experimental studies of cervical spine to investigate the mechanisms of spinal injuries. They used vertical impacts in cadaver biodynamic analysis. Some of the specimens were restrained and loaded with forces ranging from 3000 to 7000 N. The unrestrained specimens were loaded with forces ranging from 9800 to 14600 N. For restrained subjects, injuries occurred in six of eight specimens. And for unrestrained subjects, injuries included compression fracture of C3, bilateral locked facets and fracture of the odontoid. The compressions ranged from 2 to 4 cm. The authors found that intervertebral discs compressed substantially during dynamic loading.

Deng and Goldsmith, **1987** studied the response of the human head/ neck/ upper-torso and its response to impact and dynamic loading. They used a water-filled skull, plastic vertebrae, sternum and ribs, silicon rubber discs and ligaments, and fabric muscles. The head acceleration, the disc pressures, the muscles strains, the inter-cranial pressures and the skull strains were measured. The results showed that the head deceleration time was

150 ms for extension whiplash and 400 ms for flexion whiplash. The disc pressure increased during flexion and decreased during extension. The maximum pressure changes were recorded in the disc between C4 and C5 for flexion and extension whiplash and in the disc between C3 and C4 for lateral whiplash.

McElhany et al., 1988 studied the bending responses of umembalmed human cervical spine segments. They reported that the maximum failure moment ranged from 3.4 to 14.6 Nm, and the maximum axial force was between 192 and 388 N.

Pintar et al., 1989 conducted a detailed analysis of alterations of cervical spine under compressive loading and observed that the upper cervical spine injuries occurred under compression-extension and lower cervical injuries occurred under compression-flexion modes. The compressive load ranged from 1355 to 3613 N, and the displacement was between 9 and 37 mm.

Luo et al., 1991 investigated the human response to impact loading and the resulting potential damage. They used 3-D lumped-parameter system of rigid bodies to monitor the head and the thoracic reactions, the intervertebral disc pressures, the muscle elongations and some internal organ pressures. Loads were applied by deceleration from a given velocity that occurred due to the impact of the sled with a fixed aluminum block. The model predicted simulated measurements on volunteers subjected to impulsive loading for time up to 200 ms. The measurements showed that thoracic loads and motions, disc pressure, internal organ pressure and muscle strains changed significantly.

Pintar, 1990 studied the biodynamic of cadavric cervical spine with the aims to reproduce clinically relevant cervical spine injuries under controlled conditions. The peak actuator forces ranged from 5856 to 19205 N, which created distal forces in z-direction ranging between 1586 and 6193 N. The resulted head acceleration was between 281 and 489 g. The author was able to reproduce compression and compression-flexion types of fracture.

Shea et al., 1991 conducted a study to determine the biomechanical properties along the human cervical spine. They investigated the mechanism of injuries for sagittal plane loadings using 18 fresh human cadavers. The hypotheses were that differences in stiffness exist between mid- and lower cervical spine and the initial orientation of the spine and in particular spine rotation reduce the threshold of injury for flexion-compression loading. The authors applied forces to specimens that were flex to 33 degrees. The results showed that at up to 300 N axial force, all specimens were significantly stiffer in compression than in tension. The authors also applied 150 N shear force and noticed no significant difference between the posterior and anterior shear. Further test revealed that at a moment of up to 5 Nm there was minimum difference between flexion and extension.

Yoganandan et al., 1994 while trying to quantify the biodynamic response in terms of the continuous localized motions of various cervical spine components and correlating the biodynamic with the injury pathology, found out that at dynamic loading rates (1.8 -

5.1 m/min), mid and lower cervical spine injuries consistently occurred. The mean maximum load recorded was 3983 N, the corresponding axial compression was 25 to 43 mm.

Pintar et al., 1995 reported on the experimental tolerance and the force deformation response corridor of human cervical spine under dynamic compression load. The models were pre-aligned to their stiffest axis. The authors recorded injuries to the mid-column fracture of the vertebral bodies such as burst fracture, wedge and vertical fractures. The duration of the loading was 10 ms and the average failure force was 3334 N. Based on an average neck displacement of 18 mm, the authors reported an average neck stiffness of 515 N/mm.

Voo et al., 1998 quantified the quasi-static and dynamic bending responses of cervical spine intervertebral joints using 5 mid-lower cervical spine specimens. The specimens were subjected to three quasi-static load-unload cycles followed by a dynamic load in sagittal rotation motion. The resulting peak moment at the center of the intervertebral joint was between 3.8 and 6.9 Nm for quasi-static tests and between 14.0 and 31.8 Nm for dynamic tests. Based on these results the authors concluded that the dynamic response was on average 45% stiffer than the quasi-static response.

With regards to the upcoming preliminary study of this research, there have been other studies and analyses of the head motion/reaction due to the acceleration in z and x directions, (G-z and G-x), (Miller, 1993 and Perry, (1994, 1996), Sadegh (1995 and 1997)). Pilot ejection process safety had also experienced broad interest among

researchers, (Farfan et al. 1982, Guill 1989, Haemaelaeinen et al. 1992, Helleur et al. 1984, Hoek et al. 1993).

Sadegh (1995) and Sadegh et al.,1997 reported the validation of the test results for G-y acceleration and determined the forces and torques at the occipital condyle (OC) (neck/head) joint. To validate and analyze the data, Sadegh (1995) employed a model consisting of a head, neck, and upper torso, Figure 3.10. The physical and geometric parameters for each segment were supplied by body-data generator software known as GEBOD (Gross, 1991 and Cheng et al., 1994). The GEBOD program is an interactive computer program that generates human and dummy body data set for use in dynamic modeling. For the three segments, a dynamic model was created using the Articulated Total Body software known as ATB (Orbegefell, 1988). The commercial package of the ATB program is known as DYNAMAN (Shams, 1992 and 1993). In this model the head segment is joined to the neck by "Head Pin" (HP) joint and the neck is connected to the upper torso by the "Neck Pin" (NP) joint. Both joints were of the ball-and-socket type. However, at the neck pin, NP, a viscoelastic slip joint composed of parallel spring and dashpot (Voigt Model) was added. This joint allows relative axial motion between the neck and the upper torso, which simulates "compression" at this joint. The spring stiffness was modeled by linear spring coefficient, K1 (N/m) and a quadratic spring coefficient, K2 (N/m^2), while the dashpot was given only a linear damping coefficient, c (N-sec/m). Coulomb friction was assumed to be zero. The rigid body response of the model, the forces and torques were determined at the joint. The chest acceleration of the subject was used as the input to the ATB model. Sadegh, (1995), validated the model by

selecting parameters such that the ATB model predicted and duplicated the experimental data collected at the mouthpiece. Finally, the forces and the torques in all directions (x, y, z) were determined at the head pin (HP), and neck-pin (NP) joints. These validated forces and torques reported in Sadegh (1995), will be used to conduct the preliminary study of this research and gain insight into the fact that the internal responses of the cervical spine are highly non-linear and they will lead to injuries if they result from forceful and/or excessive loadings such as impact and acceleration forces.

The figures of this chapter are illustrated next followed by a condensed review and description of the mechanisms and the classification of neck injuries in chapter five.

3.4 List of figures and tables

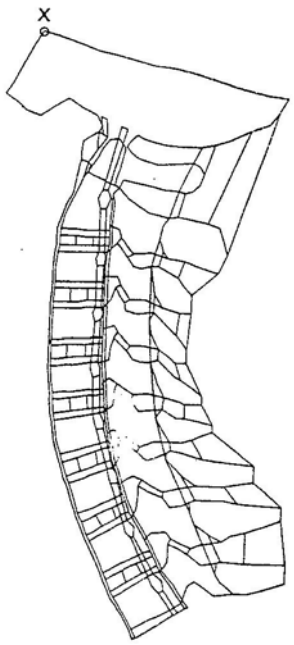

Figure 3.1: 2-D finite element model (C0-C7), Sato et al., 1991.

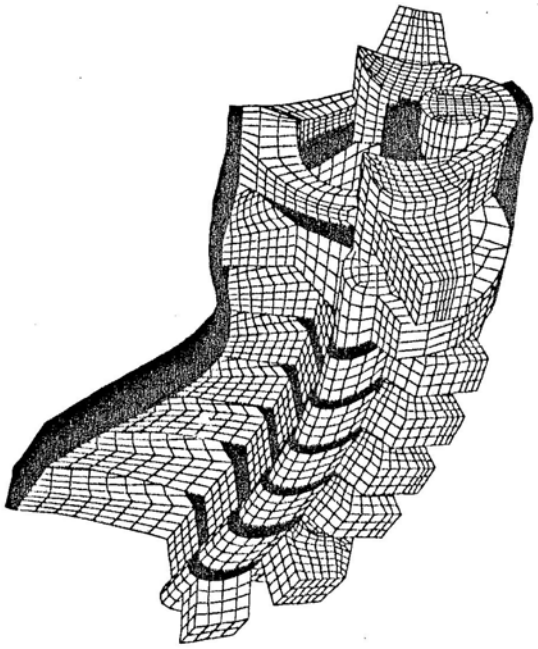

Figure 3.2: 3-D finite element model (C1-C7), Kleinberger, 1993.

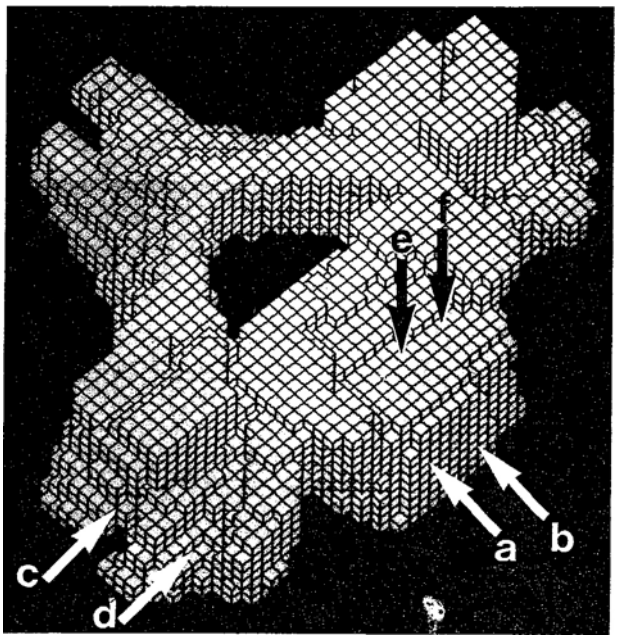

Figure 3.3: 3-D finite element model (C2), Bozic et al., 1994.

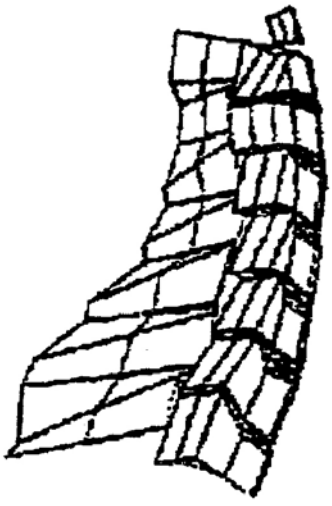

Figure 3.4: 3-D finite element model (C1-C7), Dauvillier et al., 1994.

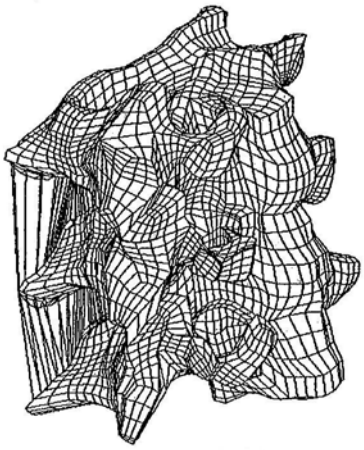

Figure 3.5: 3-D finite element model (C4-C6), Yogananda et al., 1996.

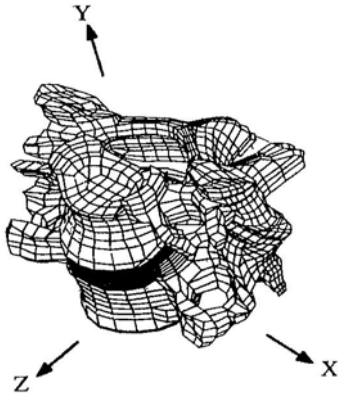

Figure 3.6: 3-D finite element model (C4-C5), Clausen et al., 1994.

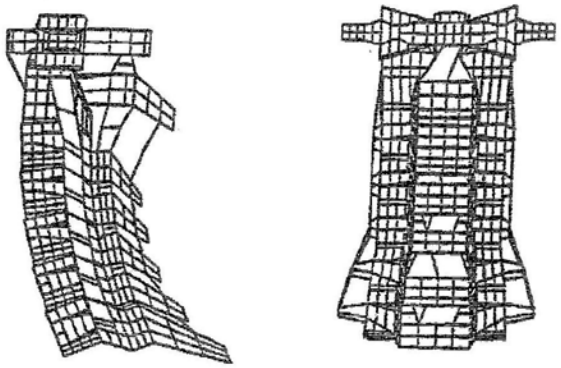

Figure 3.7: 3-D finite element model (C1-C7), Nitsche et al., 1996.

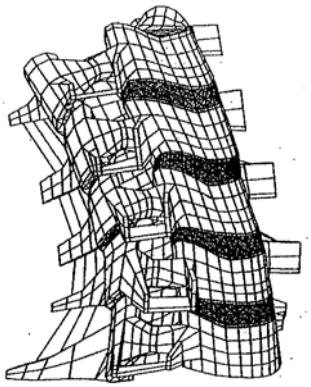

Figure 3.8: 3-D finite element model (C3-C7), Maurel et al., 1997.

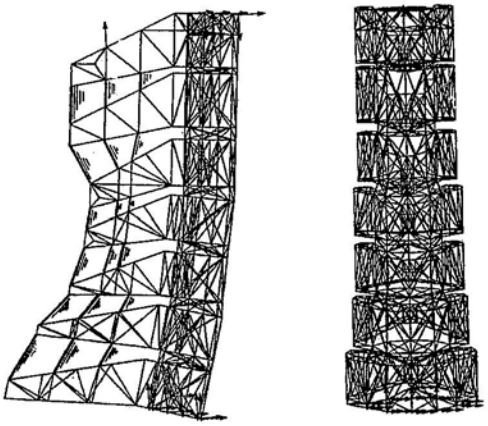

Figure 3.9: 3-D finite element model (C1-C7), Sadegh et al., 1997.

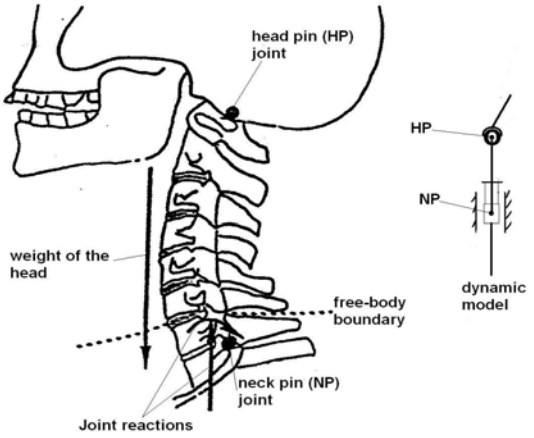

Figure 3.10: Head, neck, torso model, Sadegh et al., 1995.

4. MECHANISMS AND CLASSIFICATION OF NECK INJURIES

This chapter introduces different concepts and considerations regarding the mechanisms of neck injuries. It mainly bridges the background/review and the investigation/analytical parts of this dissertation.

4.1 Introduction

Based on the number of fatalities and survivors, cervical spine injuries contribute to about 68% of all spinal injuries in the U.S. (Grossman et al. 1999, Winkelstein et al. 1997). The basic explanation for the high percentage of cervical spine injuries is that the neck has a great mobility, has relatively small components and is the less protected weight-bearing part of the spinal column. The three major groups of structural components of the cervical spine: the osseous (vertebrae), the neurological (nerves and spinal cord) and the soft tissues (muscles, disc and ligaments) could be individually or collectively injured, Figure 4.1. For example, a fractured vertebra may involve ligaments, spinal cord and/or nerves injury as a result of bone fragment getting into the spinal canal. The cervical spine can be loaded in flexion (anterior bending of the neck), extension (posterior bending of the neck), lateral bending (right or left bending), torsion (rotation about longitudinal axis), compression (action in superior inferior direction and vice-versa) and shear (action in postero-anterior direction and vice versa). Injury to cervical spine does not result from single force or single loading mode action, but rather from multi-axial forces or coupled loading modes, see Figure 4.1 A - H. Excessive forces and/or forceful motion produced during any loading mode or combination of loading modes will lead to injuries. The breaking loads of the spinal components are given in Table 4.1 (Crowell et al. 1995).

Spinal injuries can be categorized as sprain, disc disruption, vertebral fracture or vertebral dislocation. Depending on the extent of the injuries the spinal cord or the nerves may be affected. Injuries are accurately diagnosed if their mechanisms are known. Methods of establishing injury mechanism after an accident include: description of the accident and/or the injury, laboratory investigation or recreation of particular kinds of injuries, and computer simulations using cervical spine models such as in finite element analysis.

Several experimental studies were done on cadaver cervical spines with the aim to recreate specific type of injury or elucidate the mechanism of injury. Some investigators tried to duplicate clinically observed cervical spine injuries but obtained mixed results because of the assumed boundary and restraining conditions (Bauze et al. 1978 and Yoganandan et al. 1990). Even among physicians, due to the multiple probable causes of injury, there is not a clear consensus when it comes to the classification of spine injuries. Panjabi et al., (1978) introduced the concept of major injury vector (MIV) to help simplifying the mechanism of classification of neck injuries. The concept proposes to sum all the forces (compression, anterior-posterior shear, and lateral shear) into a single resultant force. The moment, (lateral bending, extension, flexion, axial rotation), is then generated from the resultant force which is acting on the cervical spine with an eccentricity from the spine neutral axis, see Figure 4.2. Allen et al., (1982) proposed the most effective and comprehensive classification of neck injuries based on the MIV concept. They identified the six most evident structural failures to be: compressive flexion (CF), vertical compression (VC), distractive flexion (DF), compressive extension (CE), distractive extension (DE), see Figures 4.1E, D, G, C, A, and lateral flexion (LF).

Naghtingale et al., (1991) studied the influence of the degree of constraint imposed on the head by the impact contact surface. Their results suggested that the risk of cervical spine injury might strongly depend on the end condition imposed by the impact contact surface. They found the average axial load for unconstrained end to be 289 N with some models showing sign of injury. The same model with the end constrained in rotation sustained an average axial force of 1720 N and showed sign of injury. A full end-constrained model averaged 4810 N, and all specimen showed sign of injury. But in reviewing the epidemiology of catastrophic cervical spinal injury, Winkelstein et al., (1997) used the same concept as Allen et al., (1982) to show that the point of impact and the changing axis of flexion, from upper to lower cervical spine, are two major factors to be considered. They concluded that neither the head motion nor the load acting within the spine alone is sufficient to accurately define the mechanism of injury and proposed to also take into consideration the point of impact or application of the load. Based on the results of all the above cited studies, it appears that there is not a clear compromise on the classification of the mechanism of neck injury. Nevertheless it can be concluded that, a good description of the mechanism of cervical spine injuries must include the head motion, the location of impact and the type of forces and moments generated within the spine during an accident. Furthermore, it is important to recognize that the cervical spine, in any accidental situation, is probably going to be subjected to forces from different directions and/or loading modes. In the following sections some injuries typical to the cervical spine will be presented.

The injuries presented in the following sections are mainly summarized from: The Cervical Spine, Clark, editor (1998) and Pike (2002).

4.2 Soft tissues injuries

Soft tissue injury is the most common type of neck injury. Neck sprains, in which the ligaments have been stretched beyond their limits, are seen more often than any other type of spine injury. Severe injury to the ligaments can include disruption of ligamentous structures that can lead to displacement of vertebrae and/or neurological impairment, Figure 4.1 A, F, G, H.

Injury to the intervertebral disc is usually the consequence of excessive shear and compressive loadings and/or ligamentous disruption. The annulus fabrosus of the injured intervertebral disc may tear and lead to the displacement or herniation of the nucleus pulposus through a crack in the outer layer, into the space occupied by the nerves and the spinal cord. The herniated disc is a prolapsed disc if the annulus fibrosis is only partly ruptured, and is an extruded disc if there is complete rupture of the annulus. Disc bulging is a contained herniation where the annulus fibrosis remains intact and disc material slightly protrudes beyond the vertebral disc margin. Disc herniation lead to neurological injuries.

Neurological injury is the most severe type of neck injury that generally occurs in combination with vertebral fracture or ligamentous disruption. When a disc is torn or ruptured, it either bulges rearward or the nucleus pulposus prolapses or extrudes rearward and presses on the spinal nerves, which causes pain, numbness and tingling. If the herniated disc also presses on the cord, this may lead to spinal cord syndrome followed by pain, loss of sensation or even paralysis.

Cervical sprain occurs when ligaments and/or muscles are stretched to the point of minor tearing. Ligament injury may not produce neurological injury but it becomes of greater concern if it affects the ability of the ligament to maintain the relative position of adjacent vertebrae.

4.3 Vertebral injuries

Vertebral injuries are fractures that may involve its anterior part (vertebral body) or the posterior parts such as pedicles, laminae, lateral masses and spinous processes, Figures 4.1 and 4.2. The two major consequences of vertebral fracture are either the impingement of the neurological structures or the structural instability of the spine. The fracture type mostly depends on the mechanism of injury and or the physiology of vertebra.

4.3.1 Fractures of the upper cervical spine (C1-C2)

The upper cervical spine region is historically the site of the Jefferson and the hangman's fractures.

The fracture injury of the atlas (C1), Figure 4.3, occurs mostly on its posterior ring in compression-extension loading mode as the atlas is compressed between the extended head and the second vertebra (C2). The fracture usually involves the left and the right side of the ring and the disruption of the atlantal ligament (Harris et al., 1996). This fracture usually denoted the Jefferson fracture is mechanically stable and does not create neurological injury.

Fracture of the dens of the second vertebra, the axis, accounts for about 10% of all cervical fractures (Levy et al., 1986). This injury may results from flexion, extension and

occasionally from lateral bending (Anderson 1989). The dens can fracture in three different ways, Figure 4.4 (Orrison, 1989); 1) obliquely at it superior region (rare), 2) at it base (most common, 65% of the time) and results from either flexion or extension, and 3) horizontally through its body at the dens-body junction. The third mode of fracture usually occurs during excessive lateral bending, which if associated with torsion but may also result in fracture of the body, lateral mass and transverse process. The fracture is mechanically stable if there is no displacement of the dens and the third fracture type heals faster than the first two because it cuts through the soft cancellous bone of the C2 body. Extension may produce injury to the posterior elements of C2. When its lamina is excessively compressed between the laminae of contiguous vertebrae, it may fracture. If the fracture of the lamina is bilateral, it is often referred to as a hangman's fracture. Hyperflexion and hyperextension coupled with axial rotation may create dislocation with or without bony fracture at the C1-C2 joint. The so-called judicial hangman's fracture involves fracture-dislocation of the C1-C2 joint.

4.3.2 Fractures of the mid-cervical spine (C3-C5)

Injuries to the mid-cervical (C3-C5) spine are mostly fractures and dislocations of vertebral body and are attributed to a single or combination mechanisms of injury. There are four major types of fractures of the vertebra in this region of the spine, namely the compression or burst fractures, the wedge fracture (flexion), teardrop fracture (flexion) and lateral mass fracture (extension and axial rotation).

Burst fracture, Figure 4.1 D and E, is due to axial load and tends to occur when the load is applied to pre-straightened spine (Harris, 1996). Fragments of a burst fractured

vertebral body may be dispersed and consequently injure the spinal cord. Harris (1996), reported that burst fracture is frequently accompanied by fracture of one or both laminae. Unless the bilateral laminar fracture is present, burst fracture injury is generally considered stable.

Wedge Fracture, Figure 4.5, is an anterior superior vertebral body fracture resulting front flexion. The fracture occurs when the antero-inferior part of the suprajacent vertebral body compresses the antero- superior part of the subjacent vertebra. The lateral view of the fracture vertebra looks like a wedge. This injury may include the disruption of the interpinous and supraspinous ligaments. It is an unstable injury if the posterior ligamentous complex is disrupted and do not heal properly.

The teardrop fracture injury, Figure 4.6, is a violent flexion injury that breaks off a roughly triangular piece from the anteroinferior corner of the vertebral body. It is frequently accompanied by injury to the spinal cord because the anterior and posterior ligaments are disrupted and the fractured vertebra displaces posteriorly and rotates anteriorly.

Lateral mass fracture results from a combination of extension and rotation that compresses lateral pillar. The fracture is nearly vertical and occurs in the lateral mass on the side to which the head has rotated.

Beside fracture injuries of vertebrae, soft tissue injuries are also present in the mid-cervical spine and they usually lead to dislocation of the vertebrae. Dislocation injuries are ligaments and intervertebral discs related and result from vertebral displacement, Figures 4.1F, G and 4.7. Hyperextension dislocation is frequently associated with the impact to the face or forehead. A sufficient large posterior

displacement of the vertebra may disrupt the anterior longitudinal ligament and the intervertebral disc. The disc may tear horizontally and be torn away from the endplate of the suprajacent vertebra. The posterior displacement (3-6 mm) of the dislocated vertebra narrows the spinal canal and thus compresses the spinal cord to probable cause a central cord syndrome. If the extension is combined with rotation, the articular facet ligaments may be disrupted or facet may fracture.

Anterior sublaxation or partial dislocation is a flexion related injury that may occur alone or in combination with other flexion-related injuries. It is the forward translation of one vertebra with respect to the adjacent vertebrae. Anterior subluxation or anterolisthesis includes a downward angulation of the anterior vertebral body and or the forward displacement (1-3 mm), Holdsworth (1970), of the vertebral body with respect to the subjacent vertebra. Furthermore, the posterior ligamentous complex is disrupted Harris (1996) and Holdworth (1970). The injury has a high incidence of instability or delayed instability.

4.3.3 Fractures of the lower cervical spine (C6-C7)

Injuries to the lower cervical spine region (C6-C7) are mainly related to the spinous process fracture and the lateral facet dislocation, Figures 4.1D, B, and 4.8.

Spinous process fracture, historically known as clay shoveler’s fracture, is an extension related injury that occurs when the extensor muscles such as the trapezus and rhomboid, which are attached to the process suddenly and forcefully contract to react against excessive neck flexion. This type of injury frequently occurs at C6 or C7 (Orrison et al.1989). The spinous process fracture can also resulted from hyperextension leading to

forceful contact between the spinous processes of adjacent vertebrae. Ligaments disruption is minimal and the fracture is usually stable (Levy et al. 1986).

Bilateral facet dislocation is a pure flexion injury that results in the disruption of the posterior ligamentous complex, the posterior annulus of the disc and possibly tearing of the intervertebral disc and the anterior ligamentous complex. The vertebrae are relatively free to move with respect to each other and both facets move in a similar way. The displaced vertebra will injure the spinal cord leading possibly quadriplegia. Bilateral facet dislocations are mechanically and clinically unstable.

Unilateral facet dislocation occurs from the combination of neck flexion and rotation. The posterior ligamentous complex, including the posterior part of the disc, is usually disrupted. The capsular joint ligaments on the side opposite to the rotation direction may also be disrupted and the facet joint fractured.

4.4 Clinical instability

Vertebral and soft tissues injuries to the cervical spine can be categorized as mechanically / clinically stable or unstable. Clinical instability depends on the relative displacement of the involved vertebral region and/or the rupture (or no rupture but stretching) of the attaching soft tissues. Clinical instability of the lower cervical spine has a much narrower biomechanical and a much broader clinical significance. It is a traumatic sprain injury of the posterior ligaments and the intervertebral disc. The injury mostly results from flexion-compression and is associated with some of the following injuries the interspinous widening, facet joint subluxation, vertebral compression fractures and/or loss of normal cervical lordosis, which all may lead to pain and/or

neurological dysfunction, Figure 4.9, (The Cervical Spine, 1998). According to White and Panjabi (1990), a spine is diagnosed clinically unstable if in a sagittal plane flexion/extension motion localized kyphosis (thoracic-like curvature) of a disc measured between two adjacent vertebrae is greater than 11° and the horizontal displacement between the bodies of the subluxated vertebrae is more than 3.5 mm. Illustrative of the essential radiologic features used in assessing clinical instability in the cervical spine is shown in Figure 4.9. In medical practice, a clinically unstable cervical spine needs corrective surgical intervention, where as an injured but clinically stable cervical spine will heel naturally through therapeutic means.

In view of the objectives of this research one of the alternative ways of establishing injury mechanism, namely computer simulations using finite element model of the cervical spine, is considered in the coming chapters. Cervical spine models will be created in the next chapters, five and six, and the loading conditions will be applied according to major injury vector (MIV) concept. Experimentally generated and published forces will be used as distributed or single forces applied at a prescribed eccentricity to generate moment based on the head motion. The responses the cervical spine finite element models will be compared and/or correlated to experimentally or clinically observed situations.

The figures and tables of this chapter are shown next.

4.5 Figures and tables.

Table:

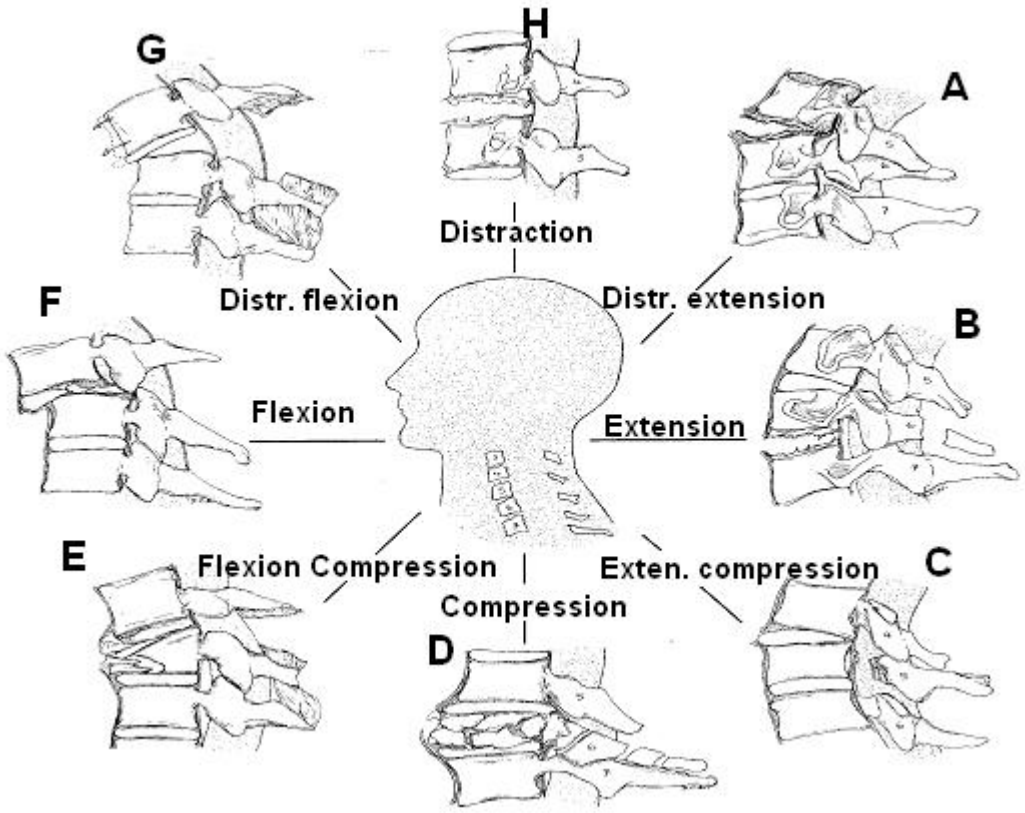

Figure 4.1: Common cervical spine injuries (The cervical spine, 3rd ed., 1998)

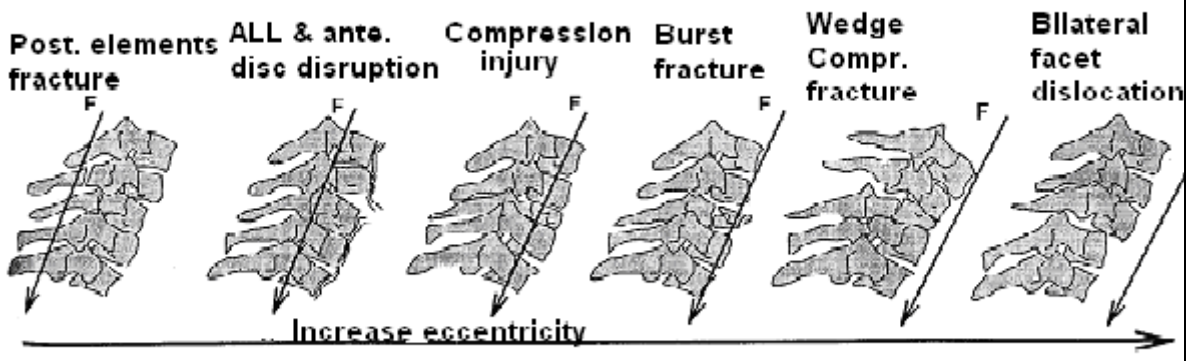

Figure 4.2: Type of injury produced as it relates to the location of the major injury vector force; from compression extension to pure compression, to compression flexion, (Winkelstein et al., 1997).

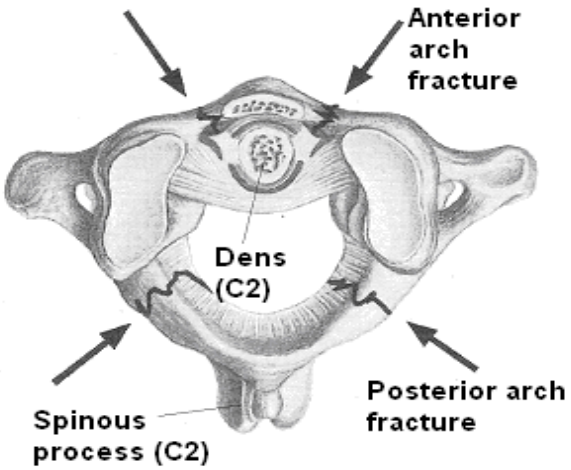

Figure 4.3: Fractures of the atlas (C1), Jefferson fractures, (Pike et al., 2002).

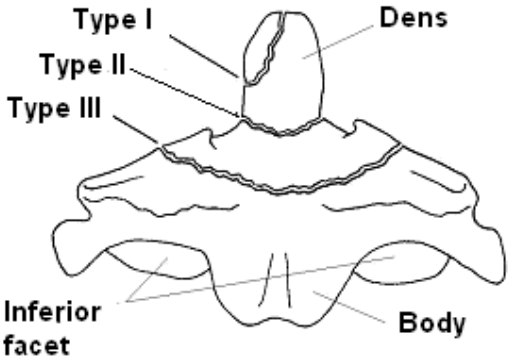

Figure 4.4: Fractures of the dens (C2).

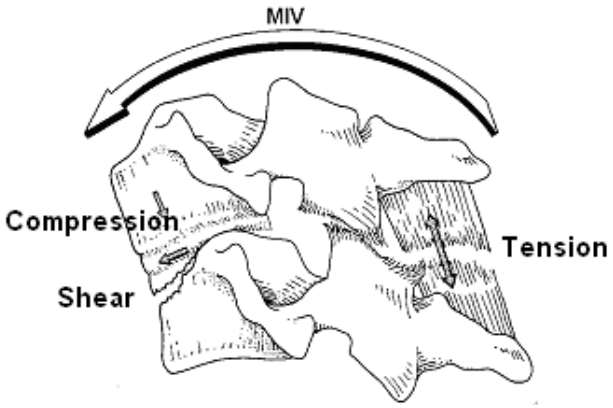

Figure 4.5: Wedge fractures of vertebra.

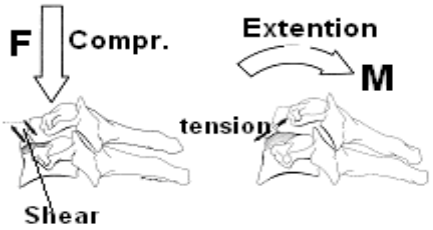

Figure 4.6: Teardrop fractures of the vertebra.

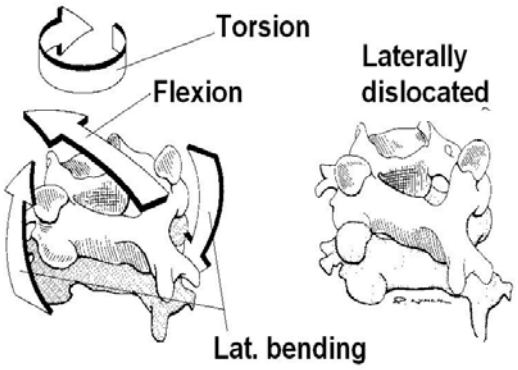

Figure 4.7: Lateral dislocation

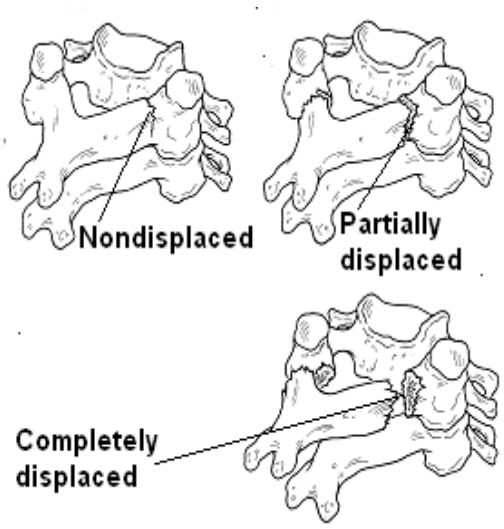

Figure 4.8: Fractures of the posterior elements.

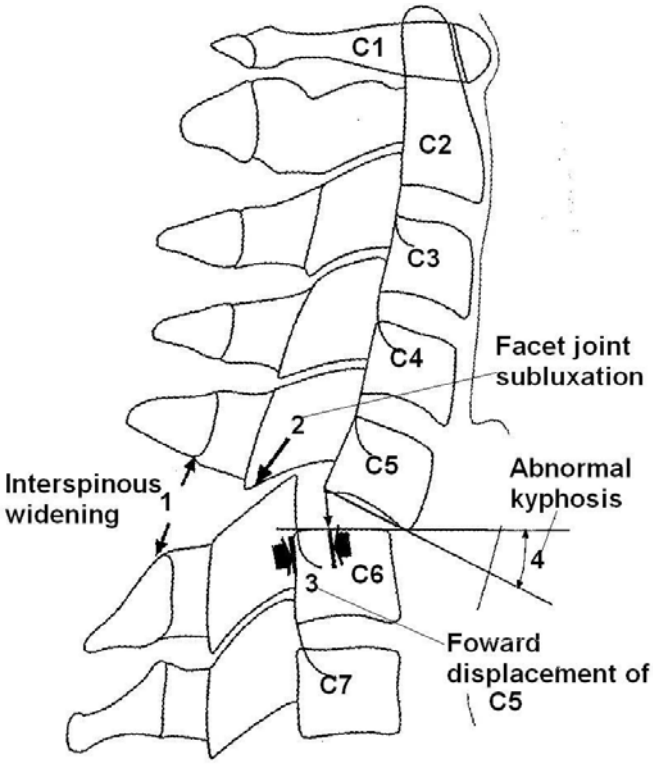

Figure 4.9: Clinical instability criteria, detail 3: forward displacement of vertebral bodies; detail 4: Relative rotational displacement of vertebrae.

Structure	Breaking load
Cervical vertebral body	2800 to 4200 N
Transverse ligament of the atlas	1000 N
Anterior longitudinal ligament (ALL)	340 N
Posterior longitudinal ligament (PLL)	180 N
Cervical disc (compression)	3200 N
Cervical disc (tension)	1000 N
Cervical disc (torsion)	6 Nm

Table 4.1: Breaking load of cervical components (Crowell et al., 1995).

5. DYNAMIC AND VISCO-ELASTIC ANALYSES

This chapter presents the preliminary studies of this research. A complete 3-D finite elements model of the cervical spine (C1-T1) was created and validated. The validated model was subsequently modified to generate a segmental elastodynamic model, and complete visco-elastic model. The two models were then loaded with dynamic forces and moments generated from high G-z accelerations sled tests. Twelve analyses, one with the elastodynamic and eleven with the viscoelastic model, were conducted and the results were reported. In the following sections, the model generation is described followed by its validation. In section 5.2 the boundary conditions generated from the sled tests are described. In section 5.4 the two models considered, followed by the results of the two models and the conclusion and discussion of the studies are presented.

5.1 The preliminary finite element model

A complete simplified 3-D finite element model of the human cervical column was created. The model (Figure 5.1) consists of a hard top plate, the seven cervical vertebrae C1-C7 and the first thoracic vertebra T1. The model was simplified in terms of anatomical details and material properties. The superior view of the solid model of each vertebra, Figure 5.2, was carefully created using the sagittal, lateral and superior planes projection of its anatomical dimensions (The Cervical Spine, 1995). The coordinate system of xyz were used, where, x is in the direction of posterior-anterior, y is in the medial-lateral direction and z is the inferior-superior direction, Figure 5.3. The complete column was then generated by stacking the individual vertebra. The proper lordosis (c-

shape), which is characteristic of the neutral position of the neck, was achieved by considering the position and orientation of each vertebra. Intervertebral discs were constructed to fill the space left between the bodies of stacked adjoining vertebrae. The major ligaments, namely, the anterior longitudinal ligament (ALL), the posterior longitudinal ligament (PLL), the intraspinous ligament (ISL) and the capsular ligament (CL) were included. Four major cervical muscles, Semispinalis Capitis and Splenius Capitis were also incorporated. These muscles are used for extension, flexion and lateral movements. A rigid plate was added to the superior surface of C1 of the model for better distribution of the applied loads and the moments. The T1 vertebra at the bottom of the model was to be used to constraint the model. The generated finite element model (FEM) has in sum 1193 elements and 560 nodes. A total number of 1142 solid tetrahedral elements were generated for the vertebrae and the discs, and 51 beam elements simulating the ligaments and muscles connections. The location of the ligaments connections are shown by numbers in Figure 5.2 and described below. There are seven beam elements connecting the inferior plane of a vertebra, C_i, to the superior plane of the vertebra C_{i+1}. Beam elements 1 to 3 were used to simulate spinous process ligaments connecting the two adjacent posterior arches. Referring to the numbers on Figure 5.2, beam elements 4 and 5 were used to simulate the articular facets. Beam elements 6 and 7 were used to simulate the anterior and posterior longitudinal ligaments, Table 5.1. Two beam elements, connecting T1 to the top plate, were used to simulate the incorporated major cervical muscles. The material and/or physical properties of the vertebrae, the discs and the ligaments are adopted from other finite element studies and are adapted during

the validation process. The material properties are given in Table 5.2. The model was generated using I-DEAS software from SDRC Inc., running on a SUN workstation.

5.2 Validation of the model

The model was validated using the anatomical range of motion in flexion extension, Table 5.3. For this purpose the experimental data obtained and the observations made by Sadegh (1995) were used in collaboration with studies done on the flexion/extension range of motion of individual segments and of the cervical column (Penning, 1978, Dvorak, 1988 White et al., 1990). The average flexion/extension range of motion of C1-C2 is 21° (White and Panjabi, 1988), which can be translated, when considering the motion at other vertebral levels, into a total saggital forward displacement of C1 of about 60 mm with respect to C7. Ghanayem et al. (1998), reported that if the cervical anatomy is normal, physiologic motion does not produce abnormal stress and strain on the cord and tissues. Sadegh (1995) observed during the sled test that at 10 G-z acceleration, the neck was completely flexed without sign of injury. Therefore, to select the material properties and validate the model the total range of motion of the cervical column model (C1-C7) in flexion was determined and compared to the anatomical physiological range of motion of the cervical spine. That is, the model was constrained at T1 and loaded at the top plate on C1 with forces obtained during the 10 G-z acceleration sled test described below. The elastic material and /or physical properties of the model components were subsequently varied and the deflection of each vertebra was determined. After each solution, the obtained maximum total (flexion) deflection of the top vertebra, C1 with respect to C7, was measured and compared to the mobility range

(Penning, 1978, Dvorak, 1988, White et al., 1990). After seventeen runs and analyses, Table 5.4, the flexion of the model matched the total anatomical range of motion, thus, the material properties were selected. This procedure also validated the model. The validated model was used to study the elastodynamic and the viscoelastic responses of the cervical spine, explained in the following sections.

5.3 Experimental data

The forces and moments used in the following studies were generated by Sadegh, (1995), from the experimental data. The data were collected from biodynamic responses of human volunteers during acceleration in the corresponding direction at the sled track or the drop tower facility located at the Armstrong Laboratory at Wright-Patterson Air Force Base (WPAFB). The facilities employ an Impulse Accelerator, which is a gas-powered actuator that accelerates a sled on two tracks. The volunteers were placed in a chair mounted on a sled facing perpendicular to the direction on the track for the Y acceleration, and facing in the direction of the track, for the X acceleration. Two sets of three orthogonal linear accelerometers were located in a chest pack and a mouth pack. These accelerometers collected the x, y and z accelerations of the torso and the head as a function of time during the acceleration impulse. The coordinate system used in the sled test or the drop test experiment is shown in Figure 5.4. The sled acceleration pulse was of the half-sine with the peak acceleration ranging from 4G to 7G and duration ranging from 31 ms to 250ms. The drop tower facility is similar to the sled facility, except that the chair is drop from a preset high on the vertical track. The forces and moments generated from the G-z acceleration experimental data were used for the current solutions. Typical

generated forces and moments from the experimental data are shown in Figure 5.5. The maximum acceleration for collected data used in this research was 12 G-z, which is below the injury level.

There is a gap between the 12 G-z acceleration and the acceleration that may cause vertebral fracture. To determine the response of the cervical column at higher acceleration, the acceleration curve of the fourth case was extrapolated from 8 G-z to 15 and 20 G-z and was labeled as cases 6 to 7, Table 5.5. In this table subjects and cells numbers are from the test laboratory. Head accelerations, neck forces and moments generated from a typical experiment are shown in Figure 5.6.

5.4 Elastodynamic and Viscoelastic models

Tow models, an elastodynamic and a viscoelastic, were developed. The elastodynamic model consists of lower cervical spine column (C5-T1) segment and was subjected to dynamic loads. The viscoelastic model was a complete cervical column model (C1-T1), where the soft tissues had viscoelastic properties and the loads where of dynamic nature.

5.4.1 The elatodynamic model

The elastodynamic model was a simplification of the complete 3-D model in that vertebrae C1-C4 were removed. These vertebrae were removed in order to reduce the model stiffness matrix and cut back on the computational time of the dynamic analysis. The model then consists of C5, C6, C7 and T1, see Figure 5.7, and was developed and used to study the responses of the cervical spine to the dynamic load. A rigid top plate

was added on top of the vertebral body of C5 for the application of forces and moments. The model was constrained at the inferior surface of T1 vertebra. The time history of the force F-z and the torque T-y obtained for 10 G-z acceleration, during the experimental study at the WPAFB, were employed. The time history ranged from 10 to 200 msec. and included the first peak values of the force and moment history. The force F-z and the torque T-y, were calculated for the C5 vertebra, that is the top vertebra in this model. Note that these forces were determined at the occipital condyle, C1. The calculated compressive force was 890 N and the calculated equivalent torque transferred C5 was 36.7 Nm. The force and the torque were applied to the rigid plate on the top of C5. The elastodynamic model has 539 tetrahedral elements, 21 beam elements and 271 nodes were used. The dynamic finite element analysis was performed using ABAQUS (KHS, Inc.) software. The dynamic analysis required adjustment of the time increments in order to achieve the convergence.

5.4.2 The viscoelastic model

The viscoelastic model was the same as the validated 3-D finite element model (Figure 5.1) except that the elastic material properties of the intervertebral disc, the ligaments and the muscles were changed to the viscoelastic properties. This model was used to study the complete viscoelastic response of the cervical column that is subjected to the dynamic impulse load. The phenomenological material model employed for this geometry, Visarius, 1994, employs quasi-linear viscoelastic theory (QLV), (Johnson, 1975). The quasi-linear viscoelastic theory can be derived from the classical linear theory of viscoelasticity. This material model has been proven to be a realistic model for

biological materials (Johnson, 1975). The material properties are defined by a Prony series representation of the normalized shear and bulk relaxation moduli, ABAQUS Manual (1997). The viscoelastic properties of the muscles and ligaments are given in Belytschko et al., 1985 and Woo et al., 1993. The viscoelastic coefficients of the materials are adopted from Visarius, (1994), and are shown in Table 5.6.

As the boundary conditions for this model, the nodes on the inferior surface of the inferior section of the main body of T1 were constrained. The loads were distributed over the superior surface of the thin rigid plate located on top of C1. The complete and exact time history (10 to 300 msec.) of all the forces, F-x, F-y and F-z and all of the torques, T-x, T-y, and T-z of the eleven cases, shown in Table 5.5, were considered. All the components of the loads and torques were applied to the model. The viscoelastic analyses of this model were performed using the nonlinear time step parameters of the ABAQUS (KHS, Inc.) software.

5.5 Results.

In the viscoelastic study, all eleven G-z acceleration cases were analyzed, as shown in Table 5.5. For each case, only the peak stress and the corresponding occurring time are given in Table 5.7. The study with elastodynamic model was conducted using only forces and moments generated from the first case (10 G-z acceleration) for a time history of 10 to 190 msec. All the forces and moments generated in each case were considered over full duration of their time history. The summary of the maximum stresses of the viscoelastic model is shown in Table 5.7 and the detailed descriptions are given below.

5.5.1 Results of the elastodynamic model

The dynamic finite element analysis was performed using ABAQUS (KHS, Inc.) software. The time history of the force and moment was input in six steps over the time range of 190 msec. The results are given in Figure 5.8 and Figure 5.9. The maximum von Mises stress found was 24.4 MPa and located in the anterior section of the mid-vertebra (C6) and occurred at about 50 msec. of the impact. The equivalent static forces of this case were determined. This was accomplished by averaging the magnitude of the forces over the total time, 190 msec. It was determined that for the first case the equivalent static force F-z was 427 N and the equivalent torque T-y was 21.8 N-m. The maximum stress in the static case was 12.7 MPa. When comparing the static and dynamic responses, the dynamic load creates about 91% more (overshoot) stress in the cervical column.

This model was a trial model to understand the behavior of the vertebral column under a dynamic load and the results show that when loaded dynamically, stresses in vertebra are almost twice as high as those sustained in static loading situation.

5.5.2 Results of the viscoelastic model

This model was used to study the complete viscoelastic response of the cervical column that was subjected to the dynamic impulse load generated from all the cases presented in Table 5.5. To capture the second peak of the stress and the rebound, the time range was expanded to 300 msec. The model was loaded with the forces and moments in 14 equal steps. On an average, each analysis took 300 increments from the onset to completion of the computation. Each increment ran, on an average up to 10 iterations to converge. It is noteworthy that due to the dynamic nature of the loads and moments, and

the complex geometry of the cervical spine, at each instant of time, one vertebra could be at its peak stress while the others are about to approach, or have passed, their peak stress. Therefore, each case should be studied individually, which makes the summarized presentation of the results very difficult. A large number of tables and graphs were generated for this model, but only a selection is presented here. The summary of the maximum values of the principal and the von Mises stresses are given with the time at which they occurred in Table 5.7. At the extrapolated 20 G-z acceleration the maximum stress was 27.1 MPa, which is close to the bone strength.

For all the eleven cases, the maximum von Mises stress of the elements on the anterior and posterior sections of all vertebrae, throughout the impulse, were determined, Figures 5.10. Note that, in some cases, the maximum stress of each vertebra does not necessarily occur at the posterior or anterior sections of the vertebra, rather it may occur at the elements on the lateral or medial side of the vertebra. The graphs of the stresses as a function of time, Figures 5.11, showed the variation of the stress for selected elements and load cases over the time history of the loads. For accurate location of the elements for the magnitudes of the maximum stresses refer to Figure 5.11.

5.6 Discussion and conclusion

The first model (C5-T1) was subjected to the dynamic load of case 1, shown in Table5.5. The model is considered as the first approximation model to examine the behavior of the neck under the dynamic load and quasi-static equivalent load. When the model was subjected to statically equivalent loads, the stresses were lower than that of dynamic loads. That is, the statically equivalent analysis of a dynamic situation leads to

comparable but lower responses. A better comparative study would have been the difference in responses between dynamic and viscoelastic solutions. The models could use the same type of loads and differ only in term of some of the material properties.

Geometrically, compared to the dynamic model, the viscoelastic model is a complete (C1-T1) 3-D model of the cervical spine. While the effect of the soft tissues, the ligaments, the articular facets and the muscles, were compensated by the beam elements in the models, more detailed nonlinear spring and dashpot elements could have been used to simulate these tissues more realistically. However, the use of nonlinear spring and dashpot, in these large models, make the dynamic analysis very difficult to converge.

Comparison of the von Mises and the Maximum principal stresses in the anterior and posterior sections of all the cases in the viscoelastic model indicate that: (a) the stresses in all the cases exhibit a similar pattern, in that there is a peak at about 40 to 100 msec. and a second peak at about 200 msec.; (b) the response of the neck to the acceleration is highly nonlinear, however, it is generally true that the maximum stresses increase as the magnitude of the accelerations increase; and (c) the maximum stress generally occurs at C4 or C6. Other than these general observations, each of the eleven cases of the viscoelastic model has its own behavior. The reason for the nonlinearity and dissimilarity of stress distributions is that the geometry of the cervical spine is complex and the material properties are nonlinear. The cervical column could be considered as a curved beam with non-uniform cross-section that is subjected to axial, bending and torsional loads. In addition, the nature of the loads and moments are dynamic which makes the prediction and justification of the response very difficult. That is, during the

time spectrum of the loads each point of a vertebra in the model may go under a stress pattern that is different from that of its adjacent one. This unpredictability of the result leads us to examine each case individually.

Observation of the results of case 1, (10 Gz), revealed that the maximum von Mises stress was 24.4 MPa and occurred at the 40th increment, at C6. The stresses at C3 and C4 were also very high. It was also noted that in most cases the maximum stress occurred on the anterior or posterior sections of a vertebra on or about the symmetric sagittal plane of the vertebra. Stresses on some group of elements are reported in Figure 5.10.

In the second case, 7 G, the stress fields at the 100th increment, where the maximum stress occurred, were determined. In this case the maximum stresses occurs in C2 and C3 vertebrae. Cases 3 and 4 show similar stress fields but with maximum occurring at C4 and C6, Figure 5.10. The peak accelerations of all the drop tower experiments were less or equal to 12 G. To examine the response of the cervical spine in higher acceleration, theoretically, the peak acceleration of the fourth case was extrapolated to 20 G-z and the stresses were calculated. This was due to the fact that the dominant acceleration of the fourth case is in the z direction and the force and torque curves are mainly in z direction. Other cases had other components of accelerations, which would make the extrapolation difficult. In the process of extrapolation, the acceleration and loading curves were proportionally increased to the equivalent of 10, 15 and 20 G-z, i.e., cases 5, 6 and 7, respectively. The stress fields of these cases were also determined. Since the model and the analyses are nonlinear the responses of the spine were not linearly proportional. That is, the magnitude of the maximum stress for the

10Gz was 20.4 MPa and for the 20 G-z was 26.3 MPa. Nevertheless, the maximum stresses generally occurred in C4 and C6 area, see Figure 5.10.

The stress field of the eighth case, 12 G-z, was determined. Due to the nature of the forces and torques, in this case the maximum stress was 34.9 MPa and occurred in C1, C2 area. The high magnitude of the stress for this case was due to its rather unusual load and torque history, i.e. its extremely high T-y that was 29.71 N-m.

The maximum von Mises stress of the ninth case, 10 G-z, was 19.8 MPa and occurred in C6 area. Note that the stress on the C4 area was also high. The reason for the high stress in this case lies in its high torque T-y. The maximum von Mises stress of the tenth case, 10 G-z, was 12.5 MPa. and occurred in C3, C4 and C6 areas. The loads in this case were rather scattered. Finally, the maximum von Mises stress of the eleventh case, 12 G-z, was 6.3 MPa., which is rather low and occurred in C6, C7 area. This is due the existence of the forces in the x and z directions. It is important to note that the time histories of acceleration, forces and torques of each case are not presented here, and Table 5.7 only shows the peak acceleration. Thus, some of the cases in Table 5.7, cases 3 and4 and cases 5, 9 and 10, have the same peak acceleration and the same time duration, their maximum stresses are different. This is due to the difference in the profile of the time histories of these cases that are not shown here. To summarize the results, the maximum stress of anterior and posterior sections of each vertebra, throughout the impulse, for all the eleven cases are presented in Figure 5.10.

The mechanical properties of cortical bone differ from that of trabecular bone by at least one order of magnitude. The modulus of elasticity of cortical bone may vary from 12 GPa (10x3 MPa) to 17 GPa, where as the modulus of elasticity of the trabecular bone

is between 0.1 GPa to 0.55 GPa (Benzel, 1995, Goel et al., 1990). Although a vertebral body has a cortical bone shell and a trabecular structure within, in this study one material that is the average of cortical and trabecular bone was employed for the vertebral body. Therefore, in these models the averaged modulus of elasticity of 2 GPa was used. The ultimate tensile strength of the cortical bone varies from 60 to 130 MPa for femoral bone (Benzel 1995). The compressive strength of trabecular bone of vertebrae is about 4.6 MPa for male and 2.7 for female, Lindahl (1976) and Goel et al., (1990). The ultimate compressive strength of wet human cervical vertebrae for ages 20 to 39 years was reported 12.7 MPa (Yamada 1970). Based on the data in the literature, and the averaged modulus of elasticity used in this analysis, it is reasonable to assume that the ultimate strength of the vertebrae of this model should be about 30 to 40 MPa. This indicates that the seventh and the eighth cases, 20 G-z and 12 G-z, respectively, are the two critical cases where the maximum stresses reached the critical strength of the vertebra. It is noteworthy that the magnitude of one of the components of the acceleration is not the only factor; rather, the combinations of forces and torques are the cause of the high stresses in the vertebrae. Also, it is difficult to predict as to where the location of the maximum stress is, simply because of the nature of the complex geometry of the cervical spine.

The biomechanics of cervical spine injury have been discussed in recent literature, (Winkelstein and Myers 1997). Myers et al. (1991) studied the viscoelastic responses of the cervical spine in torsion. Yoganandan et al. (1996) have reviewed literature of finite element analysis and modeling of a cervical spine.

There are five major mechanisms resulting in cervical injuries: compression, flexion, extension, rotation, and lateral flexion. However, upper cervical spine (C1 and C2) injuries are mainly due to hyperextension, and their dislocations are fatal.

The intervertebral discs, joints and ligaments are very resistant to compression, dislocation, flexion and extension, but very vulnerable to rotation and horizontal shearing forces such as in G-y accelerations (Roaf 1960). According to Roaf (1960), the clinical approach of a cervical dislocation or fracture-dislocation usually attributed to hyperflexion, is really the result of rotation. Belytschko et al. (1985) reported that the maximum voluntary static neck reaction is about $1.13x10^8$ dynes in tension and $1.11x10^8$ dynes in compression. A limited amount of strength data for individual components of the neck can be found in the literature.

The results of these preliminary studies give a good understanding of the responses of the cervical spine subjected to dynamic loads and with the consideration of the viscoelastic material properties. The studies confirm the hypothesis that when the cervical spine is subjected to forces and moments resulting from high g accelerations, its components endure high nonlinear internal (stresses) responses that can lead to injuries. Nevertheless, the studies showed that the components of the cervical column might tolerate acceleration forces and moments well beyond the human volunteer limit. Additional studies, to be conducted using more detailed and accurate models, are needed to compare and/or confirm the maximum stresses and the tolerance limit of the cervical spine components.

With these encouraging results, a second complete, more accurate and detailed cervical spine model was developed to test the two previously stated hypotheses of this

research as they relate to common cervical spine injuries (instability) and surgeries (discectomy). The creation of the second model and its validation are presented in the following chapter 6.

The figures and tables pertaining to this chapter are shown in the following pages.

5.7 List of figures and tables

Tables:

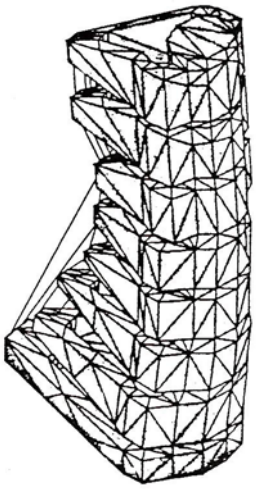

Figure 5.1: Preliminary finite element model

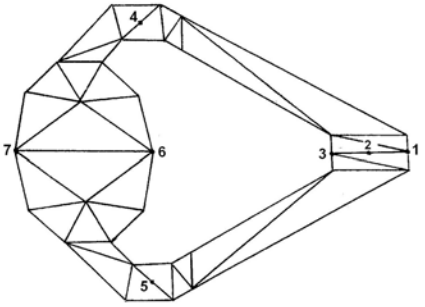

Figure 5.2: Ligamentous connection between adjoining vertebrae

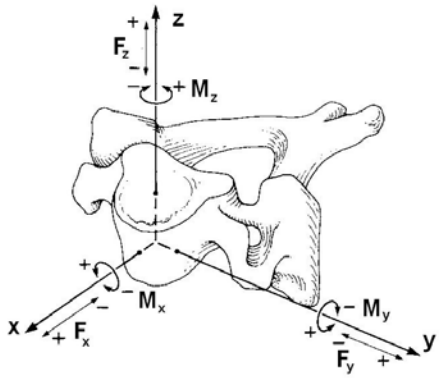

Figure 5.3: Coordinate system used for model creation.

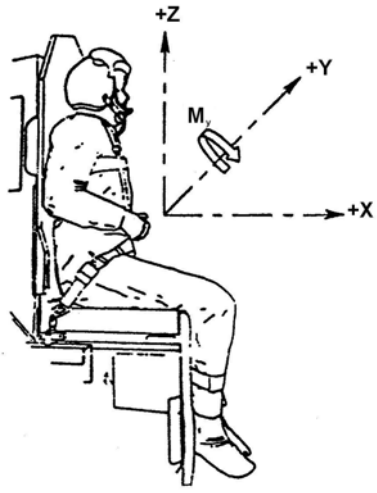

Figure 5.4: Coordinate system used in the sled test.

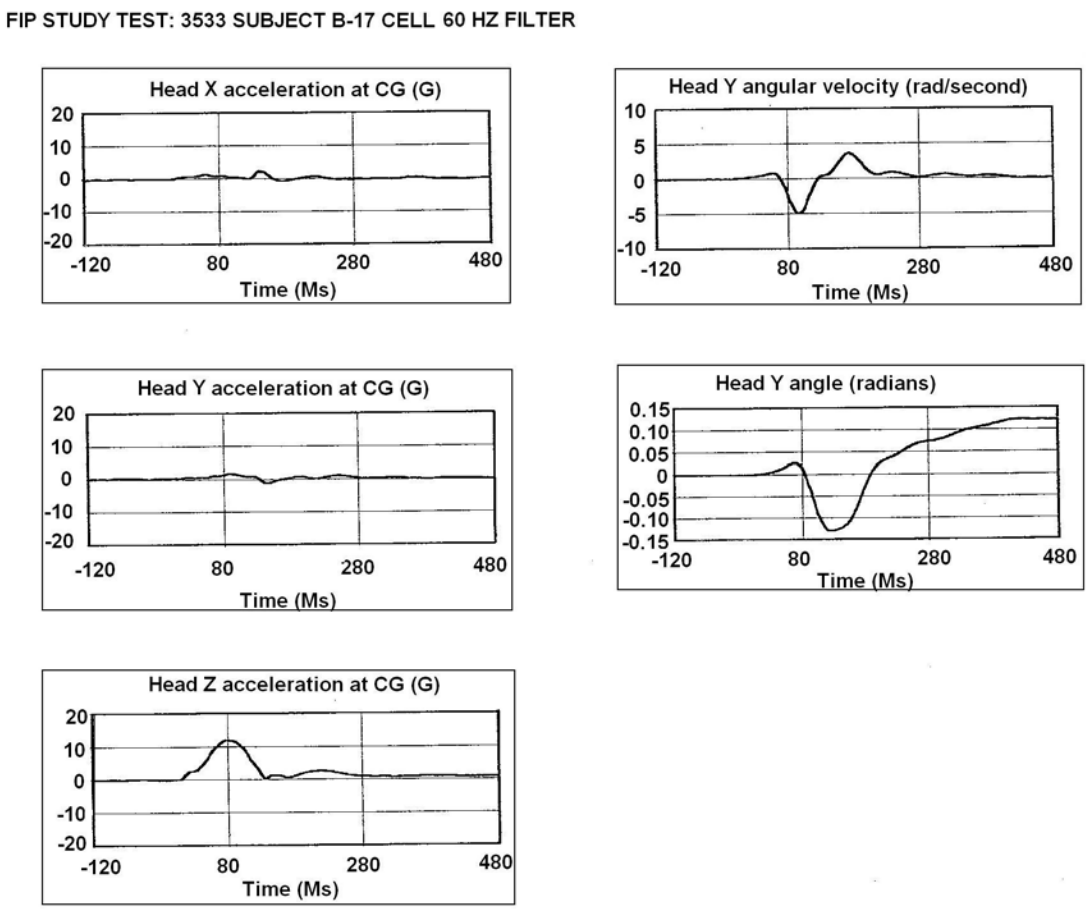

Figure 5.5: Typical acceleration and angular velocity data recorded during the drop/sled test (12 Gz acceleration) (Sadegh 1995).

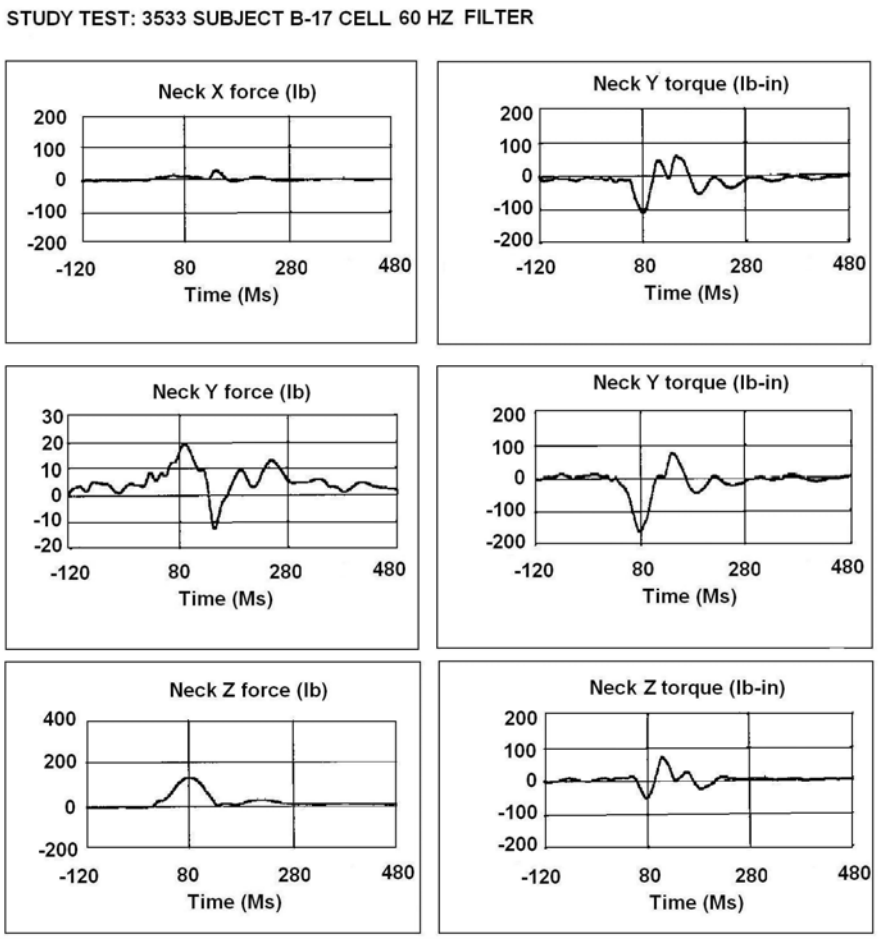

Figure 5.6: Typical forces and moments generated from the experimental data after 12 Gz acceleration, (Sadegh 1995).

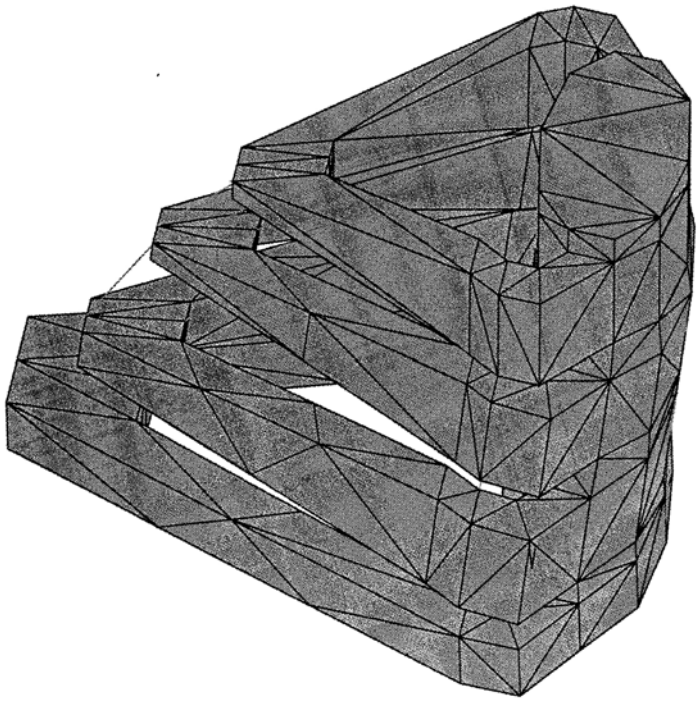

Figure 5.7: Segmental elastodynamic model (C5-T1).

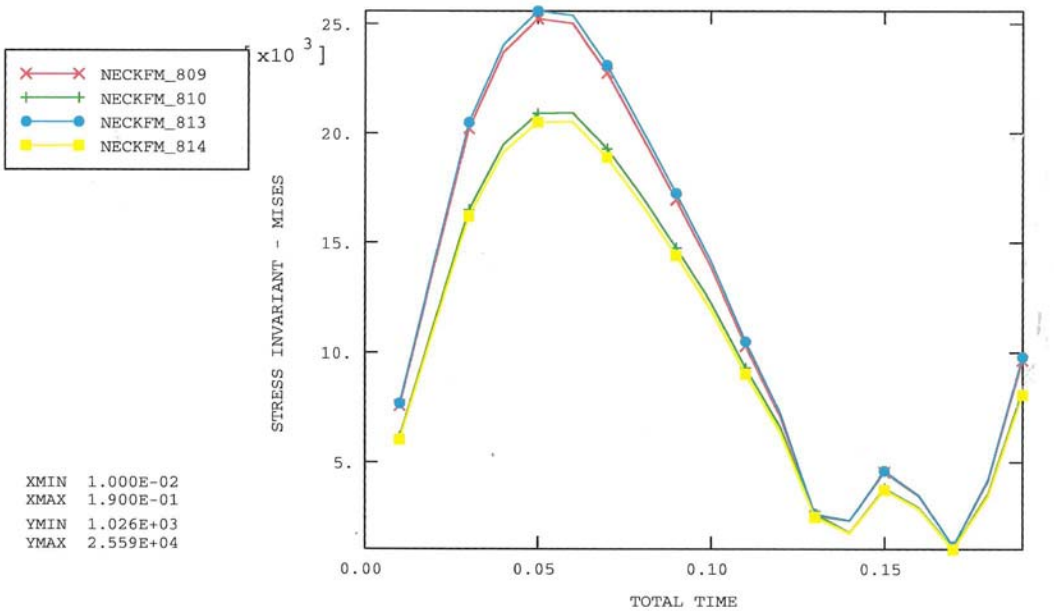

Figure 5.8: Maximum von Mises stress (KN/m^2) on selected anterior elements of the elasto dynamic (C5-T1).

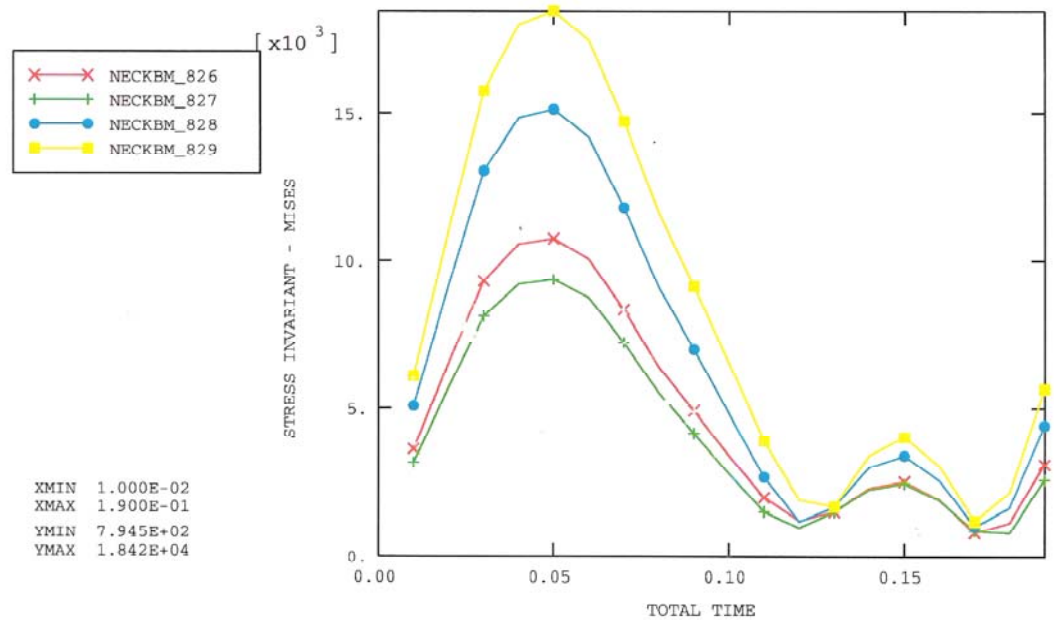

Figure 5.9: Maximum von Mises stress (KN/m^2) on selected posterior elements of the elasto-dynamic (C5-T1)

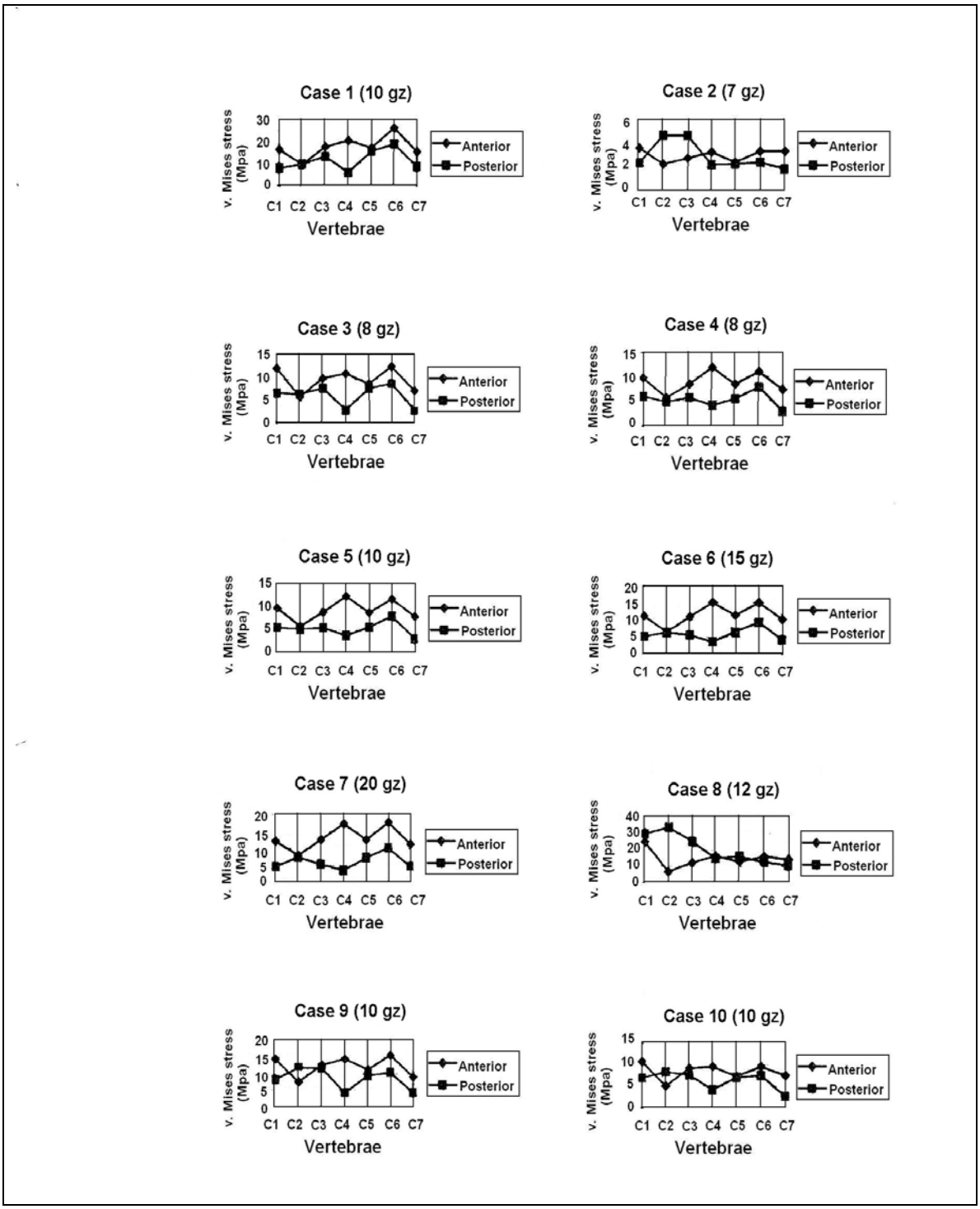

Figure 5.10: Maximum von Mises stresses in the posterior and anterior part of the vertebrae, the viscoelastic model.

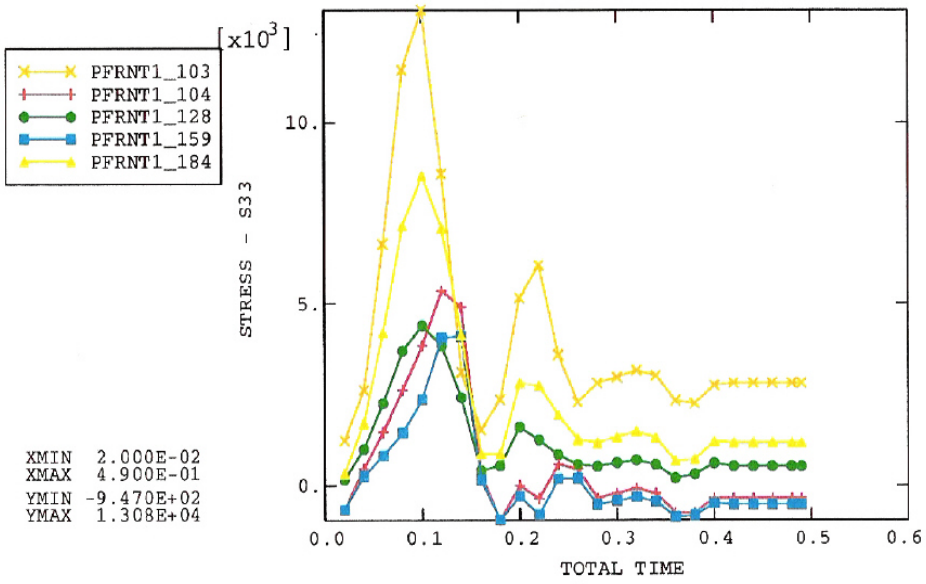

A: Anterior element

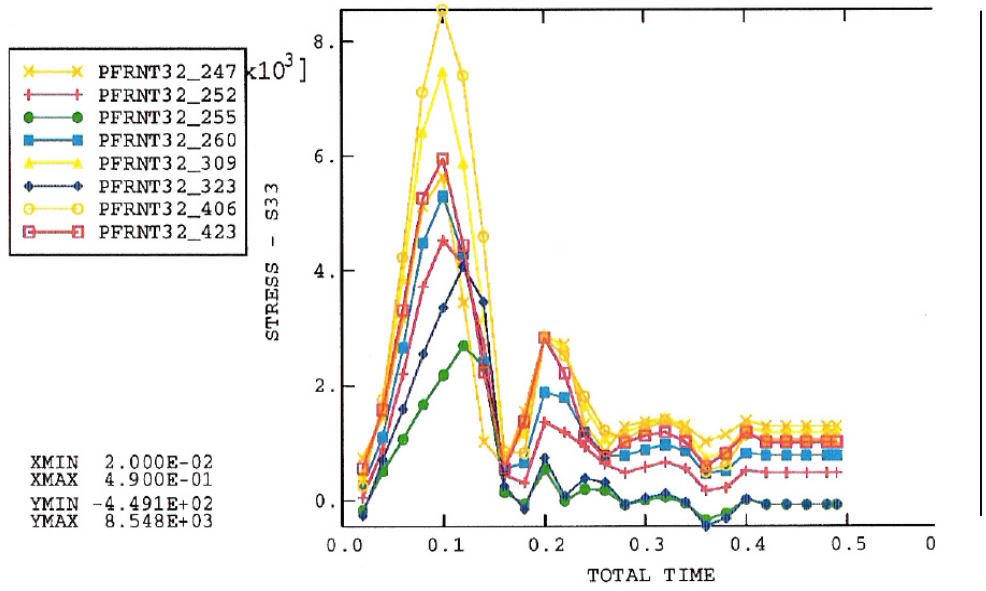

B: Posterior element

Figure 5.11: Maximum von Mises stresses (KN/m^2) in the posterior and anterior part of the vertebrae.

Positions	Explanation
1 to 3	Spinous process ligaments
4 & 5	Articular facets
6 & 7	Anterior and posterior longitudinal ligaments

Table 5.1: Beam connection number representing ligaments (ref. Figure 5.2).

	E- Modulus (MPa)	Poisson's ratio υ	Diameter Φ (mm)
Muscles	10	.38	10
Ligaments	15	.038	1.5
Discs	90	0.4	-
Vertebrae	2000	0.3	-

Table 5.2: Material properties of the spinal components.

Region	Dvorak (1988)	White and Panjabi (1990)	Penning (1978)
C1-C2		22.4	30
C2-C3	10	10	12
C3-C4	15	15	18
C4-C5	19	20	20
C5-C6	20	20	20
C6-C7	19	17	15
C7-T1		9	

Table 5.3: Average total flexion/extension rotations in degrees of healthy adults. (The cervical spine 1998).

Muscles			Ligaments			Vertebrae		Discs		Displ.
E-Modul (Mpa)	Poisson's ratio (ν)	Diameter ϕ (mm)	E-Modul (Mpa)	Poisson's ratio (ν)	Diameter ϕ (mm)	E-Modul (Mpa)	Poisson's ratio (ν)	E-Modul (Mpa)	Poisson's ratio (ν)	Max. Flexion (mm)
35	0.45	20	25	0.45	4	2000	0.3	100	0.4	32.5
35	0.45	20	15	0.45	4	2000	0.3	90	0.4	35.5
30	0.40	15	10	0.40	4	2000	0.3	90	0.4	50.57
20	0.40	15	20	0.40	4	2000	0.3	90	0.4	48
20	0.40	15	20	0.40	4	1800	0.3	90	0.4	49.3
15	0.40	15	15	0.40	4	1800	0.3	90	0.4	50.37
10	0.40	15	15	0.40	4	1800	0.3	80	0.4	54.4
10	0.40	15	10	0.40	4	1600	0.3	80	0.4	57.65
10	0.38	15	10	0.38	4	1600	0.3	80	0.4	63
10	0.38	15	10	0.38	2	1600	0.3	80	0.4	65.5
10	0.38	15	15	0.38	2	2000	0.3	90	0.4	56.3
10	0.38	15	15	0.38	2	1800	0.3	90	0.4	58
10	0.38	10	15	0.38	1.5	1800	0.3	90	0.4	58.5
10	0.38	10	10	0.38	1.5	1800	0.3	90	0.4	58.72
10	0.38	10	10	0.38	1.5	1600	0.3	80	0.4	66
10	0.38	10	15	0.38	1.5	2000	0.3	90	0.4	57.09
10	0.38	10	10	0.38	1.5	2000	0.3	90	0.4	57.09

Table 5.4: Validation of the preliminary model (*shaded row represents selected values***)**

Case number	Subject	cell	Acceleration
1	C-8	CB	10 gz
2	C-17	A	7 gz
3	B-9	A	8 gz
4	B-17	A	8 gz
5	C-17	B	10 gz
6	B-17	A	15 gz
7	B-17	A	20 gz
8	E-4	A	12 gz
9	C-17	B	10 gz
10	E-4	B	10 gz
11	B-17	C	12 gz

Table 5.5: Cases studied and acceleration measured for subject and cell numbers.

Shear relaxation (MPa)	Bulk relaxation (MPa)	Relaxation time (sec.)
G1 = 0.3991	K1 = 0.700	T1 = 3.4519
G2 = 0.3605	K2 = 0.149	T2 = 2000
G3 = 0.1082	K3 = 0.150	T3 = 7000

Table 5.6: Viscoelastic properties of discs and ligaments (Visarus, 1994).

Case	Accel.	Time (Ms)	Max. Principal Stresses (MPa)*	Max. v. Mises (MPa)*
1	10 gz	50	-26.0 +12.6	24.4
2	7 gz	100	-0.94 +5.41	5.82
3	8 gz	100	-7.08 +17.4	16.2
4	8 gz	100	-11.0 +20.2	19.3
5	10 gz	100	-10.7 +21.4	20.4
6	15 gz	200	-9.83 +24.2	23.3
7	20 gz	100	-8.97 +27.1	26.3
8	12 gz	200	-11.0 +34.9	36.1
9	10 gz	100	-9.8 +15.1	19.8
10	10 gz	100	-7.36 +12.9	12.5
11	12 gz	100	-4.83 +7.69	6.32

*** Values correspond to the first peak values.**

Table 5.7: The maximum stresses calculated at the given time, for all 11 viscoelastic cases studied.

6. THE NON-LINEAR ELASTIC MODEL

This chapter presents the creation and the validation of a new sophisticated model of the complete cervical spine. This model will be used in the subsequent chapters 7 and 8 to verify the two hypotheses of this research by investigating sport injuries and partial discectomies and fusion in the cervical spine

6.1 Model creation

An accurate 3-D FEM of the human cervical spine, see Figure 6.1, was created using digitized geometrical measurements of the vertebral bodies. This model improved upon previous model of Sadegh et al. 1997, (Figure 3.9), by accounting for digitized and accurate geometrical shapes of vertebrae, detailed meshing and for the inhomogeneous material properties of the vertebrae and discs. Specifically, each vertebra consists of two cartilaginous end plates, a cortical shell and a cancellous core each of which had individual material properties. Each disc, in this model, consists of an annulus surrounding a gel-like nucleus. The major ligaments, namely the posterior longitudinal ligaments (PLL), the anterior longitudinal ligaments (ALL), the capsular ligaments (CL), the intraspinous ligaments (ISL) and the ligamentum Flavum (LF) are also included.

Each vertebra, see Figure 6.2, was carefully created using the geometry data obtained from actual (molded) vertebrae in combination with the data published by Liu et al. (1982). The relative orientations and positions of the vertebrae were carefully generated to reflect the anatomical neutral orientation of vertebrae in a cervical spine (The Cervical Spine, 1998). The endplates and the discs**,** see Figure 6.3, were then constructed to fill the space between the bodies of adjacent vertebrae.

The material and/or physical properties are given in Table 6.1, Table 6.2 and Table 6.3 and are adopted from previous validated finite element and experimental studies of the cervical spine (Grossheim, 1989, Kumaresan, 1997, Pintar, 1986). The physical and material properties of the major muscles are given in Table 6.1. Table 6.2 gives the material properties of the vertebra (cancelous and cortical bone) and disc (annulus, nucleus and fibers), and Table 6.3 gives the non-linear spring characteristics (forces versus elongation) of the ligaments.

During the meshing phase of the FEM, the cortical shell, Figure 6.4 was first created at the surface level of the solid geometry. The solid elements of the core were then generated inside the shell. Mapped mesh was then used to create the end plates, the nucleus and the annulus. The ligaments were then carefully attached to their corresponding location. The contact elements were subsequently and automatically created between opposing articular facets. The model has 19480 eight-node solid elements, which partly represent the cancellous core part of the vertebrae, the annulus and nucleus of the disc, and the cartilaginous endplates. A total number of 7617 four-node 3-D shell elements (1 mm thickness) were used to model the cortical shells of the vertebrae. The ligaments are represented with 294 two-node 3-D non-linear spring elements with zero compression. Three-dimensional surface contact elements (960 in total) are used for the contact and sliding effect between the articular facets. The fibers of the annulus of the disc are also modeled with tension only cable elements, a method proposed by Shirazi et al. (1984), and adopted by Maurel et al. (1997). The major muscles, Table 6.1, are modeled with zero-compression cable elements and attached to the vertebrae according to the model of Deng and Goldsmith, (1987), (Figure 2.11).

The finite element software ANSYS 5.6 from ANSYS, Inc. was used to generate the geometry, the finite elements and for validation which is presented in following section.

6.2 Validation of the non-linear-elastic model

The first step in the validation process was to evaluate previous experimental and analytical techniques of other investigators to determine their applicability in obtaining load-displacement responses of the complete cervical spine. The method that seemed most suitable and easily replicable was that used by Moroney et al. (1988). Moroney tested individual Functional Units (FU) consisting of two adjacent vertebrae, (C2-C3, C3-C4, C4-C5, C5-C6, C6-C7 and C7-T1), their intervening disc, and their interconnecting soft tissues. Five primary and coupled loads (compression, compression-flexion, compression-extension, compression-lateral bending and compression-axial rotation) were applied separately, and the resulting displacements and rotations for each individual Functional Unit were measured. A compressive force of 73.6 N and a moment of 1.8 Nm were used in the experiment.

The current FE model was validated with experimental data in terms of the force-displacement and moment-rotation responses. Pure compression, compression-flexion and compression-extension, compression-bending and compression-torsion loading conditions were considered for validation. The complete cervical spine model was divided into six individual Functional Units (C1-C2, C2-C3, C3-C4, C4-C5, C5-C6, C6-C7), a typical functional unit is shown in Figure 6.5. The inferior vertebra of each

Functional unit was constrained in all directions. A rigid plate was created on top of the superior vertebra for applying the load and the moment. The rigid plate was created symmetrical with respect to the coordinate system. The compressive force was applied as a single force at the center of the superior surface of the plate. For flexion, extension, lateral bending and torsion moments, a couple of forces was applied in the respective governing direction. All the loading and boundary conditions adopted in the model were similar to the experimental setup of Moroney et al. (1988). He mounted each motion segment so that the inferior vertebra was rigidly attached to the base of the testing apparatus and the superior vertebra was free to move in response to the applied loads. The analysis included the effect of geometric (large deformation) and material non-linearities. The computed force-displacement and moment-rotation responses were compared with experimental results under similar loading (Clausen et al., 1996 and 1998, Maurel et al., 1997, Moroney et al., 1988, Panjabi et al., 1986 and Shea et al., 1991). The moment-rotation responses of the FEM were validated with experimental data under pure flexion and extension (Fuller et al., 1998, Moroney et al., 1988, Panjabi et al., 1986).

The comparison of the moment-rotation response of the model with experimental data is shown in Table 6.4. The moment-rotation responses of the FE model are within the range of the experimental results under corresponding loading mode. The FEM model is less stiff, when comparing the data obtained to those found by the Moroney's team in axial rotation. The value of less than 2 degrees rotation that they published seems low. When comparing the responses of the model with the data published by the Panjabi's group, beside the lateral bending response, the results match better. But it is worth

noticing that the lateral bending response reported by the Panjabi's team has a very large deviation.

The six validated functional units were stacked back together to reconstitute the complete cervical spine model and then the global response of the model was validated. For this purpose the experimental setup and data published by David A. Fuller et al., 1998, were used. The model (C2-T1) was completely fixed at the T1 level and subsequently flexed and extended 20 degrees and 10 degrees, respectively, in the sagittal plane. The distributions of motion across vertebral segments were recorded and compared to those obtained by Fuller under similar boundary conditions. The summary of the experimental and analytical values is presented in Table 6.5. The rotational responses of the FE model across the vertebral segments are within the range of the experimental results.

These extensive validations of the FEM in terms of moment responses and rotation responses with experimental data under primary and coupled loadings provide solid and valued confidence in using the model for biomechanical studies.

The validated finite element model was employed in the following two chapters to: 1) to simulate sport accidents that are associated with high flexion generated in the cervical spine, and, 2) to study the effect of segmental partial discectomies on the stress changes in the neighboring discs after complete fusion.

6.3 Figures and tables list

Figures:

Tables:

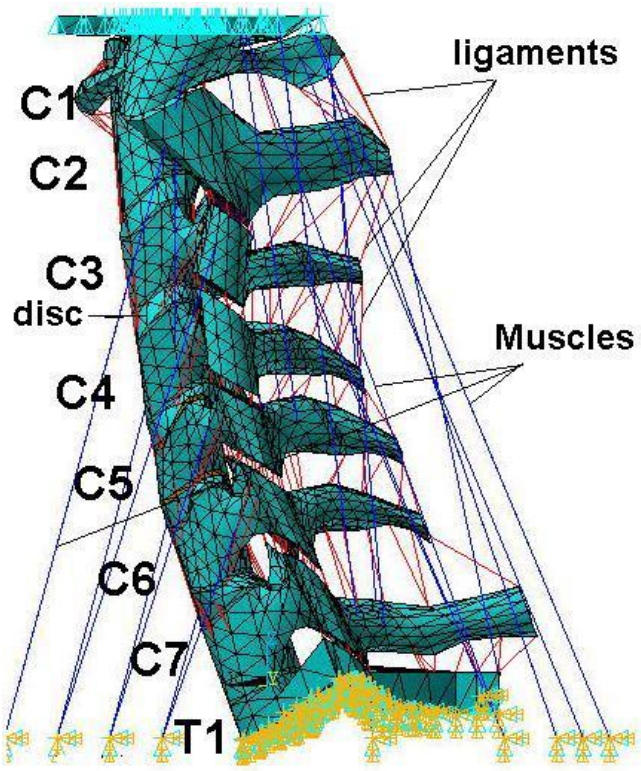

Figure 6.1: The 3-D Finite Element Model (FEM), lateral view.

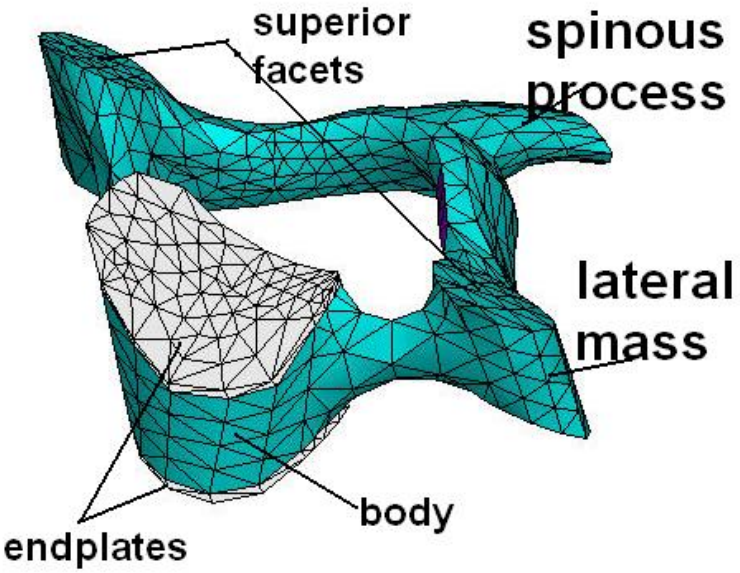

Figure 6.2: Typical vertebra of the FE model.

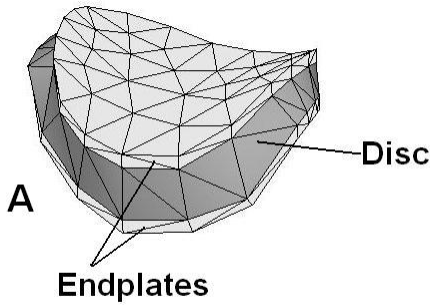

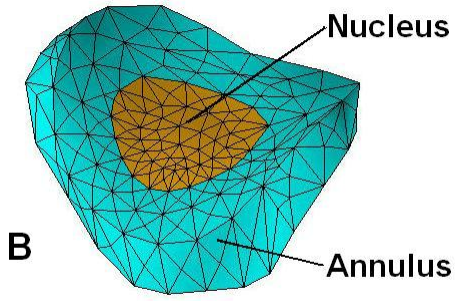

Figure 6.3: Typical disc of the FE model.

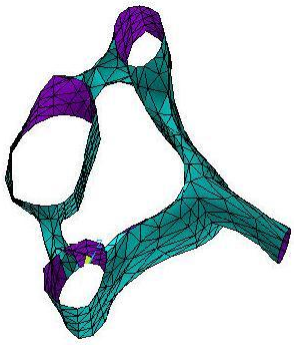

Figure 6.4: Typical cortical shell of the vertebra.

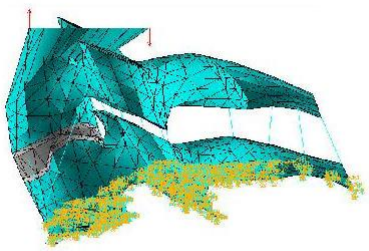

Figure 6.5: Typical Functional Units (FU) used for the FE model validation.

Muscle	Average cross-section (mm^2)	E-Modulus (Mpa)	Poisson's ratio (v)
Sternocleidomastoideus	358.6	65	0.39
Longus capitis	200	65	0.39
Longus colli	200	65	0.39
Scalenus anterior	165.6	65	0.39
Scalenus medius	43.6	65	0.39
Scalenus posterior	136.0	65	0.39
Trapezius	350.0	65	0.39
Splenius Capitis	224.4	65	0.39
Splenius capitis	84.7	65	0.39
Spinalis Capitis	80.0	65	0.39

Table 6.1: Physical and material properties of the major muscles of the cervical spine (de Jaeger, et al. 1994).

Components	Elements Type	Young's Modulus (MPa)	Poisson's Ratio
Cortical shell	3-D Shell	12000	0.29
Cancel. core	Solid 4-node	100	0.2
Endplate	Solid 4-node	500	0.4
Disc annulus	Solid 4-node	3.4	0.45
Ann. fibers	Cable 2-node	500	0.3
Disc nucleus	Fluid 4-node	3.4	0.49

Table 6.2: Elements types and material properties of the spine soft- and hard-tissues used in the Finite Element Model.

ALL		PLL		ISL		LF		CL	
Def. (mm)	F (N)	Def. (mm)	F (N)	Def. (mm)	F (N)	Def. (mm)	F (N)	Def. (mm)	F (N)
1.4	12	1.0	9.65	1.3	4.2	1.9	6.7	1.8	6.7
2.7	18	2.0	17.15	2.7	6.1	3.9	11	3.9	11
4.1	22.5	3.0	23.76	4.0	7.4	5.8	13.7	5.8	13.7
5.4	27.15	4.0	28.60	5.4	8.2	7.7	15.7	7.7	15.7
6.8	30	5.0	31.60	6.7	8.8	9.7	16.85	9.7	16.85

ALL: Anterior Longitudinal Ligament
PLL: Posterior Longitudinal Ligament
ISL : Intraspinous Ligaments.
LF : Ligamentum Flavum
CL : Capsular Ligament.

Table 6.3: Values of deformation versus force (nonlinear spring) for Ligaments properties (Grossheim 1989; Pintar 1986)

	Rotation in degree (Deviation))		
Loading Mode	Moroney Degree (deviation)	Panjabi Degree (Deviation)	Current Model Degree
Flexion	5.5 (1.84)	6.1 (3.9)	5.56
Extension	3.52 (1.94)	3.3 (1.8)	3.90
Lat. Bending	4.71 (2.99)	5.8 (5.7)	3.1
Axial Rotation	1.85 (0.67)	3.8 (1.4)	4.43

Table 6.4: Validation of the Finite Element Model with experimental data (Moroney et al., 1988, Panjabi et al., 1986) Average angular of the Functional Spine Units. (M = 1.8 Nm , F=73.6 N (compression))

	Segmental Range of Motion	
Vertebral segment	Fuller Degree (Deviation)	Current Model Degree
C2-C3	4.0 (1.4)	5.49
C3-C4	6.1 (0.2)	5.73
C4-C5	6.4 (1.2)	5.46
C5-C6	8.2 (0.8)	6.73
C6-C7	5.1 (1.5)	6.80
C7-T1	2.2 (0.5)	2.79
Total	**32.0 (0.8)**	**33.00**

Table 6.5: Validation of the Finite Element Model with the experimental Data (Fuller et al., 1998): Range of Motion between adjacent Vertebrae after 20° / 10° (flexion /extension) of the complete cervical spine model.

7. SPORT INJURIES AND SPINAL INSTABILITY

In this chapter, the mechanism of two sport injuries, namely diving and football, will be investigated. These two completely different traumatic situations are correlated to similar type of injury that could render the cervical spine clinically unstable. A clinically unstable spine could have severe consequences such as spinal cord injury and paralysis.

7.1 Introduction

The new model presented in chapter 6 is utilized to investigate two cases of cervical spine injuries resulting from hyper-flexion and compression-flexion loadings. The simulated injuries could result from recreational and professional contact and non-contact sport accidents such as motorcycle vaulting, football and diving accidents. The correlation of these types of loadings to the clinical instability of the spine and disc herniation injuries is examined, by assessing the possibility soft tissue injuries and the relative displacement of the hard tissue.

Crowell et al. (1993) found that injury to the posterior ligaments is possible in the absence of lateral flexion or axial rotation. Their in-vivo studies indicated that flexion moment of 11.6 Nm caused failure. Bauze et al. (1978) simulated, using compression load, bilateral dislocation in flexed cadaver cervical spine constrained at C5-T1 level. They concluded that compressive load on the head when the head is in flexion causes forward dislocation at C4-5 vertebrae. Maiman et al. (1983) was able to produce posterior ligament injuries in flexion and compression. Most catastrophic cervical spine injuries occur with impact loading (Viano et al., 1989). The major loading mode and the

associated type of forces generated in the neck during the impact are directly related to the impact direction, the impact location and to the orientation of the neck.

While studying catastrophic football injuries, Torg (1982) recognized that when the neck is straightened in a tackle position, flexion-compression and axial loadings are frequent mechanisms of injury. While the training methods and protecting gears have improved, neck injuries following head impact remain frequent accidents among professionals and amateur players. The hyper-flexion and compression-flexion injuries are common in football accident, motorcycle vaulting accident, automobile and diving accidents.

The correct evaluation of the severity of damage to the spinal components is crucial to the selection of appropriate treatment and the future health of the patient.

7.1.1 Biomechanics of the clinical instabilty

Moments and forces generated in the neck during accidents cause the spinal components to move relative to each other and subject them to higher internal stresses and strains. Excessive relative displacement among the vertebrae would render the spinal column clinically unstable. A spine is considered clinically unstable if it exhibits abnormal displacement under physiological load. That is, a clinically unstable cervical spine will need medical intervention such as surgery to restore its normal physiological and biomechanical functions. A clinically stable injured spine, to the contrary, will heal naturally through exercises and therapy. Clinical instability of the lower cervical spine is associated with the history of injuries related to flexion-compression, interspinous widening, facet joint subluxation, vertebral compression fractures and loss of normal

cervical lordiosis, which leads to pain and neurological dysfunction (The Cervical Spine 1998). White and Panjabi developed a checklist with a point scoring system aimed at diagnosing clinical instability (The Cervical Spine 1998). They proposed that the spine be declared clinically unstable if, in flexion-extension motion, the relative saggittal plane translation of adjacent vertebral bodies exceeds 3.5 mm and their relative saggittal plane angulation exceeds 11 degrees. Although unilateral facet dislocation may cause enough foraminal encroachment (in anterior translation) to result in nerve root symptoms, it may not be enough ligamentous damage to render the Functional Spine Unit (FSU) unstable.

Although the image techniques have enhanced the understanding and evaluation of neck injuries, misdiagnosis or non-detection of clinical instability and disc herniation are still of major concerns among radiologists. The biomechanics of the load and the injury mechanisms that could lead to an unstable spine is not well documented. Recent research (Edwards et al., 2001) showed that the failure criteria for evaluating disc injuries are still lacking and the location of the maximum stress in intervertebral disc is independent of the loading mode.

The following sections will describe the simulation of the hyper-flexion accident (football) followed by the simulation of the compression-flexion accident (diving). The results of both simulations will then be presented followed by their discussion and conclusions.

7.2 Hyper-flexion injuries

This case simulates the sudden and dramatic forward push (hyperflexion) of the neck during contact sport such as football or posterior impact of the head with a hard

object, for example, vaulting landing of a motorcyclist in an accident. In a football game, it is conceivable that, the ball-carrying player falls, and while laying on his back with his head raised, he is impacted at the helmet level by the knee of the tackling player, Figure 7.1. As a result of this impact a major shear forces is applied on the upper cervical region. A generated hyper-flexion moment combined with the applied shear forces could cause vertebral anterior displacement, subluxation and/or rotation (Onan et al., 1998). The magnitude of the shear force generated will depend on the acceleration of the impacting player and the duration of contact. The moment generate will depend on the location of impact and on the initial raised position of the head.

While investigating the effect of the height of the head rest during rear-end impact automobile accidents, Tencer et al. (2002) found that, the average shear force recorded in the cervical spine, in a head to head-rest rebound impact, was about 225 N at about 180 ms. In other studies, Crowell et al. (1993) flexed C2-C3-C4 spinal segment specimens at a mean angle of 25 degrees. They were able to generate 11.6 Nm flexion moment and an average shear force of 125 N, which caused ligamentous failure. McElhany et al. (1988) studied the bending responses of unembalmed human cervical spine segments. They reported that the maximum failure moment ranged from 3.4 to 14.6 Nm, and the maximum axial force was between 192 and 388 N.

Taking into consideration the forces used and the results of these reviewed studies, and knowing that a human thigh is about 1/6 of the bodyweight, the impacted shear force that the player would sustain is about 120 N. This is of the same of magnitude as forces used by Shea et al. (1991) and McElhany et al. (1988) for quasi-static analysis. The shear force was applied as three anterior-posterior forces to C2, C3 and C4 in such a

way that, they generated a total hyper-flexion moment of 10 Nm at T1. This flexion moment is about the average of the moments reported by McElhany et al. (1988) and Crowell et al. (1993). That is, three horizontal forces; 38.3 N, 37 N and 47.8 N were applied saggitally to C2, C3 and C4, respectively. The model was completely fixed at the T1 level. The analysis considered the large deformation and the non-linearity of the model. It also assumed a quasi-static application of the forces and moment in five equal and progressive steps. The graphical results are shown in Figures 7.2 and 7.3 and are explained in the results section.

7.3 Compression-flexion injuries

In this simulation the responses of the cervical spine to compression-flexion loads are studied. In pure compression trauma the force is generally transmitted along the axis of the vertebral bodies, when the cervical column is flexed and held almost straight. If the force is transmitted purely along the axis of the vertebral body, it may cause the rupture of the endplate and force the disc into the body of the vertebra and subsequently lead to the so-called burst fracture (Figure 4.1D, Holdsworth, 1963). However, as illustrated in Figure 7.4, with the head in ducking position, where the neck is flexed and the lower vertebrae C6 and C7 are not aligned with the upper cervical column, compression and flexion mechanisms are both present.

According to the statistics about 12 % of spinal cord injuries cord are associated with diving accidents. Diving accidents are attributed to insufficient water depth at the point of the dive. In shallow water, the head of the diver comes in contact with the bottom of the water at the point of dive. The neck is in ducking position and is being

compressed between a pushing torso and a fixed barrier (Figure 7.4). Injury will result from the fact that, the weight of the torso and of the lower limbs generates compressive load to the neck through the lower cervical vertebrae, C6 and C7, which are in alignment with the thoracic spine. As illustrated in Figure 7.4, the generated compressive force is located posteriorly at a certain eccentricity with respect to the upper cervical spine. The compression force, with the eccentricity, generates flexion moment in the cervical column. The entrapped head will tend to slip forward. The resulted flexion and forward movement of the head will add rotation and anterior displacements to the vertebrae movements.

Bauze et al. (1978) conducted an experimental study of the diving accident using cadaver cervical spine. They fixed human cadaver neck between two parallel platforms. A cylindrical bar was passed through the vertebral arches of C7, C6 in order to maintain both vertebrae fixed and aligned. Both vertebrae were free to move in inferior-superior direction. Compression forces were applied at the bottom of the C7, attached to the mobile lower platform. The vertebra C1 was attached to the fixed upper platform, and was free to move in the saggittal plane. The flexion of the neck specimen was recorded at different load, the maximum load obtained at the rupture of the posterior (capsular, inter-spinous, longitudinal) ligaments was 145 Kg. Nevertheless a significant amount of flexion rotation was well visible at 30 Kg compression load.

In simulating the Bauze et al. (1978) experimental setup, the lower part of the FE model (T1, C7 and C6) was constrained in saggital anterior-posterior and lateral translation directions and was free to translate in the inferior-superior (cranial) direction. This restraining setup simulates the alignment of C6 and C7 with the thoracic spine. The

rigid top plate sitting on C1 was only constrained in the vertical direction and was free to move in other directions. This simulates, for example, the head contact and reaction with the ground (floor) of the swimming pool. The analysis considered the large deformation and the non-linearity of the model.

A second simulation was considered with C1 and C2 also constrained. It was assumed that in ducking situation the vertebrae C1 and C2, which make up the upper axis, are aligned and will jam together after traumatic impact. In this case, T1, C7 and C6 were still constrained in saggital anterior-posterior and lateral translation directions and were free to translate in the inferior-superior (cranial) direction. The vertebrae C1 and C2 were constrained in inferior-superior direction but were free to move in other directions. The same compressive loads, 450 N (100 lbs) were used for both simulations and were quasi-statically applied at the inferior part of the body of T1, in six progressive steps. In both simulations, bottom only constrained and top and bottom constrained, the stresses and strains in the discs and the translational and rotational displacements of the vertebrae were recorded and analyzed.

7.4 RESULTS

7.4.1 Rotational and translational displacement of the vertebrae

In assessing the external responses (forward translation and saggital plane rotation) of the cervical spine for the cases simulated in this study, the relative anterior displacement of a vertebral segment was defined as the change in sliding distance between the articular facets of two adjacent vertebrae. The angular rotation was recorded as the relative change in the angle between the spinal processes of two adjacent vertebrae.

An illustrative display of the results of the hyperflexion (football) injuries simulation is showed in Figures 7.2 and 7.3. The overall results show that the mid-cervical vertebrae C3, C4, C5, and C6 experienced the most rotational and translational displacements. A closer analysis of the segment C4-C5 revealed that the relative forward translation between the vertebrae C4 and C5 was about 3 mm and the relative rotation was about 7.5 degrees. When considering the segment C5-C6, vertebra C5 translated approximately 3.45 mm and rotated about 11.5 degrees with respect to C6 (see details 1, 2, 3 on Figure 7.4).

The summary of the results for compression-flexion (diving) injuries simulation, with the model only constrained at C6-C7, is given in Figure 7.5 and Figure 7.6 at 300 N and 450 N compressive loads. Figure 7.6 illustrates the posterior-anterior displacement of vertebrae C3, C4 and C5, while Figure 7.7 shows the angular rotation of the same vertebrae at 300 N and 450 N. The results show that C3 experiences the largest forward absolute displacement at all the load steps and C4 experienced the biggest absolute saggital plane rotation. When the model was constrained at C6-T1, the maximum relative displacement obtained using sliding distance between the articular facets was 3.25 mm between C4 and C5. Also the maximum relative rotation, measured between vertebral spinous processes, was 5.5 degrees between C3 and C4 at the maximum load of 450 N. For situation where the model was constrained at C1-C2 and C6-C7 segments, the maximum absolute forward displacement was about 2.50 mm between vertebrae C4 and C5 and the maximum sagittal relative rotation of about 6.7 degree was recorded between C5 and C6. A magnified view of the displacements showed a bilateral dislocation between C5 and C6 and progressive compression between C2, C3 and C4 at the facets

levels. The deformed condition showed that the posterior portion of the disc23 and disc34 is subjected to higher compressive stresses while the anterior portion of these discs carried high tensile stresses. Note that the intervertebral discs are labeled disc**xy** where **x** and **y** represent the vertebrae Cx and Cy interconnected by the designated disc.

7.4.2 Stresses and strains of the discs

The maximum stresses and strains for the current simulations are showed Figures 7.7 – 7.9. The analysis of the results revealed that the posterior-lateral and the lateral regions of the annulus experienced the higher stresses and strains. When comparing the results of the compression-flexion simulations, the values of the compressive stresses were of the same order of magnitude for the two assumed constrains and the locations of the maximum values barely varied, Figures 7.7 B and C. The stress in disc23 is dominantly compressive. The location of the maximum von Mises stress was in the left inferior-posterior lateral portion of the annulus for compressive load up to 300 N. Then it changed to the right posterior-lateral superior portion of the annulus.

The results of disc34 and disc45 showed that, the right posterior-lateral and superior region of the annulus exhibit the maximum von Mises stresses. The posterior portion of the annulus of disc34 experienced compressive stress and its anterior portion experienced tensile stresses. The overall conclusion is that, the stress in disc45 was mainly compressive.

The results of disc34 and disc45 showed that, the right posterior-lateral and superior region of the annulus exhibit the maximum von Mises stresses. The posterior portion of the annulus of disc34 experienced compressive stress and its anterior portion

experienced tensile stresses. The maximum von Mises stress in disc56 was located in the medial lateral region of its annulus.

7. 5 Discussion and conclusion

Two cases of contact and non-contact sport accidents were simulated and the possible resulting injuries were assessed using the external and the internal responses of a cervical spine model. High stresses in soft- as well as in hard-tissues and abnormal displacement between the cervical spine components could lead to disc herniation and/or other injuries that could render the neck clinically unstable. The current studies showed that, the locations of the maximum stresses in the discs, after compression-flexion and hyperflexion trauma, are almost identical. These findings are in agreement with the works of Edwards et al. (2001), who reported that the location of the higher stresses was independent of the loading mode.

For the first simulated injury, where the spine was subjected to shear/flexion, it was observed that 120 N posterior- anterior shear force which generated a flexion moment of about 10 Nm, created 3 mm anterior facets displacement and about 7.5 degrees rotation at C4-5 level. Furthermore, vertebra C5 translated about 3.40 mm and rotated about 11.5 degrees with respect to vertebra C6. Keeping in mind that the sliding translation was obtained at the facet level, which has a saggital plane orientation of about 45 degrees, the overall translation of the vertebra is therefore smaller, and the maximum translation of C5 with respect to C6 would be about 2.4 mm. Thus, although vertebra C5 rotated almost to the limit of clinical instability set by White et al. (1990), it cannot conclusively be said that the model was clinically unstable. Nevertheless the internal

responses of the discs showed that, disc45 and disc56 experienced high stresses and forward (x-direction) strains. The von Mises stress in disc45 changed from 0.75 MPa at 2.5 Nm flexion moment to about 2.4 MPa at 10 Nm flexion moment. Disc56 had about 2 MPa stress at 10 Nm flexion moment. Adams et al. (1988) measured the ultimate tensile strength of the annulus to be 3.2 MPa. Other measurements have recorded the failure tensile strength of the annulus to be 1.4 MPa (White et al. 1990). If the failure range of 1.4 MPa- 3.2 MPa is considered, it can be concluded that disc45 would be the first disc to fail at a flexion moment closed to 5 Nm, followed by the disc56, which would fail at about 7.5 Nm (Figure 7.7 A). The maximum stress of both discs was located in the lateral posterior portion of the annulus. This location is clinically observed as the location where the disc mostly herniates. Disc23, disc34 and disc67 have maximum stress below the failure range values. Studies (Cox et al., 2001, Edwards et al., 2001, Pooni et al., 1986, Pratt et al., 1990) have showed that herniated discs are frequently misdiagnosed. Based on the stress in the discs and the assessment of the instability, the current studies showed that in hyper-flexion the absence of instability does not exclude the fact that stresses in discs could be damaging.

For the diving injuries (compression-flexion) simulations, two cases were considered; the first case assumed free movement of the head after ducking and the second case assumed the jamming (locking) of the upper vertebrae (C1-C2) after ducking. The evaluation of the clinical instability for both cases was inconclusive. With a maximum compressive force of 450 N, which is about 65 % of the body weight of normal person, the model (fixed at the bottom end) delivered about 6.7 degrees rotation and about 1.8 mm displacement between C5 and C6. Although the model was used in a

neutral position, the compressive load was applied off the neutral axis so that it could generate flexion moment. A magnified plot of the displacement solution confirmed the pattern of dislocation following instability as demonstrated by Bauze et al. (1978). Bauze demonstrated clinically that straightened cervical spine can have ligamentous failure and dislocate when it is flexed and is subjected to high compressive load. Bauze also observed that by 300 N, which was almost one fifth of the maximum force obtained during his studies, the cadavric spine had already experienced significant deformation. Flexion deformation of the traumatized neck can lead to spinal cord deformation and elongation of the neural axis. The maximum stresses and strains values for current simulations were obtained at a maximum compressive load of 450 N. Disc45 and disc56 experienced almost the same forward displacements for the two ducking simulations: the model constrained at T1-C6 only, and the model constrained at both T1-C6 and C1-C2. The values of these displacements reduced by almost 50% when the model was constrained at both ends (Figure 7.8 B and 7.8 C). Disc45 and disc56 also experienced the maximum stresses when the model was constrained at the bottom ends. Nevertheless, these maximum stress values, which were about 3.2 MPa were comfortably below the failure compressive strength of 10.3 MPa reported by Adams et al. (1988), with an ultimate compression of 35%.

Although the compressive stresses are low, the forward (x-direction) total strains were about 50% and 30%, Figures 7.8 B and 7.8 C, when the model was constrained at the bottom and at both ends, respectively. Because the model is non-symmetric, the results also provided lateral strain of up to 8%, which combined with other strains could be good indication of discs to bulging and/or herniation. When the model was

constrained at the both ends, (ducking and jamming of the upper vertebrae) the results showed that, there were less internal and external responses compare to when it was constrained only at the bottom end. This may suggest that after an impact in a ducking position, the jamming of the upper vertebrae slows the anterior-posterior movement of the neck and therefore the rotation the vertebrae. This would diminish the probability of facets dislocation and the subsequent instability, but at the same time it would increase the compressive strain and stress that could lead to disc herniation. The deformed shape of results showed potential bilateral dislocation between C5 and C6 and a progressive compression between C2, C3 and C4 at the facets levels. The deformed condition also showed that the posterior portion of the disc23 and disc34 was subjected to higher compressive stresses while the anterior portion of these discs was carried high tensile stresses. The situation would probably increase the risk of the posterior herniation of the disc and/or the anterior separation between the annulus and the endplates. The results further showed that the maximum stresses in C2, C3 and C4 vertebrae are mainly located around the lateral processes and the bodies. Studies (Adams et al. 1988) have shown that when high compression forces are associated with flexion, the risk of the sudden prolapse of the nucleus increases. Adams et al. (1988) reported that, hyperflexion stretches and thins the posterior annulus, making it the weakest structure surrounding the nucleus. A high compressed nucleus then experienced high hydrostatic pressure and bursts through the weak posterior annulus. The average compressive load for the sudden disc prolapse in the lumber spine as reported by Adams et al. (1988) was 5400 N. This amount of force can easily be reached in impact situation. Disc posterior herniation is one of the frequent undetected disc injuries in the cervical spine when using CT- scanned (Cox et al. 2001).

The evaluation clinical instability as defined by White and Panjabi was unconclusive in both simulated ducking positions.

The widely accepted criteria check list of White and Panjabi (The Cervical Spine,1998) are often used to assess clinical instability of the cervical spine after neck injuries. This study measures and analyzes the translational and rotational movements between adjacent vertebrae after hyperflexion and compression-flexion injuries. Neck injuries are reasons for a lot of anxiety among athletes, active people and physicians; fortunately most of these injuries are not permanent. The results of abnormal displacements between vertebrae are pain and dysfunction. The values for the anterior and rotational displacements found in this study were close but less than those proposed by White et al. (1990). Other criteria of these researchers cover the straining and the spraining and the destruction of the soft tissues. Although the evaluations of the clinical instability with the simulated situation were inconclusive, other clinicians supported that any degree of abnormal distraction of vertebrae has the capacity to worsen spinal cord injury Gerling et al. (2001). Palumbo et al. (1996) also concluded that abnormal relative motion between adjacent vertebrae, even as little as 1 mm, may cause significant neurologic damage. The cervical discs are relatively small when compared to the discs in other part of the spine column. Consequently the exiting space for the nerves is also small, which means that even a small abnormal disc material displacement may encroach on the nerve and cause significant pain. In hyperflexion, the posterior ligaments, which are subjected to large tension forces may be strained and/or ruptured. If the flexion moment or shear force is large enough to uncouple the articular processes then pure dislocation or subluxation may follow (Gerling et al. (2001), and Crowell et al. (1993).

Clinical examination of ligamentous instability cannot be performed (Cox et al. (2001) and this is a major handicap to the accurate evaluation of cervical instability. Some radiologists in the United States consider 2 mm anterior displacement to be average displacement for instability, Cox et al. (2001). In traumatic situation, the cervical spine is rarely submitted to pure or unique loading and the ligaments and other soft tissues will probably experience a certain degree of temporary, if not permanent, damage (Nahum et al. 1993; Thomas et al.1999).

In an asymmetric FE model, higher stresses due to coupled extension, lateral bending or axial rotation are likely to be generated. The current model FE Model model is non-linear, inhomogeneous and asymmetric. One of the advantages of an asymmetric model is that it is possible to obtain coupled values of lateral strain, which could be used to better assess the herniation and/or bulging process of discs. The combined loading modes, hyper-flexion and compression-flexion, associated with the sport accidents simulated for these studies can be found in other recreational and professional contact and non-contact sports. The forces and moments used for these studies are reasonable for a quasi-static analysis and are in the range of well-documented clinical values (Bauze et al. 1978; Crowell et al. 1993). Although the failure criteria of disc are not well documented, the observed locations of high stresses can be cautiously correlated with the frequent site of disc injuries, disc degeneration, and disc herniation. The relatively high stresses and strains recorded in the intervertebral discs without reaching the clinical instability criteria suggest that, thorough diagnosis of soft-tissues injuries and disc herniation are crucial after accident situations during which hyperflexion and/or

compression-flexion forces are generated in the neck. Clinical studies showed that about 35% of the herniated discs cases in the cervical spine are often undetected.

Injuries to cervical spine if not severe could be treated using conservative methods such as therapy, stretching test and/or use of cervical orthoses or collars. However if the injuries are severe or dysfunction or pains persist after the use of the conservative methods, surgery will be necessary to restore the integrity of the cervical structure. Surgery of the cervical may be just to relieve a compressed nerve or more drastically to remove a fracture or degenerated components. The frequently performed surgeries on the spine in general are the corpectomy (removal of the vertebral body), the laminectomy or the removal of the lamina and the discectomy or the removal of the disc. Usually the removed part is replaced by an artificial (allogenous) or natural (autogenous) piece of bone. This is discussed in detailed the next section.

Following on the successful consideration of the diving and football accidents and their consequences, the finite element model will be modified and used in the following chapter to simulate clinical application in which the injured or degenerated intervertebral disc is partially removed and completely fused. It is expected that this discectomy and fusion surgical procedures affect the overall biomechanical responses of the cervical spine and that the change in stresses in neighboring disc after complete fusion greatly contribute to the adjacent level syndrome.

7.6 List of figures

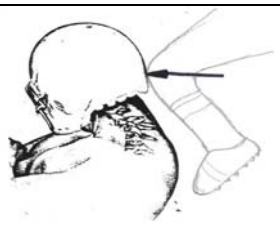

Figure 7.1: Knee to head impact during football injury, Adopted from Torg (1982)

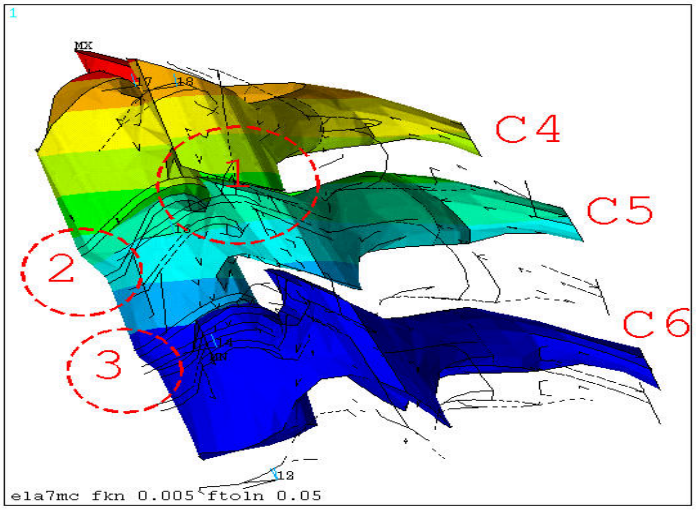

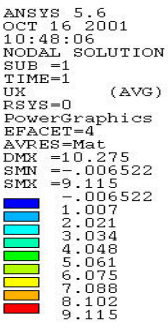

Details 1, 2, 3 show subluxation and straining

Figure 7.2: Forward displacements in mm of C4, C5, C6 after hyper-flexion simulation.

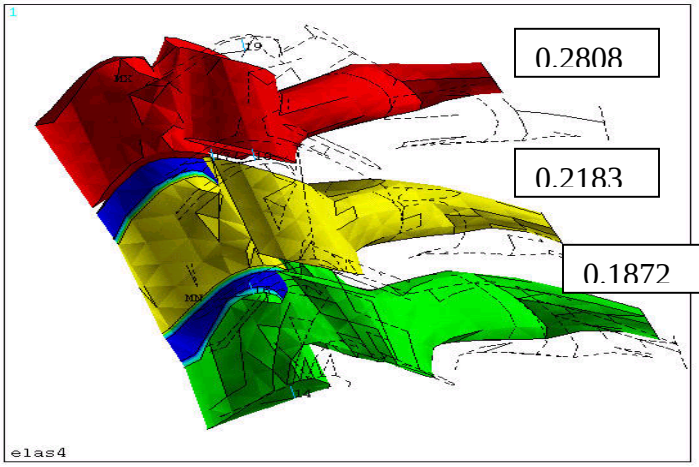

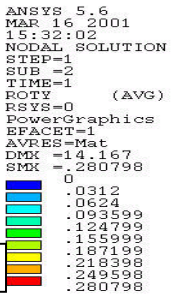

Figure 7.3: Rotational displacements in radian (boxed values) of C3-C4-C5 segment after hyperflexion simulation

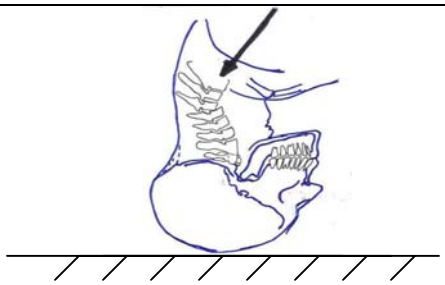

Figure 7.4: Head in ducking position during diving: adopted from Bauze (1978)

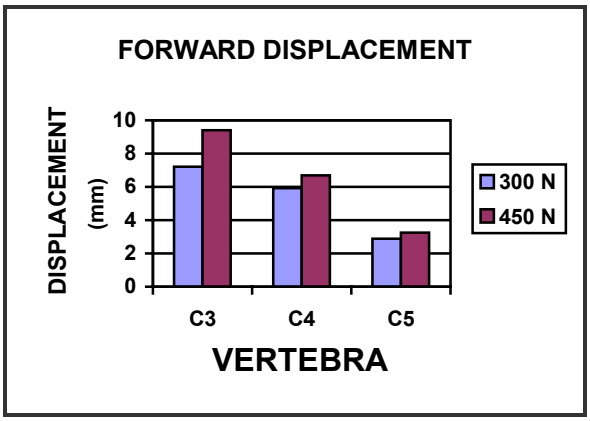

Figure 7.5: Anterior-posterior displacement of vertebra C3 over C4 and C4 over C5. Compression-flexion simulation; T1-C6 fixed in x an y directions.

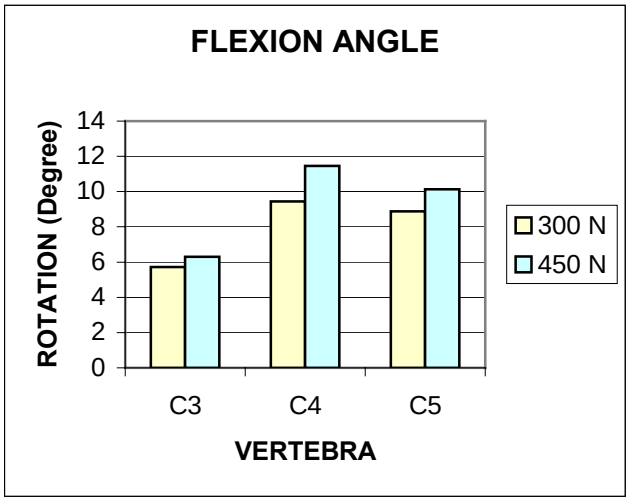

Figure 7.6: Rotational responses of the mid- vertebrae C3, C4, C5. compression-flexion simulation; T1 - C6 fixed in x and y directions.

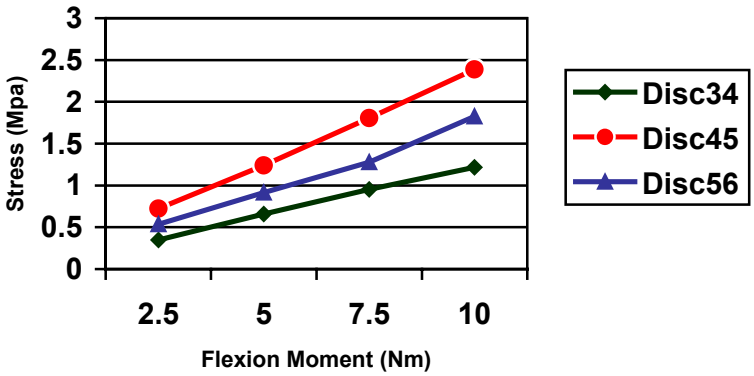

A) Hyper-flexion simulation

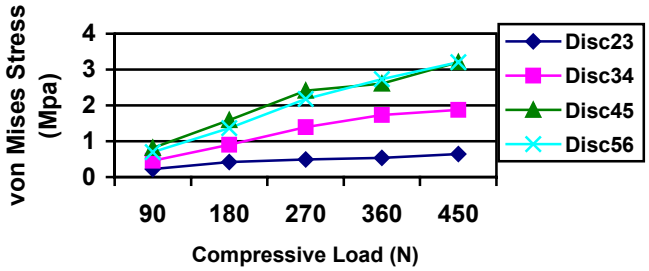

B) compression-flexion simulation : ***C6-T1 constrained*.**

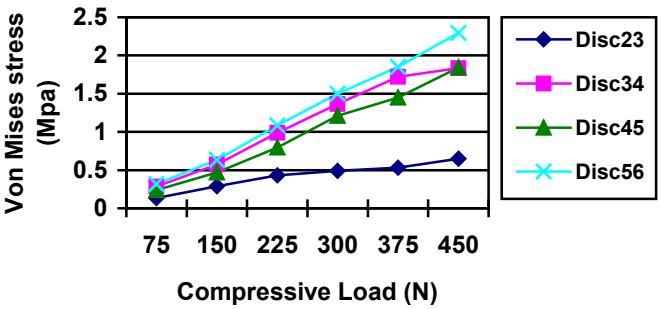

C) Compression-flexion simulation: *C1-C2 and T1-C6 constrained.*

Figure 7.7: Maximum von Mises stress in intervertebral discs as a function of: A) Flexion moment, B) and C) Compressive force.

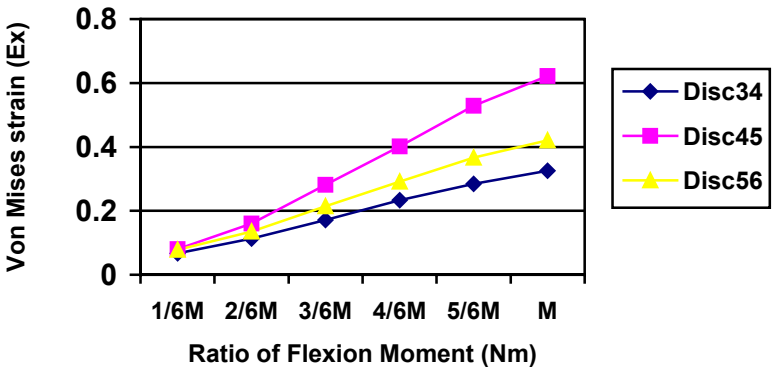

A) Hyper-flexion simulation

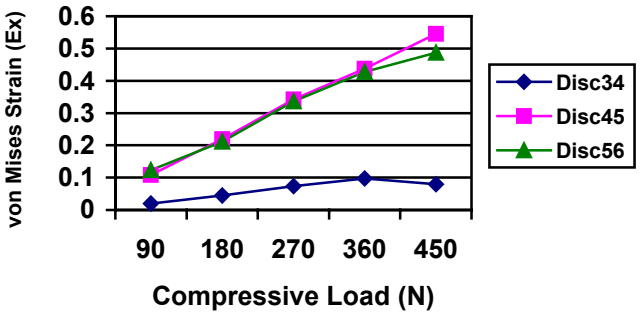

B) compression-flexion simulation:
C6-T1 contrained

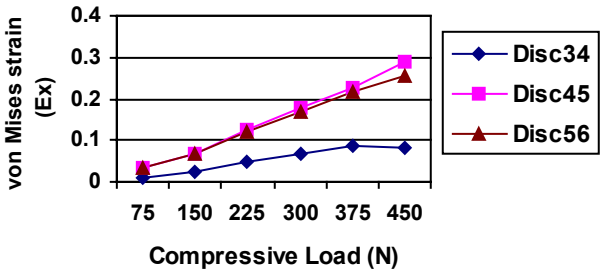

C) Compression-flexion simulation:
C1-C2 and C6-T1 constrained

Figure 7.8: von Mises Total strain (ε_x) in intervetebral discs as a function of: A) Flexion moment, B) and C) Compressive force.

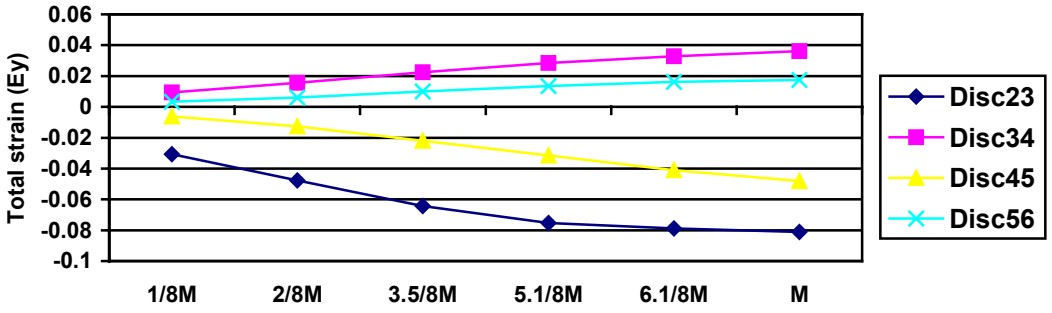

A) Hyper-flexion simulation

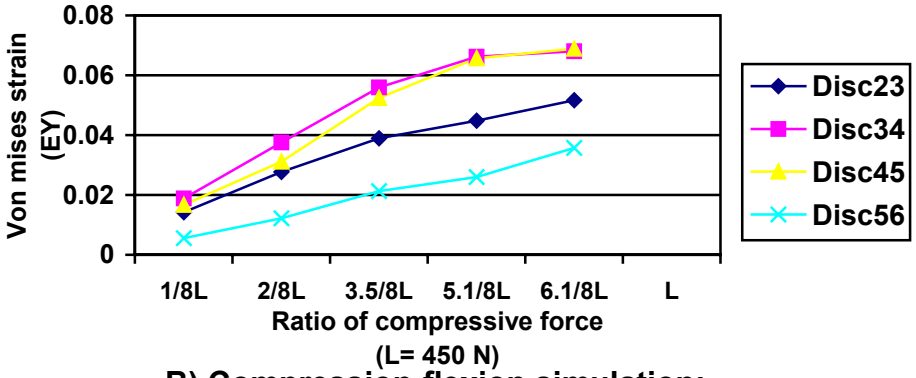

B) Compression-flexion simulation:
C6-T1 constrained

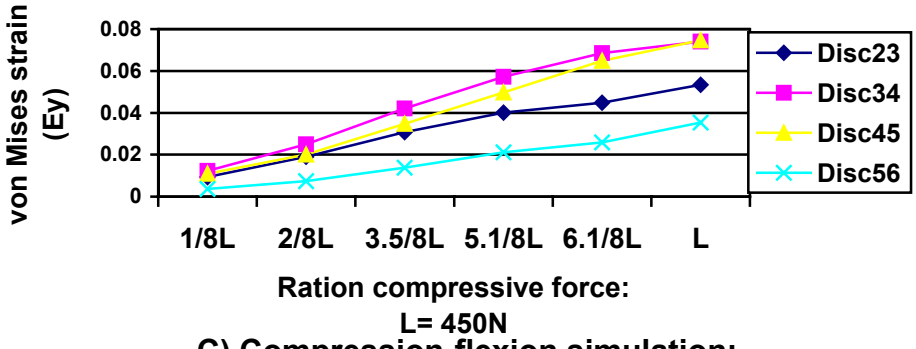

C) Compression-flexion simulation:
C1-C2 and C6-T1 constrained

Figure 7.9: Maximum strain *(εy)* in intervetebral discs as a function of: A) Flexion moment, B) and C) Compressive force.

8. PARTIAL DISCECTOMIES AND FUSION

In this chapter, the developed and validated model presented in chapter six is further used to investigate partial discectomies and fusion. Injuries or degeneration in the cervical spine, if not severe, can be treated using conservative methods such as therapy, stretching and/or use of cervical collars. However, if the injuries and degeneration are severe and dysfunction or pain persist after the use of the conservative methods, surgery will be necessary to restore the integrity of the cervical structure. Surgery on the cervical spine may be performed to relieve a compressed nerve or more drastically to remove a fracture or degenerated components. One of the frequently performed surgeries on the spine is the discectomy with subsequent fusion.

8.1. Introduction

The components of the intervertebral disc, the annulus, nucleus and vertebral endplates, act in concert to stabilize the spine and absorb and distribute load while allowing the spine to flex, extend and rotate (Shao et al. 2002). The intervertebral discs may, over time, undergoe biochemical and morphological transformations that can lead to its degeneration and/or its herniation, (The Cervical Spine, 1998). Humzah et al. (1998) and Oda et al. (1988) suggest that some irreversible changes of disc are associated with the adaptation of the intervertebral disc to alteration in prevailing mechanical (functional) conditions within the vertebral column during aging. Irreversible degenerative changes in of the intervertebral disc can create repeated and acute painful situations that will require surgery. The surgery procedure involves the removal of the damaged disc (discectomy) material, the decortication of fusion site and the placement of

a bone graft to facilitate fusion. The disc removal process can be done anteriorly (Figure 8.1) or posteriorly. Cervical spondylotic myelopathy, radiculopathy and herniation are among the degenerative diseases and/or functional pathology and injuries of the disc that are successfully corrected by discectomy and fusion. In classic spinal fusion the goal is to create over the time a solid union (or *arthrodesis*) between vertebral segment in order to correct segmental dysfunction due to herniation and degeneration of the intervertebral disc, or to correct scoliosis and kyphosis and to treat instability caused by injuries, infections or tumors. The fusion process is facilitated by placing a metallic cage or a healthy bone graft - a piece of bone usually harvested from another part of the skeleton - between two or more vertebrae (Profeta et al. 2000). Before the placement of the bone graft and/or cage, the end plates are prepared by removing the cortical cartilaginous layers. This step is important to ensure good contact between the cage/bone graft and the vertebral bodies and thus stabilize the implant and facilitate the bone in-growth. Over time the graft and the adjacent vertebrae fuse together and create a continuous bony mass. Once the cartilaginous end plates are removed the vertebrae of the cervical spine fuse with or without instrumentation (Harold 2001). Beside pain relief by decompression, it is desirable that fusion would restore the cervical lordosis and/or increase the disc height and in so doing improve the anatomy. Finally, it is necessary to minimize the secondary damage, acceleration of degeneration at adjacent levels and the possibility of instability, following fusion (Torrens et al. 2002, Cloward 1958) by allowing certain degree of flexibility.

Long-term clinical follow-ups of cervical discectomy and fusion demonstrate that the procedure is safe and associated with high rate of fusion, excellent neurological

recovery, functional improvement and pain relief (Isada et al. 2001, Hilibrand et al. 1997, Okada et al. 1991, Gore et al. 1998, and 1984). However the long-term effects of cervical discectomy and fusion on the need for re-operation and adjacent level degeneration are unknown (Shao et al. 2002). Fusion causes accelerated degenerative changes in adjacent discs (Torrens et al. 2002). These changes have been visible on weighted MRI in as early as a year (Isada et al. 2001). Several long-term clinical follow-up studies of anterior cervical discectomy and fusion have found adjacent spondylosis changes in 51% and neurological deterioration in 11%, of the patients that have had the fusion done (Teramoto et al. 1994). Other long-term clinical studies described re-operation, after fusion, for new disease at adjacent levels in 5% to 25% of the cases (Bernard et al. 1987, Hilibrand et al. 1997, Ebersold et al. 1995, Okada et al. 1991, Saunders et al. 1991, Shinomiya et al. 1993 and Clements et al. 1990). Thus up to 25 percent of patients who undergo anterior cervical fusion could have new disease due to degeneration of adjacent segments within a decade and about 16 percents will go through re-operation (Gore et al. 1998). Gore et al. (1984) reported that about 7 percents of the patients they reviewed had identifiable problems at a disc level other than the level fused. Their results also revealed that patients with spondylosis developed more recurrent pain.

Some of the practical problems facing the surgeon during discectomy and fusion are the determination of the amount of disc material to be removed, the sizing and the shaping of the bone graft. Whilst the height of the bone graft can be well defined (Lu et al., 1993), the assessment of the lateral and/or radial dimensions is more difficult. It is possible that too small piece of bone graft area will increase the risk and subsidence and a large bone graft area will lead to over-distraction of the disc space. There are many

studies that looked into the appropriate amount of distraction in disc height and the risk of bone graft dislodgment and collapse (Gill et al. 1989, Kowalski et al. 2001, and Closkey et al. 1993). Closkey et al. (1993) proposed minimum graft areas necessary to prevent subsidence in thoracic spine under moderate physiological loads. The relationship between the bone graft areas and the change in stresses in adjacent levels of the cervical spine has not been addressed.

Very few finite element analysis exist that deal with spinal fusion. Kumaresan et al. (1997) studied the effect of the fused graft on the biomechanical responses of C4-C6 spinal segment under external loadings. Nataragan et al. (1999) used finite element analysis of C4-C7 to compare the change of flexibility of C5-C6 segment and the adjacent segments, C4-C5 and C6-C7, after anterior discectomy, while considering the effect of friction between the graft and the end plate. Chen et al. (2001) studied the lumber spine (L1-L5) and analyzed the change in stresses of the discs adjacent to the fused site. Almost all these studies utilized spinal segments not a complete cervical spine column.

The hypothesis in this chapter is that there is a threshold (optimum percentage) of a size of the bone graft area over which the long-term effects of the change in stresses in adjacent discs are no longer beneficial and thus may be harmful to the dynamics of the spine. Therefore, the previously validated FEM of the cervical spine is segmentally and partially dissected and fused, and the relationship between the changes in stresses in adjacent discs and the size of the bone graft is examined. Such relationships may provide physicians wither commendations regarding the minimum or the optimum bone graft size (area) during the harvest and/or shaping phase of the discectomy and fusion procedure.

The changes in stresses in adjacent level may also help elucidate the accelerated degeneration, the adjacent level syndromes and the need for re-operation after discectomy and fusion. The main assumptions are:

1) only part of the disc is removed and replaced, and,
2) perfect healing process with complete and solid fusion after surgery has already taken place.

8.2 Finite Element Modeling of Partial Discectomies and Fusions

The detailed and previously validated 3D FEM (Figure 6.1) of the human cervical spine was modified to simulate single level segmental partial discectomies and fusion. The discs of the new models were partitioned such that only a defined proportion of the disc was considered removed and fused at a time. Seven partial discectomies (10%, 20%, 30%, 40%, 50%, 65%, and 75%), (Figure 8.2) were simulated at each of the four mid- and lower levels (disc between C3-C4 (disc34), C4-C5 (disc45), C5-C6 (disc56) and C6-C7 (disc67)) of the validated cervical spine model. Autogenous cancellous bone is frequently used in cervical fusion, and it is usually taken from the iliac crest. Thus, for this study the material properties of the corresponding disc proportion that were removed were changed to those of the iliac crest bone (E = 3500 MPa) (Nataragan et al. 1999). The iliac crest bone has a structure that makes it suitable for stability and fusion. It has a cancellous core and a cortical envelope. The cortical envelope offers the strength, thus stability, and the porous core facilitate the bone in-growth, which is necessary for successful fusion.

Assuming anterior cervical discectomy, the current study used a modified Smith-Robinson surgical technique (Smith et al. 1958). The classic Smith-Robinson procedure of the anterior cervical discectomy and fusion involves the removal of the intervertebral disc with the preservation of a small portion of the posterior annulus and the posterior longitudinal ligament. In light of the Smith-Robinson procedure, the anterior partial discectomies and fusion in this study assume the partial removal of the annulus and nucleus of the intervertebral disc with the preservation of all the unaffected portion of the annulus and the posterior ligaments. A corresponding bone graft subsequently replaces the partially removed part of the disc.

All the fused and unfused models were loaded with a compressive pre-load force of 73.6 N (representing the weight of the head) and a physiological moment of 1.5 Nm (Moroney et al., 1988). The force and the moment were uniformly distributed on the top plate. The models were loaded in compression-flexion and compression-extension, compression-bending and compression-torsion for each partial fusion. The loads were quasi-statically applied in four equal steps. The models were restrained in all the directions at the T1 level.

The finite element software, ANSYS 5.6 from ANSYS, Inc. (ANSYS User manual, 1999), was used to generate the geometry, the finite elements and for the nonlinear solution of the model.

8.3 Results

Eight partial discectomies were simulated at C3-C4, C4-C5, C5-C6 and C6-C7. This resulted, with all the physiological loading modes considered, in 132 non-linear

analyzed cases. The maximum Von Mises stress in the adjacent discs and the maximum compression of the bone graft were computed and normalized with respect to results of the intact/unfused model. The change in stresses in adjacent discs was then computed and graphed for different partial discectomies at the same disc level. The global result of the intact (unfused original) model is presented for comparison purposes in Figure 8.3. The two extreme discs, disc23 in cranial and caudal side, disc67, of the spine showed the lowest intervertebral stress. The maximum stresses are found at disc34 in all the loading modes. The ultimate maximum was about 0.67 MPa in disc34 and disc45 following lateral bending. This value is well below the maximum strength of the disc, which is between 1.5 and 10 MPa (Adams et al., 1988).

In the following section the results of the change in stresses in neighboring discs for individual segmental partial discectomies are presented followed by the results of the stress in bone grafts. In the subsequent section, the problem of bone graft subsidence is addressed. The chapter is then closed with discussions and recommendations.

8.3.1 Changes in stresses in neighboring discs

In the following presentation of the results of the individual segmental discectomies and fusion, the change in Von Mises stresses ($\Delta\sigma$) is defined as the difference between the maximum Von Mises stress (σ_f) obtained after partial discectomy and the maximum Von Mises stress (σ_{uf}) obtained after the solution of the unaltered model. The subscript "f" is for the fused and the subscript "uf" is for the undissected/unfused disc. The stress difference, $\Delta\sigma$, ($\Delta\sigma = \sigma_f - \sigma_{uf}$) is normalized with respect to the maximum Von Mises stress (σ_{uf}) obtained with the unaltered model, and is denoted as, *P*, percentage of stress

change, $P = ((\sigma_f - \sigma_{uf})/\sigma_{uf})* 100$. A positive stress difference, $\Delta\sigma$, as well as a positive percentage value, *P*, will therefore mean an increase in Von Mises stress after partial discectomy, while a negative value of $\Delta\sigma$ as well as negative value of P means a decrease in stress for the considered disc and loading mode after partial discectomy and fusions. In the following subsections (8.3.1.1 – 8.3.1.4), in terms of fused disc, the results of the percentage of the change in stresses *(P)*, for a given loading mode, flexion, extension, lateral bending and axial rotation, are presented. The results are also graphed as functions of the partial discectomy or bone graft.

8.3.1.1 Partial discectomies and fusions at disc34

The results of the partial discectomie and fusions for disc34, disc between C3 and C4, are depicted in Figures 8.4. The graphs show that the values of (*P*) vary with respect to the percentage of discectomy. In general, following partial discectomies and fusions at disc between C3-C4 and loaded in flexion, Figure 8.6A, the values of ($\Delta\sigma$) were positive ($\sigma_f > \sigma_{uf}$) in disc56 and disc45 and they were negative ($\sigma_f < \sigma_{uf}$) in disc23 and disc67 at every partial discectomy and fusion. Figure 8.4A shows that in disc67, disc56 and disc23, the values (*P*) of the Von Mises stress changes were insignificant. However disc45 exhibit the highest values of (*P*). For disc45, these (*P*) values started from 57% at a partial discectomy of 10% and continuously decreased with the augmentation of the percentage of the bone graft area to about 40% at partial discectomies of 66% and 90%.

Disc56 experienced the second largest increase in change in stress ($\Delta\sigma$) but showed an opposite trend to that of disc45. There is a slight increase of the values of *(P)* as the percentage of discectomy increases. Although the values of *(P)* in disc56 is

minimum and is about 5% at a partial discectomy of 10%, it slowly increases, with the augmentation of the bone graft area, to about 6% at a partial discectomy of 30% and remains almost constant thereafter.

When considering the loading in extension (Figure 8.4B), with the increase of the percentage of discectomy and fusions of disc34 (segment C3-C4), the results exhibited progressive increases of the values of *(P)* in disc23, disc45 and disc56 and a decrease in disc67. Disc56 had the largest values of *(P)*, which started from about 6.5% at a partial discectomy of 10% and fusion and reached about 18% at complete- 90% bone graft area, fusion. Disc23 had the second largest values of *(P)*. These changes remained minimum at about 0.5% at lower partial discectomies and fusion and progressively attained 8% at both 75% and 90% discectomy. Disc45 had values of *(P)* that relatively increase with the percentage of discectomy up to 66%. The disc then experienced an overall increase of the relative percentage change thereafter. For partial discectomy greater than 75%, the absolute change in stress gained a small percentage increase that reached about 1.5% at complete fusion. Disc67 is the only disc that experienced a continuous decrease of the values of *(P)* with the increase of percentage of discectomy. These values of *(P)* started from about -8% at partial discectomies of 10% and 20% to reach about -11% at bone graft area of 90%. For all the neighboring remaining discs the graphs of the values of *(P)* show a change of slope at about 40% partial discectomy and fusion.

In case of lateral bending mode (Figure 8.4C), the values of *(P)* were positive in three out of the four neighboring discs; disc45, disc23 and disc56. The largest value of (*P*) was in disc45 and was about 35% at partial discectomy of 30%. The value then decreased to about 30% with 66% discectomy and remained almost constant thereafter.

The values of *(P)* in disc56 and disc23 are very close in magnitude with little variations. Disc67 is the only neighboring disc in this loading mode with negative values of *(P)* for all the partial discectomies. The *(P)* values started from about -8% at partial discectomy of 10% and relatively increased to about -2% with 90% discectomy.

Following the loading in axial rotation (Figure 8.4D), the values of *(P)* in disc45 and disc56 show a steady increase that reached a maximum at about 40% discectomy, and then experienced a continuous decrease. Disc45 had the largest absolute and relative percentage of the change in stress of about 55%. The second largest percentage change in stress was about 15% in disc56. Disc23 experienced negative values of *(P)* with partial discectomy under 50% and a relative small increase beyond 50% partial discectomy. In disc67, the values of *(P)* had small magnitude and remained negative throughout the partial and complete discectomy. In general, the changes in disc 23 and disc67 seemed to be of minimum significance.

In summary for the partial discectomies and fusion at disc between C3 and C4, disc45 experienced the largest values of *(P)* in flexion, lateral bending and axial rotation. Disc67 experienced negative values of *(P)* in all the loading modes and throughout all the partial discectomies.

8.3.1.2 Partial discectomies and fusions at disc45

Figure 8.5 summarizes the results of the partial discectomies and fusions of the intervertebral disc45. In flexion (Figure 8.5A), segmental partial discectomy at disc45, disc between C4 and C5, showed that the discs above (disc23 and disc34) and the discs below (disc56 and disc67) the fused site revealed opposite reactions. Disc23 and disc34

experienced an increase in values of *(P)* with the biggest increase occurring between 40%and 50% partial discectomies. These values of *(P)* then remained almost at constant values of about 1% in disc34 and 2% in disc23 beyond 50% discectomy. The maximum increase in values of *(P)* was about 2.5% in disc23. Disc56 and disc67 started with a minimum increase of the values of *(P)* for partial discectomy below 40%. These *(P)* values then decrease to about –4.5% in disc56 and about –0.7% in disc67 beyond partial discectomies of 40%. Beyond 50% partial discectomy the decreases showed a slow linear progression. In general, the values of *(P)* were minimum, in the flexion loading, for all the partial discectomies at C4-C5 segment.

The results of the partial discectomies of segment C4-C5 loaded in extension (Figure 8.5B), although lower in magnitude, showed similar trend to those obtained with the partial discectomies at disc34 and also loaded in extension. All the discs except disc67 experienced an increase in the values of *(P)* with the increase of the percentage of discectomy. The values of *(P)* in disc23 and disc34 are the largest and are almost overlapping. The biggest relative increase of the values of *(P)* occurred between 40% and 50% partial discectomies. The graphs of the values of *(P)* in disc23, disc34 and disc56 revealed a change in the slope at about 40%-50% discectomies. Beyond 50% discectomy, the values of *(P)* slowly converged to the maximum values at full/90% discectomy. The maximum value of *(P)* was about 9% in disc 34. Disc67 is the only disc that experienced only decreases of the values of *(P)* in the extension loading mode. The graph exhibited a quiet linear decrease in change in stress until 50% discectomy and fusion. Beyond 50% partial discectomy, the values of *(P)* remained almost constant at about 4.70%.

Following the right lateral bending mode (Figure 8.5C), all the neighboring discs experienced an increase in values of *(P)* for partial discectomies less than 50%. The values of *(P)* in disc56 decreased after 50% partial discectomy to an insignificant value of almost zero percent with 90% discectomy. Disc67 and disc23 experienced similar and almost overlapping patterns of the values of *(P)* beyond 50% partial discectomy. The average value of *(P)* in these two discs was about 4%. For lateral bending the largest percentage change in stress *(P)* was about 9% in disc34, at full/90% discectomy

Following the axial rotation simulation of C4-C5 segmental discectomies (Figure 8.5D), all the neighboring discs experienced positive values of *(P)* for partial discectomies up to 40 % discectomy. Disc67 experienced almost no changes in the values of *(P)* for partial discectomies under 40%. But beyond 40% discectomies, the values of *(P)* then decreased to minor change of about 3% at discectomy of 66% and remained almost unchanged thereafter. The values of *(P)* in disc23 also, remained almost constant, at about 2%, partial discectomies equal or greater than 40%. Disc34 is the only disc in this loading mode with a steady increase of the values of *(P)* when the percentage of discectomy increases. The changes slowly converge to about 8% at bone graft area of 90%. All the discs experienced a relative jump in percentage change in stress *(P)* between 50% and 66% partial discectomies. The values of *(P)* remained also almost constant beyond 66% partial discectomies.

In summary, disc34 experienced the maximum values of *(P)* in all the loading modes except in flexion. The magnitudes of the *(P)* values are relatively lower in all the loading modes when compared to the values obtained after partial discectomies and fusion at disc34.

8.3.1.3 Partial discectomies and fusions at disc56

Disc56, disc between C5 and C6, is the transition between the mid and the lower cervical spine. When partially dissected then fused and loaded in flexion all the neighboring discs showed significant changes in stress, ($\Delta\sigma$). The percentages of the changes in stresses *(P)*, **(**Figure 8.6A), remained almost constant up till partial discectomy of 75%. Disc23, the most upper disc in the cervical spine, is the only disc to show increases (positive values) in the values of *(P)*. The maximum value of *(P)* was about 16% at partial discectomy of75%. Disc67, disc45 and disc34 had continuous negative values of *(P)* for partial discectomy below 75%. The largest average value of *(P)* was about -26% in disc45, followed by about -12% in disc34 and -10.5% in disc67.

Following the extension loading mode **(**Figure 8.6B) of the partial discectomy and fusion of segment C5-C6, the values of *(P)* in all the adjacent discs had little variation. The values of *(P)* in disc23 went from minimal negative values below 40% discectomy to positive values then after and reached a maximum value of about 2.5% at full/partial discectomy of 90% and fusion. The values of *(P)* in disc67 continuously decreased from about -13.5 % at graft area fusion of 10% to about -17% at graft area fusion of 75%. Between 75% and 90% graft area fusion, the progression of the value of *(P)* in disc67 changed to positive *(P)* values and there is a relative increase of about 15%. The average values of *(P)* in disc67 was about -14.9%. In disc34 and dis45, the values of *(P)* were negative and decreased linearly with the increase of the discectomy area up to 75%. The graphs then changed the slope between 75% and 90% discectomies.

Considering the lateral bending loading mode **(**Figure 8.6C), there were almost no relative changes of values of *(P)* in all the neighboring discs throughout the simulated

partial discectomies. Although disc23 is the only disc with increases in the values of *(P)*, the values remained almost constant at about 43% for all the partial discectomies simulated. Other discs showed similar trend in the *(P)* values. The values of *(P)* in disc34 and disc67 are overlapping and are about 5% in average. The largest percentage decreases are to be found in dis45 and the average were about -20% for discectomies beyond 50%.

For partial discectomies and fusions at C5-C6 segment and loaded in axial rotation **(**Figure 8.6D), disc23 experienced positive value of *(P)*, but the value of about 10% remained constant throughout the partial discectomies. Disc45, disc34 and disc67 all experienced negative values of *(P)* with the largest decrease of about -25% recorded in disc45. The second largest decrease was showed in disc34 and was about -15% in average. The smallest percentage decrease was in disc67 and was about -5% in average.

In summary, with partial discectomies and fusions at disc56 the values of *(P)* in the neighboring discs remained almost constant throughout partial discectomies. In all the loading modes, disc32 experienced the maximum while disc45 experienced the minimum *(P)* values.

8.3.1.4 Partial discectomies and fusions at disc67

The results of the flexion loading mode (Figure 8.7A**)** of the partial discectomies of disc67, disc between C6 and C7, showed that the values of *(P)* in all the neighboring discs showed minor variation. Disc56 experienced the most significant changes in stresses and had an average value of *(P)* of about 25%. The *(P)* values in disc23 and disc34 were very close and their averages were about 5%. Disc45 is the only disc to

exhibit a decrease or negative values of *(P)* in this loading mode. The average percentage of the change in stresses in disc45 was -15%.

Following partial discectomies of disc67 in extension loading mode (Figure 8.7B) only one disc, namely disc56, showed increases or positive values of *(P)*. The (P) value remained almost constant beyond 30% discectomies and was about 16% in average. Disc23, dis34 and disc45, all experienced negative values of *(P)*. Disc45 had about –28% in average value of *(P)*, followed by disc34, which had –7.5% and disc23 with 6%.

The results of the partial discectomies of the segment C6-C7 loaded in lateral bending (Figure 8.7C) revealed that the values of *(P)* in disc56, disc34 and disc23 slightly increased with the augmentation of the percentage of discectomy. In general the increases in neighboring discs are minor. All the values of *(P)* are almost constant with little variation between partial discectomies. Disc56, which is the disc adjacent to the fused segment, had the largest value of *(P*), which was about 30% at 50% and 90% discectomies. The second disc above the fusion site experienced negative values of *(P)*, which diminished with the increase of the percentage of discectomy.

When model was partially dissected and fused at segment C6-C7 and loaded in axial rotation (Figure 8.7D), only disc56 exhibit an increase or positive values of *(P)*. These *(P)* values in disc56 increased with the increase of the percentage of discectomy. The average of the values of *(P)* in disc56 was about 20%.

Disc34, disc23 and disc45 showed decreased or negative values of *(P)* at all the partial discectomies, with average of -2%, -8% and -13% respectively.

In summary, for partial discectomies and fusions disc between C6 and C7, disc56 showed the maximum values of *(P)* all the loading modes. The values of *(P)* in disc45 were negative for all the loading modes.

8.3.2 Stress in the bone graft

Beside the incidence of subsidence one of the other factors that should be clinically considered in partial discetomy is the stress concentration and the maximum stress in the bone graft. The iliac crest tricortical bone graft has a strength of about 10 MPa ((An et al. 1994)). When considering fusion at disc34 and disc45, the stress in the bone graft was above its maximum strength for partial discectomies below 40%. The larger stress occurred in extension loading modes and is located on the posterior portion of the graft. The maximum von Mises stresses for the bone graft in disc34 was 16 MPa at 10 % partial discectomy, which progressively diminished to about 9.5 MPa, at 40% discectomy and fusion. Bone graft in disc45 had the second higher stress values of 13 MPa at 10% partial discectomy. This stress value decreased with the augmentation of the bone graft proportion to 9.2 MPa at 40 % partial discectomy. The bone grafts in disc56 and disc67 had reasonable compressive and Von Mises stresses under the maximum tolerable values for all the partial discectomies.

8.3.4 Subsidence of the bone graft

Subsidence of the bone graft into the vertebral body may lead to the collapse of the disc space, the recurrence of spinal deformity, and probably failure of the fusion (Kowalski et al. 2001 and Gercek et al. 2003). Subsidence can lead to post-surgery

complications that may lead to reoperation. The outcome of discectomy and fusion greatly depends on the quality of the bond (fusion) between the bone graft and the surrounding vertebral bodies. Therefore, in satisfactory discectomy and fusion care should be taken during the surgery to minimize the graft subsidence. According to Kowalski et al. (2001), three factors that directly affect the occurrence and extend of the subsidence are: a) the closeness of fit between the bone graft in the vertebral body, b) the surface area of contact between the bone graft and vertebral body, and c) the character or quality of the contact surfaces. The different between the modulus of elasticity of the hard iliac crest bone graft and of the soft cancellous bone facilitates subsidence. In flexion-extension loading the bone graft is subjected to compression forces, which enhance the bone healing process and fusion as stated in Wolff law (Cowin, 1986, Cowin et al. 1992). Clearly, the smaller the bone graft contact area the higher will be the stress concentration between the bone graft and the vertebral body. Higher stress concentration correlate with larger amount of subsidence. Studies have showed that subsidence can average as high as the preoperative intervertebral height (Kowalski et al. 2001, Gercek et al. 2003, Kumar et al. 1993, and Patel et al. 2002).

In our studies subsidence was defined as any compressive change in height of the bone graft. Only the results of the flexion and extension loading modes, which generated opposite compressions into the bone graft, were considered.

The maximum compression (disc space reduction) values were obtained for flexion loading modes. The values were almost twice as those recorded in extension loading modes. Grafts in disc34 and disc45 experienced the largest subsidence values, which were about 1.4 mm and 1.3 mm at 10% discectomy, respectively. The remaining

had subsidence values are under 1 mm, with the minimum subsidence value of 0.220 mm recorded at 75% discectomy.

8.4 Discussion

There are many variables (biomechanical, biological and pathological) that could influence the success of discectomy and cervical spine fusion. The bone fusion is analogous with solid union or arthrodesis, which stiffens a previously flexible spine segment and can induce changes in stress in the neighboring spinal elements. This process thus takes away the flexibility of the spine by attenuating motion between vertebrae segment. Clinical studies (Epstein, 1998, Caspar et al., 1999, Wirth et al., 2000) have show that fusion occurs in about 6 to 12 months after discectomy. Using a C5/C6 segmental finite element model to study anterior cervical discectomy with fusion, Wirth et al. (2000) and Nataragan et al. (1999) were able to show decrease of stiffness after discectomy and an increase of stiffness after fusion with autologious bone graft and trapezoidal plate osteosynthesis.

In this study four segmental partial discectomies and fusion of the cervical spine were investigated and the relationship between the bone graft area and the changes in stress in adjacent discs was studied. Although most of the radiographic evaluations of the spine after fusion are done only in flexion and extension, this study considered all the major physiological loading modes, flexion extension, lateral bending and axial rotation. Families of curves (Figure 8.4 through 8.7) relating percentage of bone graft areas of a disc and changes in stress in neighboring discs were created for every fused disc and every loading mode.

The results of these analyses indicated that the change in stress at adjacent level could be related to the areas of the bone graft used at the fusion site. Such relationship can be used clinically by the surgeon as a practical guide in determining the adequate graft area for spinal fusion. According to Martins (1976) and Dowd et al. (1999), some evidences exist that show that additional length in time of the fusion procedure and the increased retraction required for the bone graft placement may increase the incidence of local complications. Some studies recognized the significance of graft related complications and donor site morbidity (Flynn et al. 1982). As noted by Pilitsis et al. (2002), good sizing of bone component is critical for optimizing bone fusion outcome. A precise fitting and shape of the bone graft would minimize the chance of graft dislodgement and other forms of failure. The surface area of contact between the bone graft and the vertebral body will not only affect the incidence of subsidence, as this study shows, but also the change in stress in adjacent levels. The extent of subsidence is inversely proportional to the surface area of contact between the bone graft and the vertebral body. The largest the surface area of contact the less the subsidence occurs and vice-versa. Thus, it is important to maximize the contact area between the bone graft and the vertebral body without over-sizing it. Gill et al. (1989) suggested that between 50% and 80% of the vertebral body end-plate area been covered by the graft for interbody spinal fusion. Closkey et al. (1993), using thoracic vertebral bodies, showed that, in order to prevent graft subsidence under moderate physiological loads, the minimum graft area must be between 30% and 40%.

Therefore, there must be a threshold of a size of the bone graft area over which the long-term effects of the change in stresses in adjacent discs are no longer beneficial

and thus can even be harmful to the dynamics of the spine. This investigation showed that, such a size depends on the segment fused. For example, this study suggested that for fusion of segment C3-C4, a bone graft area between 50% and 75% is recommended. Whilst for fusion of segment C4-C5, a bone graft area between 30% and 50% would be sufficient to balance the redistribution of stress in the neighboring segments. These findings could be explained by the fact that the responses of the cervical spine to loads are non-linear. Furthermore, the fusion of the two caudal discs (disc56 and disc67) in the lower cervical spine showed little variations in change in stress between partial discectomies. This suggests that small and large discectomies and fusions would have almost the same effect on the neighboring discs. As previously noted, the change in stresses alone may not be the only consideration in selecting the size of discectomy/ bone graft. Other factors such as the amount of subsidence and the stress in the bone graft itself must also be taken into consideration while evaluating the success of discectomy and fusion. Therefore a piece of bone graft, large enough to prevent the risk of subsidence and able to tolerate the maximum stress, would be recommended (Closkey et al. 1993). It is also of interest to note that in the discs adjacent and subjacent to the fused segments may experience change in stresses in opposite direction, meaning the percentage change in stress could be decreasing (negative) or increasing (positive).

Fuller et al. (1998) concluded that under given load, a particular unaltered motion segment in multilevel specimen would undergo similar deformation regardless of mechanical alterations occurring at other segments. Goel et al., (1994) found comparable motion before and after an arthrodesis at segment adjacent to a fused segment. Van Mameran et al., (1992) undertook a detailed analysis of cineradiographs of healthy

individuals performing flexion and extension of the cervical spine and discerned a general pattern. He found that flexion and extension follow specific sequence amount the spinal segments and are initiated in the lower cervical spine (C4-C7). At the start of the of flexion motion, the C6-C7 segment regularly flexes to its maximum contribution, before C5-C6 segment begin flexing, then, follow the segments C4-C5, C2-C3, and C3-C4. And in extension, the order of contribution of individual segments is variable at the beginning of the motion but become regular in the final phase in the following order: C4-C5, C5-C6, C6-C7, C2-C3 and C3-C4. These patterns explain the nonlinear behavior of the vertebrae and may explained why some neighboring discs experienced more distinctive changes in stresses than other after partial discectomies in adjacent levels.

In general, the gradual partial segmental discectomies and fusion of the discs of the cervical spine revealed that the percentage changes in stress are not evenly distributed in the neighboring segments. The overall trend of the percentage of the change in stress was fairly noticeable in all the loading modes. The direction (negative or positive) of the percentage change in stress after fusion at each level also varies with the location of the neighboring segment. It is also worth noticing that the fusions of the centrally located disc45 showed a balanced redistribution of stress in all the neighboring discs.

Literature review shows that, the change in stresses in adjacent discs of a complete cervical spine, after partial discectomy and fusion of a disc, and its relation to the bone graft size has not been addressed.

Degenerative disc disease most frequently involves the mid and lower cervical spine (C4-C7) and clinical studies have shown that the discs between C4 and C5, and C5 and C6 are the frequent fusion sites in the cervical spine (Gore et al., 1984). Furthermore,

in their studies on the operative techniques of cervical discectomy, Wirth et al. (2000), found that the degeneration and diseases were most prevalent in disc67 followed by disc56, disc45 and disc34. They also found that the anterior cervical discectomy with fusion had few recurrences at same level but an increased number at neighboring levels. Age-related changes in disc biophysical characteristics occur in all individuals. The anatomic and cellular changes are associated with fluctuations in disc mechanical stiffness, which decreases during early degeneration and increases again with more advanced stages. Although the mechanisms for these changes are unclear and controversial, most agree that they reflect a combination of mechanical and biological events (Lotz et al., 2001).

Before the works of Cloward (1958), Robinson and Smith (1958), and Barley et al. (1960) on anterior discectomy combined with bone graft placement, intractable radiculopathy or myelopathy due to the nerve root or spinal cord compression was regarded as clinical disc disease. The advent of improved new technology has changed this perception and spinal fusion has become common practice among spinal surgeons. But the adjacent levels syndrome remained controversial among spinal surgeons. Long-term clinical studies showed that up to 25 percent of patients who undergo anterior cervical fusion could have new disease due to degeneration of adjacent segments within a decade and about 16% will go through re-operation (Gore et al. 1998). Recurrent pain and possibly re-operation can be huge burdens to the society in term of worker compensation and treatment cost and it can also greatly affect the quality of live of those suffering and for their family members.

The change in biomechanics and dynamics, and thus in stress, is only one of the many factors that can lead or start a degeneration process in the spine component. Mechanical stress is usually seen as a stimulant during the healing process after cervical discectomy and fusion, but it can also induce pain and accelerate the degeneration of healthy spine components after arthrodesis. Excessive stress due to large distraction in disc size (height) can lead to dislodgment of the bone graft. Although spine fusion is clinically well documented, the biomechanics and the analytical studies remained poorly explored domains. This investigation has made a major analytical contribution with the current model used herein, which is a complete and more realistic cervical spine model and therefore is more reliable.

8.5 List of figures

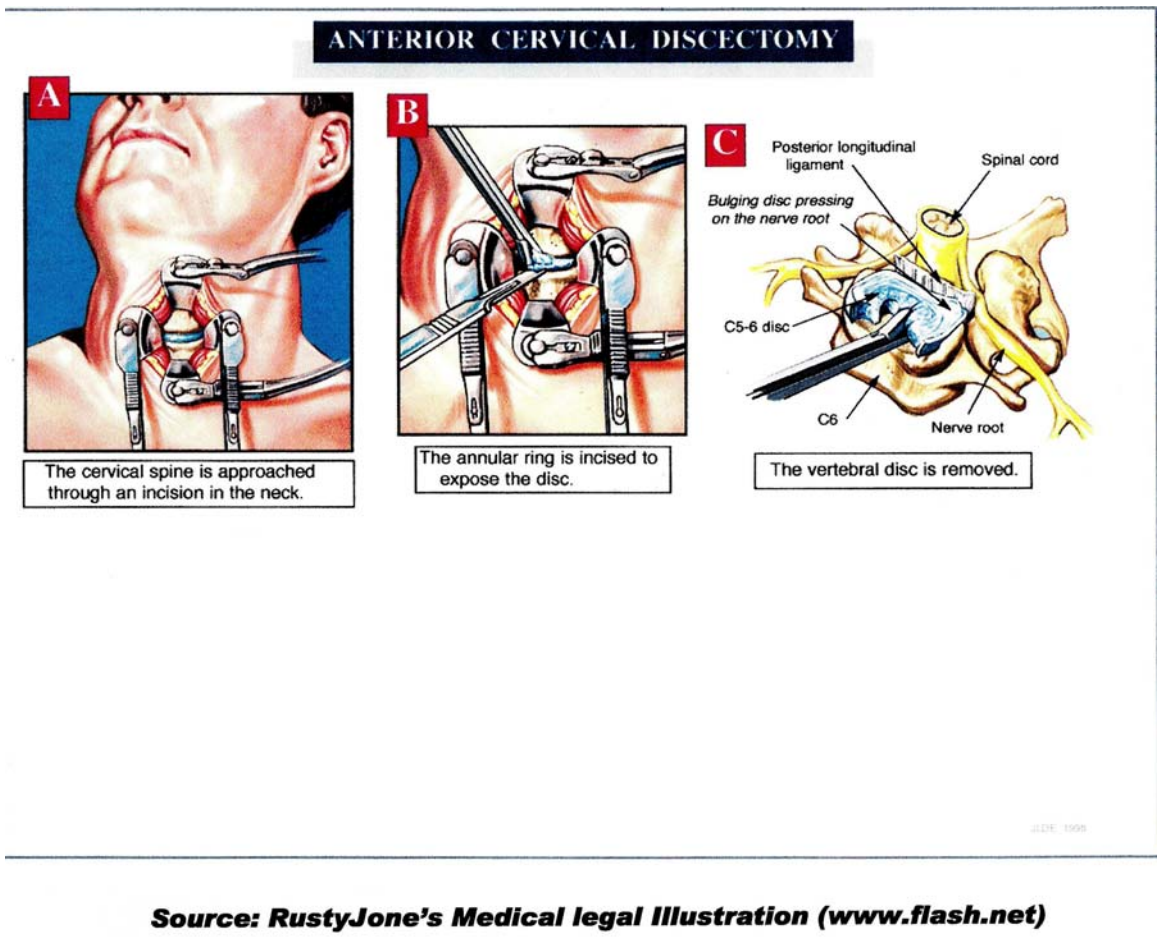

Source: RustyJone's Medical legal Illustration (www.flash.net)

Figure 8.1: Anterior cervical discectomy and fusion (ACDF)

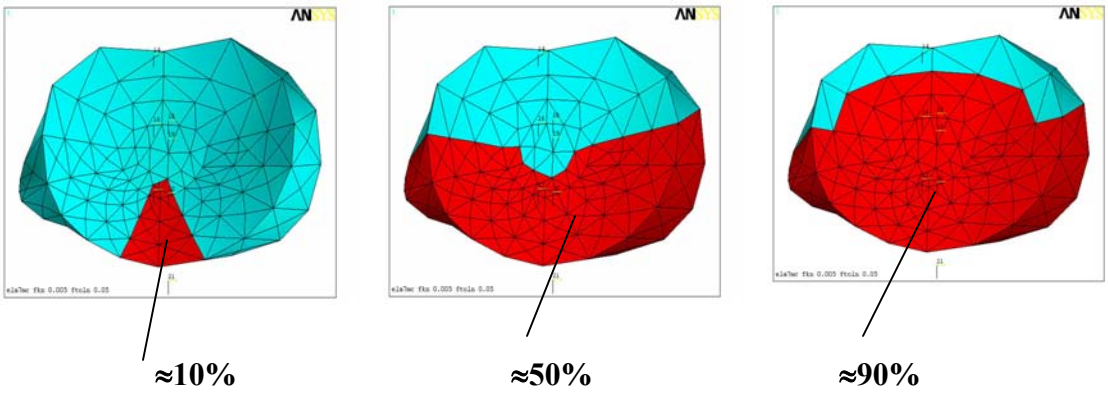

Figure 8.2: Examples of simulated partial discetomies and fusion showing approximate percentage of the bone graft area.

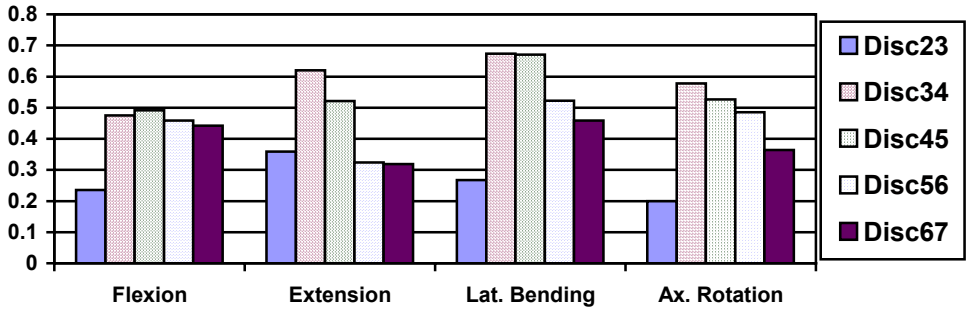

Figure 8.3: Maximum Von Mises stresses in intervertebral disc of intact Model (Loads: 1.5 Nm moment and 73.6 N preload)

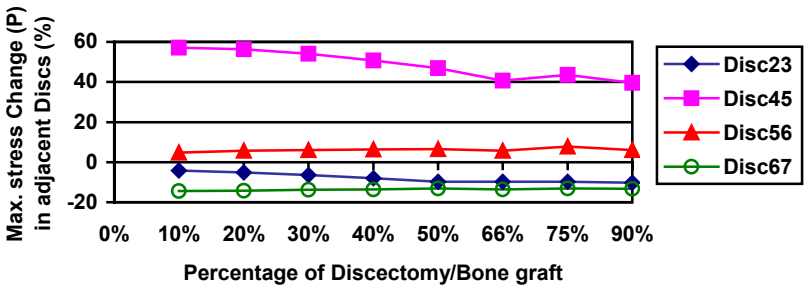

A

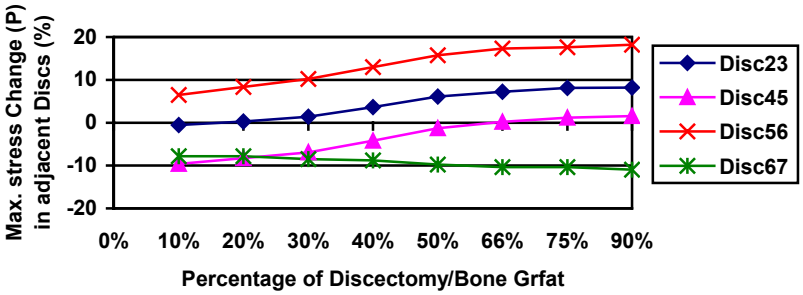

B

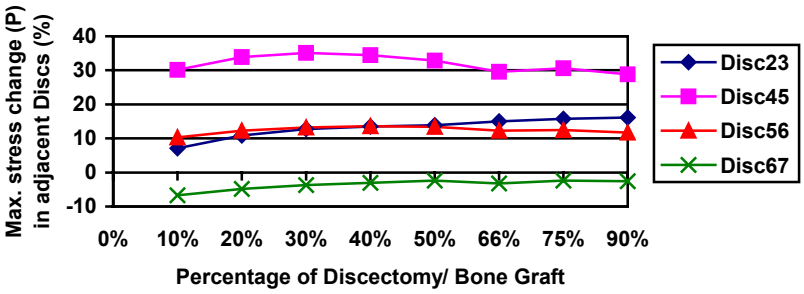

C

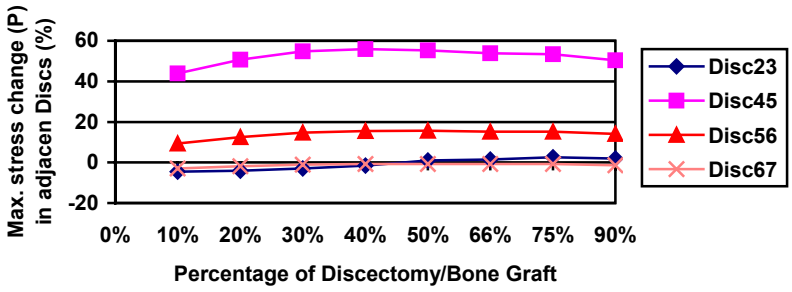

D

Figure 8.4: Percentage of change in stresses in adjacent discs as a function of the percentage of discectomy/bone graft and fusion at Disc34 – with the models loaded *in: A) Flexion, B) Extension, C) Lateral Bending and D) Axial Rotation.*

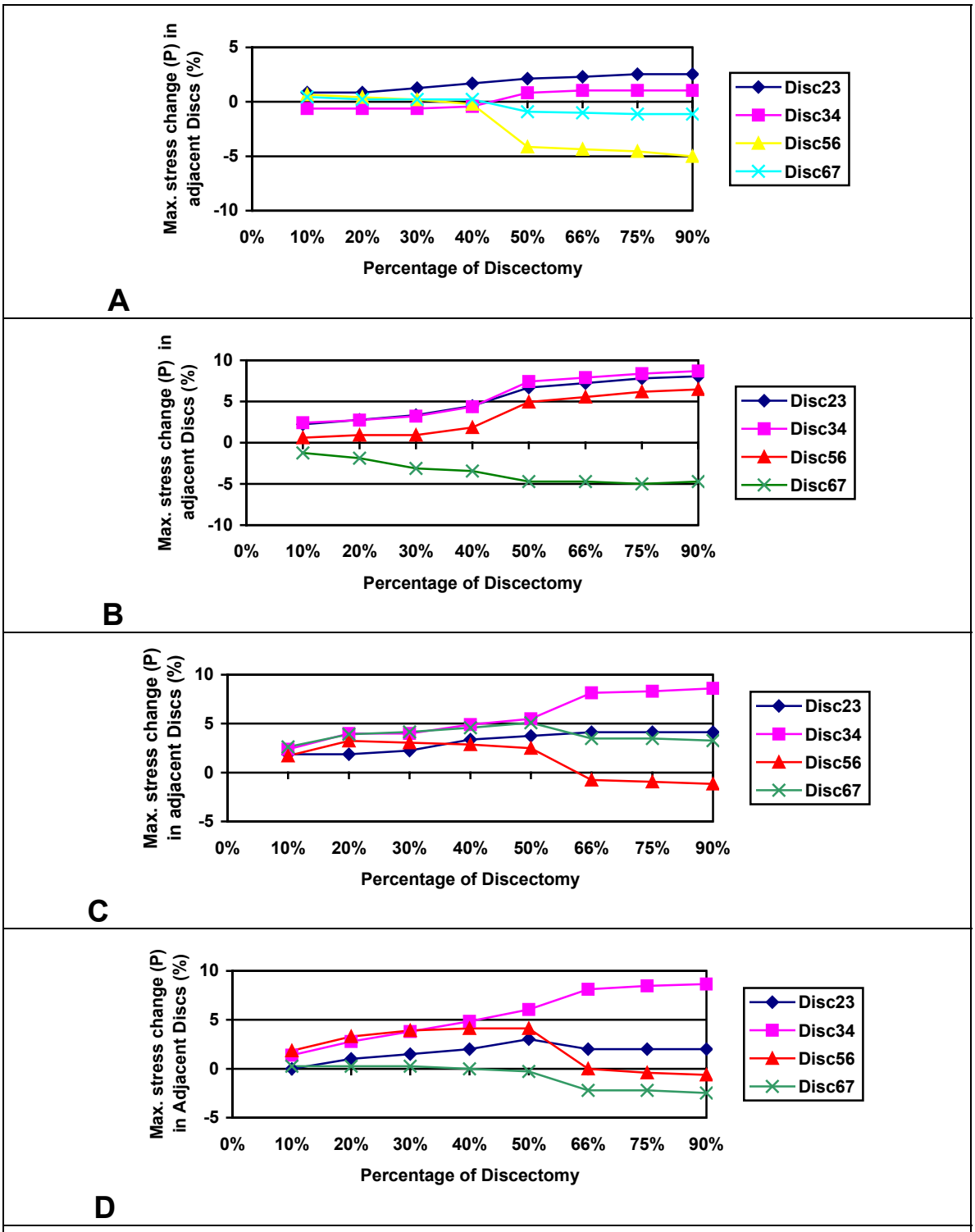

Figure 8.5: Percentage of change in stresses in adjacent discs as a function of the percentage of discectomy/bone graft and fusion at Disc45 – with the models loaded *in: A) Flexion, B) Extension, C) Lateral Bending and D) Axial Rotation.*

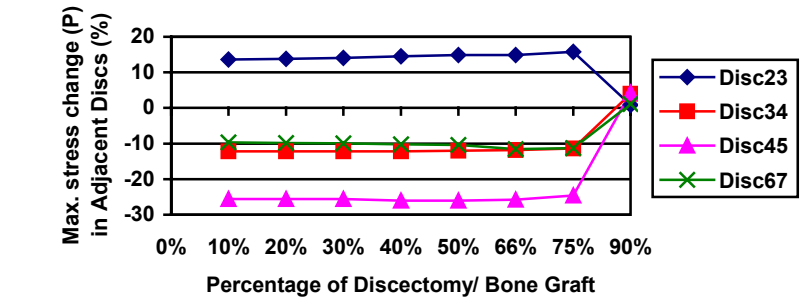

A

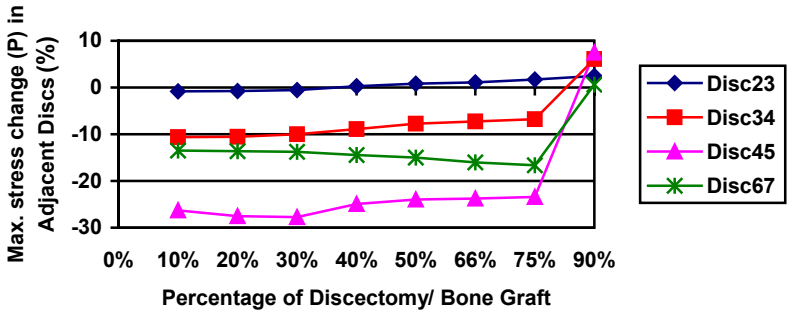

B

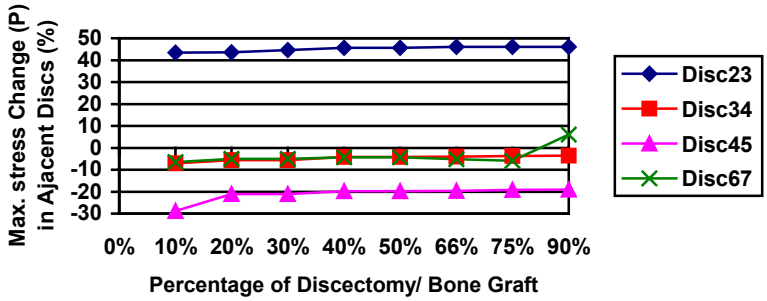

C

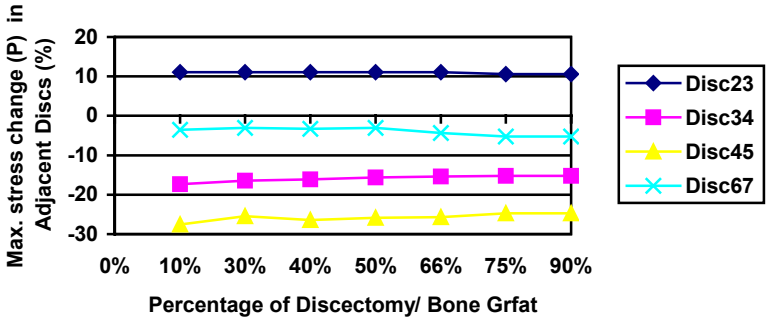

D

Figure 8.6: Percentage of change in stresses in adjacent discs as a function of the percentage of discectomy/bone graft and fusion at Disc56 – with the models loaded *in: A) Flexion, B) Extension, C) Lateral Bending and D) Axial Rotation.*

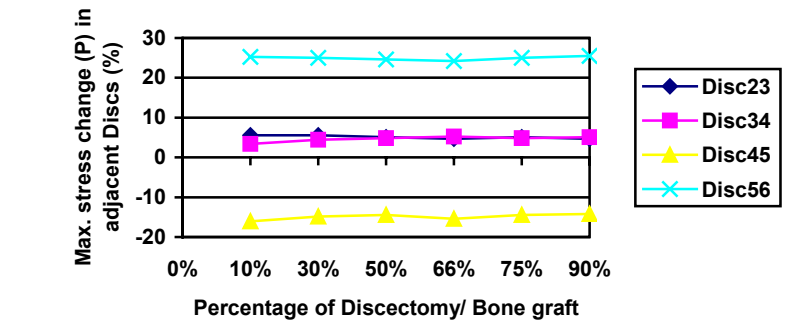

A

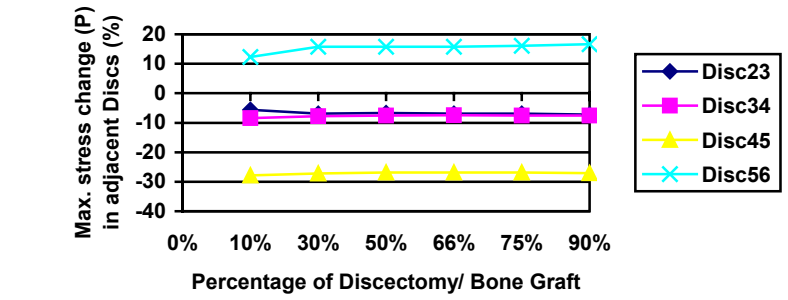

B

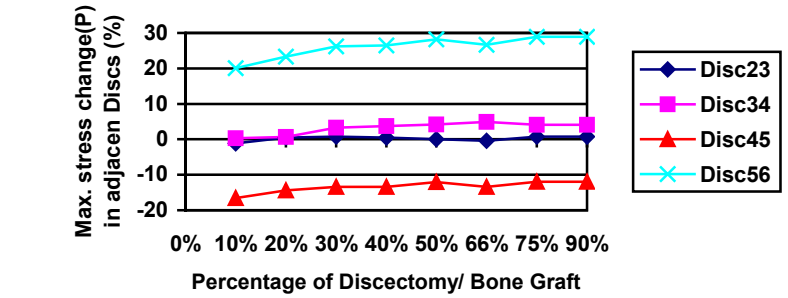

C

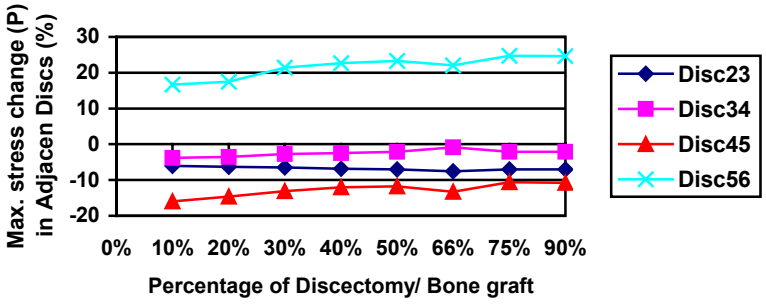

D

Figure 8.7: Percentage of change in stresses in adjacent discs as a function of the percentage of discectomy/bone graft and fusion at Disc67 – with the models loaded *in: A) Flexion, B) Extension, C) Lateral Bending and D) Axial Rotation.*

9. RESEARCH SUMMARY

The aims of this research project were to create, validate and utilize an anatomically accurate and complete FE model of the cervical to investigate the following two hypotheses:

3) The stresses in the intervertebral disc reach critical values before the onset of the translational and rotational displacements, of adjacent vertebrae, that lead to the clinical instability. That is, disc herniation and/or bulging occur before the clinical instability.
4) Segmental discectomy and fusion induces changes in stresses in neighboring discs of the cervical spine. These changes in stresses are non-linear and are directly related to the percentage of contact area between the bone graft and the vertebral body. There is an optimum percentage of bone graft and partial discectomy for each disc, an average of 20% – 60%, at which the changes in stresses in adjacent discs are less critical.

To investigate the stated hypotheses, broad reviews of the anatomy and preview of analytical and experimental studies, pertaining to the cervical spine, were presented in chapters 2 and 3.

The mechanisms of neck injuries were presented in chapter 4

The pilot study was presented in chapter 5. The pilot study of this investigation employed an approximation model of the cervical spine to examine the behavior of the neck under the dynamic load and quasi-static equivalent load. More results and discussion are given in previous publication (Sadegh et al. 1997, 1998 and 2000). The

part of the results selected for this research includes eleven cases of dynamics/viscoelatic analysis. The experimental results of these cases were taken from WPAFB laboratory tests, in Dayton, Ohio. Comparison of the von Mises and the Maximum principal stresses in the anterior and posterior sections of all the cases in the viscoelastic model indicate that:

a) The stresses in all of the cases exhibit a similar pattern, in that there is a peak at about 40 to 100 msec. and a second peak at about 200 msec.

b) The response of the neck to the acceleration is highly nonlinear, however, it is generally true that the maximum stresses increase as the magnitude of the accelerations increase.

c) The magnitude of one of the components of the acceleration data is not the only factor, rather, the combinations of forces and torques are the cause of the high stresses in the vertebrae.

d) The maximum stress generally occurs at C4 or C6, which is clinically known as a site of high incidence of injuries.

e) Based on the assumed ultimate strength of the vertebrae of this model (30 to 40 Mpa). The seventh and the eighth cases, 20 G-z and 12 G-z, respectively, are the two critical cases where the maximum stresses (26.3 Mpa and 36.1 Mpa) are very close to the critical strength of the vertebra.

In an attempt to close the gap between the human tolerable (safe) acceleration in the experiments and the threshold of injuries, two cases were extrapolated. The maximum stresses of the two extrapolated accelerations, 15 G-z and 20 G-z, are also critically close to assumed vertebral strength in this study.

A new anatomically sophisticated and validated FE model of the cervical spine was presented in chapter 6. This is a new and more detailed model of the cervical spine that was created and used to study the biomechanics of sport injuries and their correlation to cervical spine instability. In chapter 7, two cases of contact and non-contact sport accidents (football and diving) were simulated and the possible resulting injuries were assessed using the displacement and stress responses of the FE model. The following conclusions were reached for the football injuries.

a) The locations of the maximum stresses in the discs, after compression-flexion and hyperflexion traumas, are almost similar. That is, different loading modes could lead to similar injuries. The motion generated between the spinal components, in hyperflexion and compression-flexion is very important factor in characterizing the type of injuries.

b) In the football injury simulation, where the spine was subjected to shear/flexion, it was observed that 120 N posterior- anterior shear force would generate about 3 mm anterior facets displacement and about 7.5 degrees rotation at C4-5 level. This shear force can place the cervical spine column at the onset of the clinical instability.

c) The shear force created high stresses at disc45 and disc56, which exceeded the disc ultimate stresses. The maximum stress of both discs was located in the lateral posterior portion of the annulus. This location is clinically observed as the location where the disc mostly herniates.

e) For the football accident simulation, it can be summarized that the absence of clinical instability in hyper-flexion does not exclude the fact that stresses in discs could be damaging.

For the diving injuries (compression-flexion) simulations, two cases were considered; the first case assumed free movement of the head after ducking and the second case assumed the jamming (locking) of the upper vertebrae (C1-C2) after ducking. The following conclusions were reached.

a) When the model was constrained at the both ends, (ducking and Jamming of the upper vertebrae) the results showed that, there were less displacement and stress responses compare to when it was constrained only at the bottom end (ducking).

b) The pattern of dislocation leading to instability as demonstrated by Bauze et al. (1978) was confirmed for the type of loading simulated. The deformed shape of the results showed a potential bilateral dislocation between C5 and C6, and a progressive compression between C2, C3 and C4 at the facets levels.

c) Disc45 and disc56 experienced the maximum stresses for both simulations. Nevertheless, these maximum stress values, which were about 3.2 Mpa, were comfortably below the failure compressive strength of 10.3 Mpa, reported by Adams et al. (1988). The posterior portion of these discs was subjected to higher compressive stresses while the anterior portion of these discs was carried high tensile stresses. The situation

would probably increase the risk of the posterior herniation of the disc and/or the anterior separation between the annulus and the endplates.

d) The evaluation of both cases for clinical instability was inconclusive. The largest displacement and rotational values were about 6.7 degrees flexion rotation and about 1.8 mm displacement between C5 and C6 and were obtained when the model was in simple ducking without jamming.

e) The results further showed that the maximum stresses in C2, C3 and C4 vertebrae are mainly located around the lateral processes and the bodies. These could be recognized as a potential fracture site due to compression.

For the summary of the compression-flexion injuries, it can be said there is a high risk of bilateral dislocation in the mid-cervical region and a potential high risk of disc herniation with increase compression.

All the above-discussed results support and conclude the first hypothesis, which stated that the stresses in the intervertebral disc reach critical values before the onset of the translational and rotational displacements, of adjacent vertebrae, that lead to the clinical instability. That is, disc herniation and/or bulging occur before the clinical instability.

Minor neck injuries are reasons for a lot of anxiety among athletes, active people; fortunately most of these injuries are clinically stable, and not of permanent nature, and therefore do not require surgical intervention. Although the evaluations of the clinical instability with the simulated situations could be seen as inconclusive, Gerling et al., (2001) supported that any degree of abnormal distraction of vertebrae has the capacity of worsening the spinal cord injury. Palumbo et al., (1996) also concluded that abnormal

relative motion between adjacent vertebrae, even as little as 1 mm may cause significant neurological damage. This is due to the fact that exiting space for the nerves in cervical spine is small, and even a small abnormal disc material displacement may encroach on the nerve and cause significant pain. Thus, Some radiologists in the United States consider 2 mm anterior displacement to be average displacement for instability (Cox et al. 2001). In hyperflexion, the posterior ligaments, which are subjected to large tension forces may be strained and/or ruptured. If the flexion moment or shear force is large enough to uncouple the articular processes then pure dislocation or subluxation may follow (Gerling et al. 2001, Crowell et al. 1993). Clinical examination of ligamentous instability cannot be performed (Cox et al. 2001) and this is a major handicap to the accurate evaluation of cervical instability. The repair of a clinically unstable cervical spine may require disceetomy and fusion.

The final investigation of this research covered the partial discectomies and fusion in the cervical spine column and is presented in chapter 8. It is accepted that discectomy and fusion surgical procedures affect the overall biomechanical responses of the cervical spine and that the change in stresses in neighboring disc after complete fusion greatly contribute to the adjacent level syndrome. In this study it was assumed that the proportion of disc removed and replaced control the degree of change in stresses in adjacent levels. Partial discectomies and fusions were considered for intertevertebral discs between C3-C4, C4-C5, C5-C6 and C6-C7 with the objectives of localizing the optimum proportion of discectomy that generates less stress in adjacent levels. The following summarizes the conclusion for each segmental fusion:

1) For the partial discectomies and fusions at C3-C4, disc45 was the critical disc with the maximum change in stress in all of the loading modes except in extension. For this reason disc45 should be used to optimize the percentage of partial discectomy at disc34. Partial discectomy of about 65 % induces a minimum change in stress in disc45, has lower subsidence, and is in the range recommended by Gill et al., (1989) and Closkey et al., (1993).

2) For the partial discectomies at C4-C5, there was a balanced redistribution of stresses. Although disc34 was the disc with the maximum percentage of stress changes in all the loading modes but flexion, all the changes in stress are of the same order in all of the discs. A general observation revealed that the necessary bone graft area with minimum changes in stresses was between 30% and 50% of the surface of vertebral body.

3) A global indication of the results of the segmental partial discectomies at C5-C6 showed that disc23 would be the critical disc when it comes to selection of the appropriate bone graft area, because it has the higher percentage of changes in stress. Even if the change in stresses in this disc did not vary significantly between partial discectomies. The minimum bone graft area of about 30% to 50% would reduce the risk of subsidence and should be considered.

4) For the segmental partial discectomies at C6-C7, the cranial discs (disc23 and dis34) showed an almost constant and overlapping percentage in change in stresses. Dics56 is one of the cervical discs frequently subjected to diseases and degeneration. Any bone graft size that will diminish the adjacent level syndrome in this disc will be

recommended. Similar to the case of fusion at C5-C6, there are insignificant variations in percentage between partial discectomies. The recommendation for the minimum amount of bone graft, 30% to 50%, should be take into consideration to minimize the effect of bone graft subsidence.

The above-mentioned summaries of the partial discectomies confirm the second hypothesis of this research that the changes in stresses in adjacent discs after discectomies and fusion are non-linear and are directly related to the percentage of contact area between the bone graft and the vertebral body. The optimum percentage of bone graft and partial discectomy depends on the disc dissected and fused. The average optimum percentage value is between 30% and 65%, when the amount of subsidence is taken into consideration.

The problems of subsidence and stress concentration equally affect the outcome of the solid fusion and must always be taken into consideration before, during, and after the surgery. Depending on the segment fused, a small size of the bone graft may lead to higher stresses that subsequently lead to the failure and collapse of the disc space. The same will happen if the subsidence is too pronounced.

When the cervical spine is fused, its biomechanics is altered; it looses some of its flexibility and becomes stiffer. This study indicates all the neighboring discs experience stresses changes after adjacent level fusion. The changes in stresses are not evenly distributed to the neighboring discs. The percentage of change in stress can be related to the area of vertebral body covered by the bone graft implant. This study suggested the optimum area depends on the segment fused but the fusion area should be large enough to avoid subsidence and should be between 30% and 65 % of the vertebral body surface.

REFERENCES:

Adams M.A., Huton W.C., Mechanics of the intervertebral disc. The biology of Intervertebral disc vol. II, Peter Ghosh, CRC press, 1988.

Allen, B.L., Ferguson, R.L., Lehman, T.R., O'Brien, R.P., A mechanistic classification of closed, indirect fractures and dislocations of the lower cervical spine. Spine (1) 1-27, 1982.

An, H.S., Xu, R., Lim, T.H., McGrady, L., Wilson, C., Prediction of bone graft strength using dual-energy radiographic absorptiometry. Spine 19 (20) 2358-2363, 1994.

Anderson, L., Clark, C., Fractures of the odontoid process of the axis, in Sherk, H.H. (ed.), The Cervical Spine, 2nd edition, The Cervical Spine Research Society, Lippincott (Philadelphia), 325-341, 1989.

ANSYS User Manual, version 5.6 , Swanson Analysis Systems, Inc, Houston, PA, 1999.

Barley, R.W., Badgley, C.E., Stabilization of the cervical spine by anterior fusion. Journal of Bone Joint Surgery Am 42, 365-94, 1960.

Bauze, R. J., Ardan, G. M., Experimental Production of Forward Dislocation in the Human Cervical Spine, J. of Bone and Joint Surgery, 60B: 239-24, 1978.

Belytschko T. Rencis M. and Williams, Head-Spine structure modeling: enhancements to secondary loading path model and validation of head-cervical spine model, AAMRL-TR-85-019, 1985.

Benzel, E. C., Biomechanics of Spine Stabilization, principles and clinical practice, Biomedical Engineering Handbook , Editor J. D. Bronzino, CRC Press, 1995.

Bernard, T.N.J., Whitecloud, T.S. III., Cervical spondylotic myelopathy and myeloradiculopathy. Anterior decompressionand stabilization with autogenous fibula strut graft. Clin. Orthop., 221, 149-160, 1987.

Bozic, K. J., Keyak, J. H., Skinner, H. B., Bueff, H. U. and Bradford D. S. Three – Dimensional finite element modeling of a cervical vertebra: An investigation of burst fracture mechanism, J. Spine Disord., 7, 102-110, 1994.

Caspar, W., Pitzen, T., Anterior cervical fusion and trapezoidal plate stabilization for re-do surgery. Surg. Neurol. 52: 345-52, 1999.

Chang, D.G., Tencer, A.F., Ching, R.P., Treece, B., Senft, D., Anderson, P.A., Geometric Changes in the cervical spinal canal during impact, Spine 19: 973-980, 1991.

Chen C.S., Cheng, C. K., Liu, C. L. Lo, W.H., Stress analysis of the disc adjacent to interbody fusion in lumbar spine. Med. Eng. & Phys. : 23, 483 –491, 2001

Cheng, H. Obergefell, L. and Rizer A., Generator of Body Data (GEOBOD) Manual, Report AL/CF-TR-1994-0051, Armstrong Laboratory, Air Force Materiel Command, WPAFB, March, 1994.

Clausen, J., Goel, V. K., Traynelis V. C., and Wilder, D. G., Cervical spine Biomechanical investigation using an experimentally validated FE model of C5-C6 motion segment, Trans. 42nd Ann. Meeting, Orthop. Res. Soc., Atlanta , GA, February 18-22, p 657, 1996.

Clausen, J. D., Goel, V. K., Prediction of Load Sharing Among Spinal Components of a C5-C6
Motion Segment Using the Finite Element Approach, Spine 23: 684-691, 1998.

Clements, D.H., O'Leary, P.F., Anterior cervical discectomy and fusion.
Spine 15:1023-1025, 1990.

Closkey, R.F., Russell Parsons, J., Lee , C.K., Blacksin, M.F., Zimmerman, M.C., Mechanics of Interbody spinal Fusion: Analysis of critical bone graft area.
Spine 18: 1011-1015, 1993.

Cloward, R.B., The anterior approach for removal of rupture cervical discs.
Journal of Neurosurgery 15: 602-17, 1958.

Cowin, S.C., Wolff's law of trabecular architecture at remodeling equilibrium.
J Biomech Eng. Feb;108(1):83-8, 1986.

Cowin, S.C., Sadegh, M.A., Luo, G.M. An evolutionary Wolff's law for trabecular architecture. J Biomech Eng. Feb;114(1):129-36, 1992.

Cox, M. W., McCarthy, M., Lemmon, G., Wenker, J., Cervical Spine Instability: Clearance Using Dynamic Fluoroscopy. Current Surgery, Vol. 58, No. 1, 2001.

Crowell, R. R., Edwards, W. T., White, A. A., Mechanism of ijury in cervical spine: Experimental evidence of biomechanical modeling. In The cervical spine, 2nd ed., Philadelphia, JB Lippincott 70 -90, 1995.

Crowell, R. R., Shea, M, Edwards, W. T., Clothiaux, P. L., White, III, A. A., Hayes, W. C., Cervical Injuries under Flexion and Compression Loading,
J. of Spine Disorders 6: 175-181, 1993.

Dauvilliers, F, Bendjellel, F, Weiss, M, Lavaste, F and Tarriere, C. Development of a finite element model of the neck 38th Stapp Car Crash Conference, 77-91, 1994.

de Jager, M., Sauren, A., Thunnissen, J., Wismans, J., : A Three-dimensional Head-Neck Model: Validation for Frontal and Lateral Impacts. Society of Automotive Engineers. SAE paper No. 942211, 1994.

Deng, Y. C., Goldsmith, W., Response of a human head/neck/upper – torso replica to dynamic loading – I. Physical model. J. Biomechanics, Vol. 20, No. 5, 471 – 486, 1987.

Deng, Y. C., Goldsmith, W., Response of a human head/neck/upper – torso replica to dynamic loading – II. Analytical/ numerical model. J. Biomechanics, Vol. 20, No. 5, 487 – 497, 1987.

Dietrich, M., Kedzior, K., and Zagrajek, T., A biomechanical model of human spinal System Proceedings of the Institution of Mechanical Engineers Part H, J. Eng. Med., 205(H) 19-26, 1991.

Dowd, G.C., Wirth, F.P., Anterior Cervical discetomy: Is fusion necessary ? Journal of Neurosurgery 90, 8-12, 1999.

Dvorak J., Froehlich D., Penning L., Baumgartner H., Panjabi M.M., Functional radiograghic diagnosis of the cervical spine: Flexion/extension, Spine13: 748-55, 1988.

Ebersold, M.J., Pare, M.C., Quast, L.M., Surgical treatment for cervical spondylotic myelopathy. Journal of Neurosurgery 82, 745-751, 1995.

Edwards, W.T., Ordway, N.R., Zheng, Y., McCullen, G., Han, Z., Yuan, H.A. Peak Stresses observed in posterior lateral annulus. Spine 2001, Vol. 26, # 16.

Epstein, N. E., Evaluation and treatment of clinical instability associated with pseudarthrosis after anterior cervical surgery for ossification of the posterior longitudinal ligament. Surg. Neurol. 49: 246-52, 1998.

Farfan H., Gracovetsky, S., and Helleur C., Cervical spine analysis for ejection injury prediction, US AFOSR #81-0012, 1982.

FicK, R., Handbookder Anatomie and Mechanik der Gelenke. Jena, Verlag G. Fischer, 1910

Flynn, T.B., Neurologic complications of anterior cervical interbody fusion. Spine 7:172-86, 1982.

Francis, C.C., Variations in the articular facets of the cervical vertebrae Anat. Record , 589-609, 1955.

Fuller, D. A., Kirkpatrick, J. S., Emery, S. E., Wiber, R. G., Davy, D. T., A Kinematic

Study of the Cervical Spine Before and After Segmental Arthrodesis,
Spine 23: 1649-1656, 1998.

Gercek, E., Arlet, V., Delisle, J., Marchesi, D., Subsidence of stand-alone cervical cages in anterior interbody fusion: warning,
Journal of Neurosurgery Vol. 12, No. 5, PP 513-516, 2003.

Gerling, M. C., Davis, D. P., Halmiton, R. S., Morris, G. F., Vilke, G. M., Garfin, S. R., Hayden, S. R., Effect of Surgical Cricothyrotomy on the Unstable Cervical Spine in a Cadaver Model of Intubation,
The Journal of Emergency Medicine, Vol. 20, No 1, pp. 1-5, 2001.

Ghanayem J. A.., Zdeblick A. T., Dvorak, J., Functional anatomy of joints, ligaments, and discs. In the Cervical Spine, 3rd ed., chap 3, 45-52, 1998.

Gilbertson, L.G., Goel, V.K., Kong, W.Z., Clausen, J.D. Finite element methods in spine biomechanics research. Crit. Reviews Biomech. Engr. 23 (5&6): 411-473, 1995

Gill, K., Lin, P.M, Lumbar interbody fusion. Rockville, Maryland Aspen Pub, 3-7, 1989.

Goel,V.K.and Weinstein, J., Biomechanics of the spine , CRC Press, 1990.

Goel, V.K., Park, H., Kong, W.,Investigation of vibration characteristics of the ligamentous
lumbar spine using the finite element approach. J. Biomech Engr. 116 (1) 377-383, 1994.

Gore, D.R., Sepic, S.B., Anterior Cervical fusion for degenerated or protruded discs: A review of one hundred forty six patients. Spine 9, 667-671, 1984.

Gore, D.R., Sepic, S.B., Anterior Discectomy and fusion for painful cervical disc disease. A report of 50 patients with an average follow up of 21 years.
Spine 23 : 2047-2051, 1998.

Gross, M., The GEOBODIII Program User's Guide and Description,
Report AL/CF-TR-1991-0102, Armstrong Laboratory, Air Force Materiel Command, WPAFB, March, 1991.

Grossheim, L. Morphology of the human cervical spine, Masters Thesis,
Marquette University, Milwaukee, WI, 1989.

Grossman, M.D., Reilly, P.M., Gillett, T., Gillett, D., National survey of the influence of cervical spine injury and approach to cervical spine clearance in U.S. Trauma Centers. J. Trauma, 47, (4), 684-690, 1999.

Guill , F.C., Ascertaining the causal factors for "Ejection associated" injuries ,

Aviat., Space, Environ. Med., 60 (10 suppl.): B48 –B71, 1989.

Guill, F.C., Herd, G.R., Aircrew Neck Injuries: A new, or an existing misunderstood phenomenon?, Neck Injury in Advanced Military Aircraft Environment, AGARD, conference Preceedings No. 471, 9-12, 1990.

Habitt, Karlsson, & Sorensen, ABAQUS User Manual, 1997.

Haemaelaeinen, O., Vanharanta, H., Effect of Gz forces and head movements on cervical Erector spinae muscle strain. Aviat., Space, Environ. Med., 63: 709-16, 1992.

Harold, D., Portnoy, Anterior Cervical discectomy and fusion. Surg Neurol, 5, 178-80, 2001.

Harris, J., Mirvis, S. Radiology of acute cervical trauma, 3rd Edition. Williams & Wilkins (Baltimore), 1996

Helleur, C., Gracovetsky, S., Farfan, H.Tolerance of the human cervical spine to high acceleration: a modeling approach. Aviat., Space, Environ. Med. 55: 903-909, 1984.

Hilibrand, A.S., Yoo, J.U., Carlson, G.D., Bohlman, H.H., 1997. The success of anterior cervical arthrodesis adjacent to previous fusion. Spine 22: 1574-1579, 1997.

Hoek van Dijke, G.A., Snijders, C.J., Roosch, E.R., Burgers, P.I., Analysis of biomechanical and ergonomic aspects of the cervical spine F-16 flight situations. J. Biomechanics, 26: (9), 1017-1025, 1993.

Holdsworth, H., Fractures, Dislocations, and Fracture-Dislocations of the Spine. The Journal of Bone and Joint Surgery, Vol. 45B:6 1963.

Holdsworth, H. Fractures, dislocations and facture-dislocation of spine. J. of Bone and Joint Surgery. 52A:1534, 1970.

Hukins, D.W.L, Disc structure and Function, The biology of Inter vertebral Disc Vol I, Peter Ghosh, Crc Press, 1988.

Humzad, M.D., Soames, R.W., Human Intervertebral disc: Structure and function, review, Anat Rec 220, 337-56. 1998.

Isada, T., Goya, T., Nakano, S., Kodama, T., Moriyama, T., Wakisaka, S., Serial changes in signal intensities of the adjacent discs on T2-weigthed sagittal images after surgical treatment of cervical spondylosis: Anterior interbody fusion versus expansive laminoplasty. Acta Neurochir 143, 707 – 710, 2001.

Johnson , RW., Crelin, E. S., White III, A. A., Panjabi, M. M. and Southwick, W. O., Some new observations on the functional anatomy of the lower cervical spine, Clin. Orthop: 3, 192-200, 1975.

Kabo, J. M., Goldsmith, W., Response of the human head-neck model to transient saggital plane loading, J. Biomechanics, Vol. 16, No. 5, 313-325, 1983.

Katake, K., Studies on the strength of human skeletal muscles. J Kyoto Med Univ 69:463, 1961.

Kleinberger, M., Application of Finite Element Techniques to Study of Cervical Spine mechanics, Proc 37th Stapp Car Crash Conf., San Antonio , TX , Nov. 7-8, 1993, pp. 261-272.

Kowalski, R.J., Ferrara, L.A., and Benzel, E.C., Biomechanics of bone fusion, Neurosurg. Focus 10 (4), 2001.

Kumar, A., Kozak, J.A., Doherty, B.J., Dickson, J.H., Interspace distraction and graft subsidence after anterior lumbar fusion with femoral strut allograft. Spine 18: 2393-2400, 1993.

Kumaresan, S.C., Clinical studies of the human cervical spine using finite element modeling. Ph D. Thesis, Umi Dissertation Services, 1997.

Laporte, C., Laville, C., Lazennec, J. Y., Rolland, E., Ramare, S., Saillant, G., Severe hyperflexion sprains of lower cervical spine in adults. Clinical Orthopaedics and Related Research, 363, 126 – 134, 1999

Levy, R.C., Hawkins, H., Barsan, W.G. Radiology in emergency medicine. Mosby (St louis), 1986

Lindahl, O, " Mechanical properties of dried defatted spongy bone", Orthop. Scand. 47, 11-19, 1976.

Liu, Y. K., Krieger, K. W., Njus, G., Ueno, K., Connors, M. P., Wakano, K., Thies, D., Cervical Spine Stiffness and Geometry of the Young Human Male, Air Force Medical Research Laboratory, Ohio, 1982.

Lotz, J.C., Hsieh, A. H., Walsh, A. L., Palmer, E. I., Chin, J. R., Mechanobiology of the intervertebral disc. Biochemical Society Transactions. Vol. 30, 6: 853-858, 2002.

Lu, J, Ebraheim, NA, Yang, H, Rollins, J, Yeasting, RA, Anatomic bases for anterior Spinal surgery: surgical anatomy of the cervical vertebral body and disc space. Surg. Radiol Anat 21: 235-239, 1993.

Luo, Z., Goldsmith, W. Reaction of a human head/neck/torso system to shock, J. Biomechanics, Vol 24, 1991

Maiman, D. J., Sances, A. Jr., Myklebust, J. B., Larson, S. J., Houterman, C., Chilbert, M., Ghabit, A. Z., Compression Injuries of the Cervical Spine: A Biomechanical Analysis, Neurosurgery, 13: 254-260, 1983.

Malanga, A.G., Kim, D. Cervical spine sprain/strain injuries, www.E-medicine.com, 2002

Martins, A., Anterior Cervical discectomy with and without interbody bone graft. Journal of Neurosurgery 44, 290-5, 1976.

Maurel, N., Lavaste, F., Skalli. W., A Three-Dimensional Parameterized Finite Element Model of the Lower Cervical Spine. Study of the Influence of the Posterior Articular Facets, J. Biomech., 30: 921-931, 1997.

McElhany, J. H., Doherty, B. J., Paver, J. G., Myers, B. S., Gray, L., Combined bending and axial loading response of human cervical spine, SAE paper # 881709, pp 21-28, 1988.

Mckenzie, J. A., Williams, J. F., The dynamic behavior of the head and cervical spine during 'whiplash. J. Biomechanics, 4: 477 –490, 1971.

Miller, H. L. and Schneck D. J., Biodynamic responses to emergency ejections under conditions of added head mass, WPAFB, research contract, 1993.

Moroney, S. P., Schultz, A. B., Miller, J. A., Anderson, G. B., Load Displacement Properties of Lower Cervical Spine Motion Segments, J. Biomech., 21: 769-79, 1988.

Myers B., McElhaney J. and Doherty, B., The viscoelastic responses of the human cervical spine in torsion: experimental limitations of quasi-linear theory, and a method for reducing these effects, J . of Biomechanics, Vol. 24, No 9, pp 811-817, 1991.

Nahum, AL, Melvin JW, Accidental Injury, Biomemechanics and prevention Springer Verlag, 1993.

Nataragan, R.N., Chen, B.H., An, H.S., Anderson, G.B.J., Biomechanical analysis of cervical discectomy and fusion using a three segment model, 23rd annual meeting of the American Society of Biomechanics, Pittsburgh, 1999.

Netter FH, Atlas of Human Anatomy, second edition, Novartis, East Hanover, NJ, 1999

Nightingale, RW, Myers, BS, McElhany, JH, Richardson, WJ, Doherty, BJ: "The influence of end condition on human cervical spine injury mechanisms." 35th Stapp Car Crash conf. SAE paper #9129115: 391-399, 1991.

Nitsche, S., Krabbel, G., Appel, H., and Haug, E.,Validation of a finite element model of the human neck. International IRCOBI Conference on Biomechanics Impact, Dublin, Ireland, 107-108, 1996.

Obergefell, L, Gardner, T., Kaleps, I, Fleck J. "Articulated Total Body Model Enhancements User's Guide" Report AAMRL-TR-88-043, Armstrong Aerospace Medical Research Laboratory, Air Force System Command, WPAFB, January, 1988.

Oda. J., Tanaka, H., Tsuzuki, N., Intervertebral disc changes with aging of human cervical vertebrae from the neonate to the eighties. Spine 13, 1205-11, 1988.

Okada, K., Shirasaki, N., Hayashi, H, Oka, S., Hosoya, T., Treatment of cervical spondylotic Myelopathy by enlargement of the spinal canal anteriorly, followed by arthrodesis, Journal of Bone and Joint Surgery 73, 352-364, 1991.

Onan, OA, Heggeness, MH, Hipp, JA "A motion analysis of the cervical facet joint." Spine 23 (4) 430-439, 1998.

Orrison, W. Introduction to neuroimaging. Little Brown, Boston, 1989

Palumbo, M. A., Hulstyn, M. J., Fadale, P. D., Obrien, T., Shall, L., The Effect of Protective Football Equipment on Alignment of the Injured Cervical Spine, Am. J. Sports Med., Vol. 24 (4), 446-453, 1996.

Panjabi, M. M., White, A. A., Keller D., Southwick, W. O., Friedlaender, G., Stability of The spine under tension. J. Biomechanics, 11,189 –197, 1978

Panjabi, M. M., Summers, D. J., Pelker, R. R., Viedeman, T., Friedlander, G. E., Southwick, W. O., Three Dimensional Load-Displacement Curves Due to Forces on the Cervical Spine, J. Orthop., 4: 152-161, 1986.

Patel, S.S., Timon, S.J., Dawson, E.G., Wang, J.C., 2002. Anterior Lumbar Discectomy and Fusion Using Femoral Ring Allografts, American Academy of Orthopaedic Surgeons, Dallas, TX, February 13 – 17, 2002.

Penning L.,Normal movement of the cervical spine, AJR 130: 317-26, 1978.

Perry, C. E., Vertical impact testing of two helmet-mounted night vision systems, AL/CF-SR, 1994-0013, 1994.

Perry, C.E., Gz Impact acceleration test results for human subjects and manikin. internal communications of the test results. 1996.

Pike A. J., Neck Injury: The use of X-Rays, CTs, and MRIs to study crash-related injury

mechanism. Society of Automotive Engineers, Inc. Warrendale, PA. 2002.

Pilitis, J.G., Lucas, D.R., Rengachary, S.R.: Bone Healing and Spinal Fusion. Neurosurg Focus 13(6), 2002.

Pintar, F.A.,Yoganandan, N., Reinartz, J., Sances, A., Harris, G., Larson, S. J., Kinematic and anatomical analysis of the human cervical spinal column under axial loading. SAE paper # 892436, 191 – 214, 1989.

Pintar, F. A., Yoganandan, N., Suh, J.K., L., Cusick, J. F., Maiman, D. J., Sances, Larson, S. J. Unger G. Biodynamic the human cadavric cervical spine, SAE paper 902309, 55-72, 1990.

Pintar, F. A., Yoganandan, N., Voo, L., Cusick, J. F., Maiman, D. J., Sances, A. Dynamic characteristics of the human cervical spine, SAE paper 952722, 1995.

Pintar, F. A., Biomechanics of Spine Elements, Doctoral Dissertation, Marquette Univ., Milwauke, WI, 1986.

Pooni, J.S., Hukins, D.W.L., Harris, P.F., Hilton, R.C., Davies, K.E., Comparison of the structure of human intervertebral discs in the cervical, thoracic and lumbar regions of the spine. Surgical-Radiologic Anatomy, 8, 175-182, 1986.

Pratt, ES, Green, DA, Spengler, DM, Herniated intervertebral discs associated with unstable spinal injuries. Spine 15: 662-666, 1990.

Profeta, G., de Falco, R., Ianniciello, G., Profeta, L., Cigliano, A., and Raja, I.A., Preliminary experience with anterior cervical microdisectomy and interbody titanium cage fusion (Novus CT-Ti) in patients with cervical disc disease. Surg Neurol 53, 417-26, 2000.

Roaf R., A Study of the Mechanics of Spinal Injuries. J. Bone Joint Surg., 42B, 810-823, 1960

Sadegh, M. A., Analysis of loads on the neck and head joints due to G-y acceleration. SFRP report, AL/CFBE, WPAFB, 1995.

Sadegh, M.A., Perry C.E., and Knox F., Loads on Neck and Head Joints Due to G-y Acceleration, Advances in Bioengineering, Edited by B. Simon, BED/ASME, Vol. 36, pp 229-230, 1997.

Sadegh, M.A., Tchako, A., " A neck model for predicting human tolerance to G-y and G-z accelerations, Math. Model. Scientific computing, Vol 8, 1997.

Sadegh, M. A., Tchako, A., A Cervical Spine Model to Predict Vertebral Stresses in High Accelerations, Advances in Bioengr., BED/ASME, Vol. 36, pp. 213- 214, 1998.

Sadegh, A.M., Tchako, A., Vertebral Stress of cervical spine modelunder dynamic load. Technology and Health Care 8, 143-154, IOS Press, 2000.

Saito, T., Yamamuro, T., Shikata, J., Oka, M., and Tsutsumi, S., Analysis and prevention of spinal column deformity following cervical laminectomy I. Spine, 16, 494-502, 1991.

Saunders, R.L., Bernini, P.M., Shirreffs, T.G.J., Reeves, A.G., Central corpectomy for cervical spondylotic myelopathy: a consecutive series with long term follow-up evaluation. J. Neurosurgery 74:163-170, 1991.

Shams, T., Weerappuli, D., Sharma D., Rangarajan, N., DYNAMAN Program Manual Version 2.0, Report AL/CF-TR-1992-0184, Armstrong Laboratory, Air Force Materiel Command, WPAFB, December, 1992.

Shams, T., Weerappuli, D., Sharma D., Nurse, R., Rangarajan, N, DYNAMAN User's Manual Version 2.0 Report AL/CF-TR-1993-0076, Armstrong Laboratory, Air Force Materiel Command, WPAFB, December, 1993.

Shao, Z., Rompe, G., Schiltenwolf, M., 2002. Radiographic Changes in the lumbar intervertebral discs and lumbar vertebrae with age. Spine 27: 263-268, 2002.

Shea, M., Edwards, W.T., White, A. A., Hayes, W. C., Variations of stiffness and strength along the human cervical spine, J. biomechanics 24: 95 – 107, 1991.

Shea, M., Edwards, W. T., White, A. A., Hayes, W. C., Variations of Stiffness and Strength Along the Human Cervical Spine, J. biomechanics 24: 95 – 107, 1991.

Shinomiya, K., Okamoto, A., Kamikozuru, N., Furuya, K., Yamaura, I., An analysis of failures in primary cervical anterior spinal cord decompression and fusion. Journal of Spinal Disorders 6: 277-288, 1993.

Shirazi-Adl, A., Ahmed, A.M., Shrivasta, S.C. Stress analysis of the lumbar disc-body unit in compression – a three-dimensional nonlinear finite element study. Spine 9: 120-134, 1984.

Shirazi-Adl, A., Ahmed, A. M., Shrivasta, S. C., A Finite Element Study of a Lumber Motion Segment Subjected to Pure Sagittal Plane Moments, J. Biomechanics, 19: 331-350, 1986.

Smith, G.W., Robinson, R.A., The treatment of certain cervical spine disorders by Anterior removal of the intervertebral disc and interbody fusion. Journal of Bone Joint Surgery 40A, 607-624, 1958.

Tencer, A. F., Mirza, S., Benselt, K., Internal Loads in the Cervical Spine During Motor

Vehicle Rear-End Impacts, Spine 27: 34-42, 2002.

Teo, E.C., Paul, J.P., and Evans, J. H., Finite element stress analysis of a cadaver second cervical Vertebra. Medical & biological Engineering & Computing 32: 236-238, 1994.

Teramoto, T., Ohmari, K., Takatsu, T., Inove, H., Ishida, Y., Suzuki, K., Longterm results of anterior cervical spondylosis. Neurosurgery 35: 64 – 68, 1994.

The Cervical Spine, 2nd ed., Charles R. Clark, Editor, Lippincott-Raven Publishers, Philadelphia, 1995

The Cervical Spine, 3rd ed., Charles R. Clark, Editor, Lippincott-Raven Publishers, Philadelphia, 1998

Thomas, BE, McCullen, GM, Yuan, HA, Cervical spine injuries in football players J. Am. Acad. Orth. Surg. 7 (5): 338-47, 1999.

Torg, J., Athletic Injuries to the Head and Face, Lea and Febiger, Philadelphia, 1982.

Torrens, M.J., Miliaras, G., Cervical spondylosis. Part II: Surgical management. Current Qrthopaedcs 16: 300-310, 2002.

Van Mameran H, Sanches H., Beursgens J. Cervical spine motion in the sagittal plane. II. Position of segmental averaged instantatneous centers of rotation-a Cineradiographic study. Spine 17: 467-74, 1992.

Viano, D. C., King, A. I., Melvin, J. W., Weber, K., Injury Biomechanics Research: An Essential Element in the Prevention of Trauma, J. Biomech, 22: 403-417, 1989.

Visarius, H., On the experimental and mathematical modeling of the viscoelastic behavior of human spine, Dissertation, Wayne State Univ., 1994.

Voo, L. M. Pintar, F. A., Yoganandan, N., Liu, Y.K., Static and dynamic bending responses of human cervical spine, J Biomech.Engr.,120: 693 – 696, 1998.

Walz, F, Biomechanische Aspekte der HWS-Verletzungen. Orthopaede 23: 262-267, 1994.

White, A. A., Johnson, R. M., Panjabi, M. M., Southwick, W.O., Biomechanical analysis of the clinical stability in the cervical spine. Clin Orthop 109:85-95, 1975

White, A. A., Southwick, W.O., Panjabi, M. M., Clinical instability in the lower cervical spine. Spine 1: 15-27, 1976

White, A. A., Panjabi, M. M., The problem of clinical instability in human spine: A systematic approach. In White AA and Panjabi MM (eds). Clinical Biomechanics of the spine, 2nd ed., Philadelphia, JB Lippincott 302-327, 1990.

Williams, JL, Belystschko, TB, A three-di,mensional model of the human cervical spine for impact simulation. J. Biomech. Engr. 105: 321-330, 1983.

Winkelstein, BA, Myers, BS "The biomechanics of cervical spine injury and implications for injury prevention" Med. Sci. Sports Exerc. 29: supp. S246-S255, 1997.

Wirth, F.P., Dowd, G.C., Sanders, H.F., and Wirth, C., Cervical discectomy: A prospective analysis of three operative techniques. Surg Neurol 53, 340-8, 2000.

Woo SLY, Johnson GA., Smith B." Current concepts in modeling of ligaments and tendons, ASME Bioeng. Conf. 1993, BED-Vol 24, 298, 1993

Woodburne, RT, Essentials of Human Anatomy, 7th ed., Oxford University Press, Oxford, 1982.

Yamada, H., Strength of Biological Materials, edited by Evans, FG, The Williams & Wilkins Company Baltimore, 1970.

Ylikoski, M, Tallroth, K, Measurement variations in scoliotic angle, vertebral rotation, vertebral body height, and intervertebral disc space height. J. Spinal Disord. 3: 387-391, 1990.

Yoganandan, N., Sances, A., Maiman, D. J., Myklebust, J. B., Pech, P., Larson, S. J., Experimental spinal injuries with vertical impact. Spine, Vol. 11, pp 855 – 860, 1986.

Yoganandan, N, Myklebust, JB, Ray, G, Sances, A, Mathematical and finite element Analysis of spines injuries. CRC Crit. Rev. Biomed. Engr. 15: (1) 29 – 92, 1987.

Yoganandan, N, Sances, A, Pintar, FA, Maiman, DJ,:Reinartz, J, Cusick, JF, Larson, SJ, Injury biomechanics of the human cervical spine. Spine 15 :1031-39, 1990.

Yoganandan, N, Pintar, FA, Arnold, P., Maiman, DJ, Sances, A, Strenght and motion analysis of the human head-neck complex. J. Spin. Disord. 4: 1, 73-85, 1991.

Yoganandan, N., Pintar, F. A., Arnold, P., Reinartz, J., Cusick, J. F., Maiman, D. J., Sances, Larson, S. J., Continuous motion analysis of head-neck complex under impact. J. Spinal Disord. 7: 420-428, 1994.

Yoganandan, N., Kumaresan, S. C., Voo L., Pintar, F. A. and Larson, S.J, Finite element modeling of C4-C6 cervical spine unit, Med Eng & Phys: 18 (7), 569-574, 1996.